Rep. Prog. Phys. **60** (1997) 1217–1304. Printed in the UK PII: S0034-4885(97)38914-3

# Spin-polarized photoemission

Peter D Johnson
Physics Department, Brookhaven National Laboratory, New York 11973, USA

Received 18 April 1997

**Abstract**

Spin-polarized photoemission has developed into a versatile tool for the study of surface and thin film magnetism. In this review, we examine the methodology of the technique and its application to a number of different problems, including both valence band and core level studies. After a detailed review of spin-polarization measurement techniques and the related experimental requirements we consider in detail studies of the bulk properties both above and below the Curie temperature. This section also includes a discussion of observations relating to unique metastable phases obtained via epitaxial growth. The application of the technique to the study of surfaces, both clean and adsorbate covered, is reviewed. The report then examines, in detail, studies of the spin-polarized electronic structure of thin films and the related interfacial magnetism. Finally, observations of spin-polarized quantum well states in non-magnetic thin films are discussed with particular reference to their mediation of the oscillatory exchange coupling in related magnetic multilayers.

0034-4885/97/111217+88$59.50 © 1997 IOP Publishing Ltd 

**Contents**

## 1. Introduction

Driven by the requirements for new information storage technologies the last two decades have seen a rapid increase in research devoted to studies of surface and thin film magnetism (Falicov *et al* 1990). New technologies such as molecular beam epitaxy, previously developed in the semiconductor industry, are now being applied to the development of new magnetic materials with unique properties. The understanding of the properties of these two-dimensional (2D) systems has in turn provided a number of exciting challenges for the scientific community, both experimental and theoretical.

On the experimental side a whole range of electron spectroscopies previously developed for the study of metallic surfaces have been 'spin-sensitized' through the addition of spin polarimeters. Electron-based techniques are particularly suited to the study of surfaces and thin films because the strong Coulomb interaction between electrons results in a relatively short mean free path and associated probing depth.

In this review we examine in detail the development of one such technique, spin-polarized photoemission. Photoemission itself has already seen widespread application to the study of the electronic structure of a whole range of different materials (Kevan 1992). As we shall see, the spin-polarized counterpart has a history spanning a period in time that is almost as long as this 'modern' era of photoemission. However, it has taken several years for the complete angle-resolved, spin-resolved photoemission experiment to be developed to the point where it provides spectra with a signal-to-noise ratio comparable to that of its non-spin-resolved counterpart.

Several reviews of spin-polarized photoemission (SPES) have already appeared in the literature (Feder 1985, Kisker 1987, Johnson 1995a). The present review represents an attempt to provide a perspective on the rapid developments in the last ten years. The article is divided into a number of different sections. We first examine the physics of the photoemission process itself with particular reference to the excitation of spin-polarized electrons. The experimental aspects including the different spin polarimeters that are currently available and the unique aspects of a polarimetry measurement are discussed. We then review a whole range of different experiments, moving from bulk studies, which cover the traditional areas of research in magnetism, through clean and adsorbate covered surfaces to thin films and their interfaces. Finally, we examine the quantized electronic structures found in thin film systems and review the physics of these states with particular reference to the unique properties observed in the related magnetic multilayers.

We would note that this review is not exhaustive in that some areas of endeavour are probably under represented. Indeed the majority of the experiments that are discussed represent studies of ferromagnetic systems, in part reflecting the authors own research interests. However, using incident circularly polarized light, studies of non-magnetic or unpolarized systems are possible. Indeed such experiments have been used to more fully determine the symmetry of different states or bands in solids and to characterize the quantum numbers, dipole matrix elements and phase-shift differences of wavefunctions in the photoionization of free or adsorbed atoms (Heinzmann 1987). Some experiments of this type are discussed but on a more limited basis. Finally, we note that almost every day brings new insights and new applications of spin-polarized photoemission. Hopefully these will be the subject of analysis and review in some future article.

## 2. The photoexcitation process

Photoemission represents the excitation of an electron from an initial state, below the Fermi level in the case of condensed matter systems, to a final state above the vacuum level. As

illustrated in figure 1, the initial state may fall within the delocalized valence bands or it may represent a more localized core level. Excellent reviews of photoelectron spectroscopy have been presented elsewhere (Plummer and Eberhardt 1982, Himpsel 1983, Smith and Himpsel 1983). In general, these authors begin with a description of the interaction between the electron and the photon written within the framework of the non-relativistic Schrödinger equation. In such a picture the interaction is accounted for simply by replacing the momentum operator in the Hamiltonian $\boldsymbol{p}$ by $\boldsymbol{p} - (e/c)\boldsymbol{A}$ with $\boldsymbol{A} = \boldsymbol{A}_0 \mathrm{e}^{\mathrm{i}\omega t}$ the vector potential of the electromagnetic field. In doing so this also introduces a term that reflects the scalar potential of the electromagnetic potential $\phi$. However, it is always possible to chose a gauge such that the latter is zero.

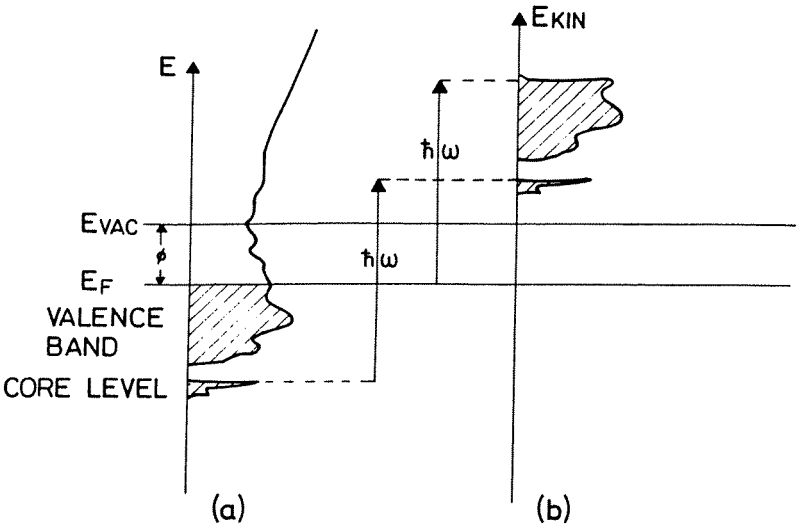


**Figure 1.** A schematic of the photoemission process. The incident photon with energy $\hbar\omega$ excites an electron from an initial state below the Fermi level $E_{\mathrm{F}}$ to some final state above the vacuum level $E_{\mathrm{vac}}$. The left panel shows the electron originating either from the valence band or the more localized core level. The right panel displays the excited electron energy distribution in the final state.

The Schrödinger approach effectively treats the electron as 'spinless'. The Dirac equation, therefore, represents a more appropriate starting point for any description of spin-polarized photoemission. Here the Hamiltonian is written

$$H = \frac{1}{2m}\left(\boldsymbol{p} - \frac{e}{c}\boldsymbol{A}\right)^2 + e\phi - \frac{e\hbar}{2mc}\boldsymbol{\sigma}\nabla \times \boldsymbol{A} + \frac{\mathrm{i}e\hbar}{4m^2c^2}\boldsymbol{E}\cdot\boldsymbol{p} - \frac{e\hbar}{4m^2c^2}\boldsymbol{\sigma}(\boldsymbol{E}\times\boldsymbol{p}) \tag{1}$$

where the first two terms are again identical to the Schrödinger description. The third term, proportional to $\boldsymbol{\sigma}\nabla \times \boldsymbol{A} = \boldsymbol{\sigma}\cdot\boldsymbol{B}$ with $\boldsymbol{\sigma}$ the spin of the electron, represents the interaction of the magnetic dipole with the magnetic field. The fourth term is a relativistic correction to the energy and the final term, proportional to $\boldsymbol{\sigma}(\boldsymbol{E}\times\boldsymbol{p})$, represents the spin–orbit coupling. The spin-dependent terms in the Dirac equation provide new avenues for inducing spin-polarization effects in the photoemitted beam. The $\boldsymbol{\sigma}\cdot\boldsymbol{B}$ term leads to spin-flip transitions which can lead to a measurable spin-polarization at high photon energies. However, at photon energies typical of the ultraviolet (UV) and soft x-ray range, the probability of spin-flip to spin-conserving transitions is of the order $2 \times 10^{-2}$ (Feuchtwang *et al* 1978). The

spin–orbit term, $\boldsymbol{\sigma}(\boldsymbol{E}\times\boldsymbol{p})$, can lead to observable spin-polarization effects both in the initial and final states as will be discussed in later sections.

In the absence of spin–orbit coupling it can be shown for linearly polarized incident light that the Schrödinger description represents an adequate description of the spin-conserving transitions. Thus from Fermi's Golden rule the differential cross section $\mathrm{d}\sigma/\mathrm{d}\Omega$ for excitation from some initial state $|\psi_i\rangle$ to some final state $|\psi_f\rangle$ is given by

$$\frac{\mathrm{d}\sigma}{\mathrm{d}\Omega}(E_f, \hbar\omega, k_f, \boldsymbol{A}) \propto \sqrt{E_f}\sum_i |\langle\psi_f|(\boldsymbol{A}\cdot\boldsymbol{p}+\boldsymbol{p}\cdot\boldsymbol{A})|\psi_i\rangle|^2\,\delta(E_i - E_f - \hbar\omega) \tag{2}$$

where the $\delta$ function describes the energy conservation of the process. Measuring the kinetic energy of the electron in the final state $E_f$ and knowing the incident photon energy, $\hbar\omega$, the experimenter can trace back to the binding energy of the electron in the initial state $E_i$.

Neglecting the diamagnetic term $|A|^2$ which is always small and noting that $\nabla\cdot\boldsymbol{A}$ is non-zero only in the surface region, equation (2) is usually reduced to the simpler form

$$\frac{\mathrm{d}\sigma}{\mathrm{d}\Omega} \propto \sum_i |\langle\psi_f|(\boldsymbol{A}\cdot\boldsymbol{p})|\psi_i\rangle|^2\,\delta(E_i - E_f - \hbar\omega). \tag{3}$$

The matrix element introduces selection rules which can be exploited to determine the symmetry of the initial state. In the non-relativistic limit, excitation by linearly polarized light between one electron states of the form $|nlm_l\rangle$ is restricted to transitions such that $\Delta l = \pm 1$ and $\Delta m_l = 0$. In the event that the incident light is circularly polarized, the second selection rule becomes $\Delta m_l = \pm 1$ dependent on the handedness of the polarization. In the full relativistic treatment with spin–orbit coupling included, the selection rules become $\Delta j = 0, \pm 1$ and $\Delta m_j = \pm 1$ with $j$ and $m_j$ now referring to the total momentum.

A more complete description of the photoemission process will allow for the many-body response of the system to the excitation. Here the $\delta$ function of equation (3) is replaced by a self-energy correction represented by the function

$$A(h\nu, E_i) = \frac{1}{\pi}\frac{\mathrm{Im}\sum(h\nu, E_i)}{\pi\{[h\nu - E_i - \mathrm{Re}\sum(h\nu, E_i)]^2 + [\mathrm{Im}\sum(h\nu, E_i)]^2\}} \tag{4}$$

where $\mathrm{Re}\sum(h\nu, E_i)$ and $\mathrm{Im}\sum(h\nu, E_i)$ represent the real and imaginary parts of the self-energy, respectively. This correction results in a broadening and shifting of the peaks that would characterize the one-electron spectrum. In ferromagnetic systems, because of the spin polarization of the electronic structure, we may anticipate a spin dependence in the response of the system.

Extending the technique and measuring the photoemitted current at some well defined angle $\vartheta$ it becomes possible to map the dispersion of the different initial-state bands. As illustrated in figure 2, at a well defined $k_\parallel$, the process represents a direct transition between two bands of the same spin. In the solid state momentum conservation is maintained through the mediation of the crystal momentum giving

$$\boldsymbol{k}_f = \boldsymbol{k}_i + \boldsymbol{G} \tag{5}$$

where $\boldsymbol{k}_i$and $\boldsymbol{k}_f$ are the wavevectors associated with the initial and final states and $\boldsymbol{G}$ represents a suitable lattice vector. To within a reciprocal lattice vector the parallel momentum $k_\parallel$ of the photoelectron given by

$$k_\parallel = \left(\frac{2m}{\hbar^2}\right)^{1/2} E^{1/2}\sin\vartheta \tag{6}$$

is conserved on crossing from the solid into the vacuum. Thus a measurement of this component in the vacuum supplies a good measure of the parallel component in the solid.

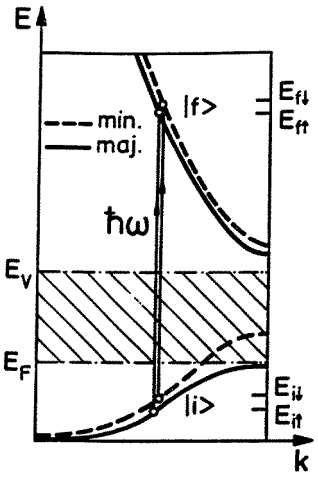


**Figure 2.** A schematic of the direct $k$-conserving transition in the photoemission process. The incident photon excites an electron from an initial state $E_i$ below the Fermi level $E_F$ to some final state $E_f$ above the vacuum level $E_V$. Spin conservation is maintained in the transition.

The perpendicular component is less well defined. Without a detailed knowledge of the relationship between $E$ and $k_\perp$ in the solid some approximations have to be made. However, even with this limitation there have been an enormous number of successful measurements of bulk band dispersions in a wide variety of solids. One approach has been to approximate the final state with a free-electron-like band defined from some 'adjustable' inner potential (Plummer and Eberhardt 1982). Another method that has been very successful has involved the calculation of the initial- and final-state bands via some method such as the combined interpolation scheme (Smith 1979).

Throughout this review we will make reference to studies using the complementary technique, inverse photoemission (Dose 1985, Himpsel 1986, Smith 1988, Johnson 1992). This technique, which may be viewed as the time reversed mechanism, allows the study of the momentum-resolved unoccupied electronic structure above the Fermi level. A refinement of the technique allows the spin resolution of the unoccupied bands through the use of a spin-polarized electron source (Donath 1994).

## 3. The experimental approach

### *3.1. Spin polarimetry*

In this section we examine the methodology of the spin-polarized photoemission experiment. In particular, we concentrate on the different types of spin polarimeter that are available and discuss the practicalities of a spin polarization measurement.

A review of spin-polarized electrons and spin polarimetry has been provided elsewhere by Kessler (1985). Here we will examine particular aspects of spin polarimetry as applied to the photoemission technique. It is well known that a neutral atomic beam may be polarized in the inhomogeneous field of the Stern–Gerlach apparatus. Unfortunately, the presence of the Lorentz force acting on the charged electron prohibits the use of the same technique for determining the polarization of an electron beam. However, techniques based on the use of

either spin–orbit or exchange scattering have been developed and we discuss these in the following sections.

*3.1.1. Spin polarimetry via the spin–orbit interaction.* Much of the pioneering work in spin-polarized photoemission was carried out with spin polarimeters of the high-energy Mott-scattering type (Kisker *et al* 1982). Here the electrons to be analysed are scattered off gold atoms at energies typically of the order of 100 keV. Spin–orbit coupling of the electron in the potential of the gold atom, as shown in figure 3, leads to an asymmetry in the scattering, left and right, dependent on the spin of the electron.

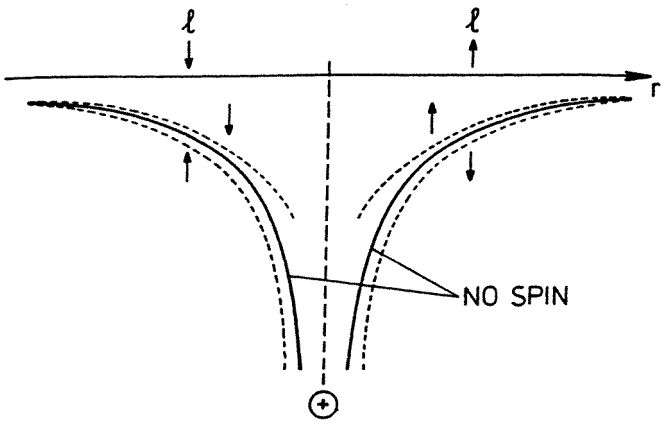


**Figure 3.** The potential curves experienced by an electron with spin up or spin down in the vicinity of a gold scattering atom both with (- - - -) and without (——) spin–orbit coupling.

Because of the high energies involved in the earlier designs, Mott polarimeters tended to be large. However, there have recently been a number of successful modifications that have allowed the polarimeter to be scaled down in size. Figure 4 shows the configuration used in one such device as described by Tang *et al* (1988). After initially passing through a deceleration lens the incident beam of electrons is accelerated onto the gold foil at an energy of 20 keV. As in the earlier designs (Kisker *et al* 1982), those electrons elastically scattered through 120° are detected by two symmetrically opposite channeltrons. Retarding fields in front of the latter collectors remove any electrons that have undergone inelastic losses. The spin polarization $P$ of the incident electron beam is given by

$$P = \frac{1}{S}\frac{I_A - I_B}{I_A + I_B} \tag{7}$$

where $S$, the Sherman function of the device, is a measure of its ability to distinguish different spins and $I_A$ and $I_B$ represent the intensities measured in opposite channels. Mott polarimeters of this type are now sufficiently small that they can readily be moved inside a vacuum system and, therefore, be used for angle-resolved polarization measurements.

The figure of merit (FOM) used in comparing different polarimeters is defined as

$$\text{FOM} = S^2\frac{I}{I_0} \tag{8}$$

where again $S$ is the Sherman function, $I$ is the sum of the current collected by the two opposite detectors and $I_0$ is the incident beam current (Kessler 1985). The FOM for the

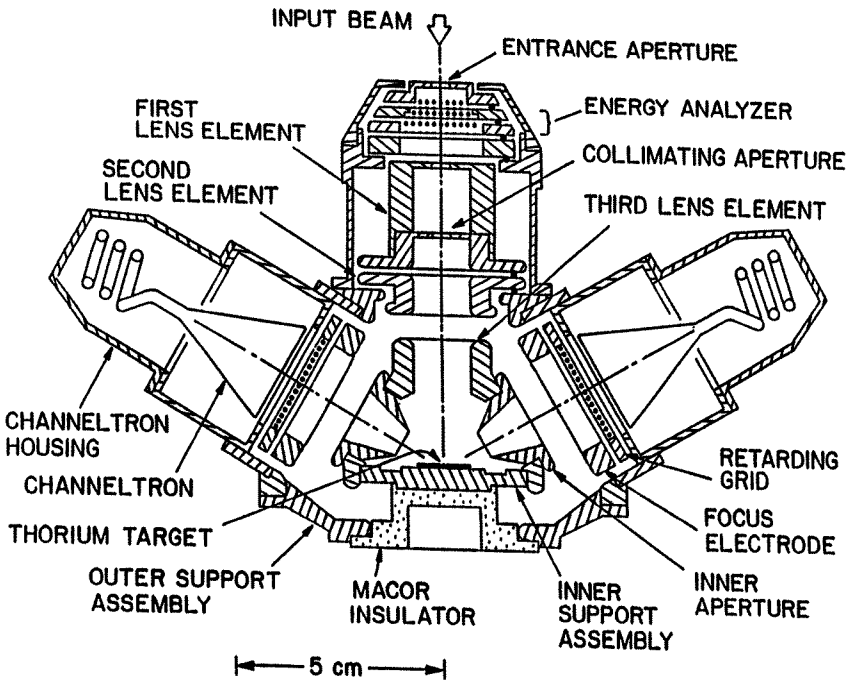


**Figure 4.** Representative configuration of the micro-Mott spin detector showing the various elements in the incident lens, the scattering target and the collecting electrodes or channeltrons.

traditional Mott polarimeter is typically $10^{-4}$; that of the compact low-energy Mott device has been approximately $2 \times 10^{-5}$ (Tang *et al* 1988). However, more recently, the FOM of the compact device has been improved to approximately $1.6 \times 10^{-4}$ through the use of large-area electron detectors and careful optimization of the electron optics (Burnett *et al* 1994). The possibility of pushing the FOM even higher with better defined electron optics has been examined by Huang D-J *et al* (1993).

It has recently been demonstrated that the low-energy diffuse scattering type of detector, originally designed for use in secondary electron microscopy with polarization analysis (SEMPA) studies (Unguris *et al* 1986, Scheinfein *et al* 1989), also proves an excellent device for energy- and angle-resolved spin-polarized photoemission studies (Johnson *et al* 1992). Rather than the high energies, characteristic of the Mott devices, the electrons to be spin analysed are now scattered from a polycrystalline gold surface at the much lower energy of 150 eV, an energy at which the Sherman function of gold exhibits a local maximum. The back-scattered electrons pass through retarding grids to remove low-energy secondary electrons, and are then collected by four discrete anodes. This allows a measurement of two components of the polarization to be made in parallel. Shown later in figure 7, this type of detector has an FOM of the order of $1.0 \times 10^{-4}$ (Unguris *et al* 1986), i.e. comparable to the traditional Mott detector.

If the scattering surface is a single crystal rather than polycrystalline it is possible to use spin-dependent diffraction to measure the polarization. The spin asymmetry in the scattering again reflects the spin–orbit interaction. Detectors of this type include a low-energy detector of Kirschner and Feder (1979) which relies on spin–orbit effects in the diffraction of the electrons from a single-crystal tungsten (001) surface. The intensities of the symmetrically

opposite $(2, 0)$ and $(\bar{2}, 0)$ diffracted beams are measured with the electrons incident at an energy of 100 eV. The authors report an FOM for this detector of $1.6 \times 10^{-4}$.

*3.1.2. Spin polarimetry via the exchange interaction.* Spin polarimeters based on an exchange interaction fall into two categories, those employing reflection and those employing transmission. A detector based on low-energy reflection from a ferromagnetic film has been described by Tillman *et al* (1989). Here the scattering surface is a 400 Å thick Fe(001) film grown on an Ag(001) substrate. Reflected intensities are measured when the electrons to be analysed are incident on a magnetized iron surface at an energy of approximately 10.0 eV.

The asymmetry in the scattering, $A$, in such a detector is given by

$$A = \frac{1}{P}\frac{I^{\uparrow\uparrow} - I^{\uparrow\downarrow}}{I^{\uparrow\uparrow} + I^{\uparrow\downarrow}} \tag{9}$$

where $P$ is the spin polarization in the incident beam and $I^{\uparrow\uparrow}$ and $I^{\uparrow\downarrow}$ are the scattered intensities obtained when the target and primary beam magnetic moments are parallel and anti-parallel, respectively. The FOM of such a device is then given by

$$\text{FOM} = A^2 \frac{I_\text{R}}{I_\text{P}} \tag{10}$$

where $I_\text{R}$ and $I_\text{P}$ are the reflected and primary beam currents, respectively. One difficulty with an instrument of this type is that with the reflecting or analysing surface being effectively another 'sample', two samples have to be successfully prepared and magnetized. However, at 10.6 eV analysing energy, the authors report a value of 0.21 for $A$ and an FOM of $3.5 \times 10^{-3}$.

Turning to transmission, Schonhense and Siegmann (1993) have suggested the possibility of using the spin-dependent transmission through ferromagnetic thin films as a means of detecting spin polarization. That such a spin dependence in transmission exists is evident in that the low-energy secondary electron cascade in all electron spectroscopies is known to display an enhanced spin polarization. Indeed, the latter polarization is considerably larger than would be expected simply on the basis of the bulk valence band polarization.

Whilst no spin polarimeter based on transmission has been developed and routinely used, a number of experiments have examined the spin-dependent transmission of electrons through thin films. In a detailed study, Pappas *et al* (1991) examined the transmission of unpolarized d-electrons from a copper (001) substrate through a thin face-centred cubic (fcc) Fe overlayer. The study found that for electron energies below 40 eV, the mean free paths for the two spin states clearly diverged as shown in figure 5. Furthermore, they found that both of these mean free paths or escape depths were less than would be expected on the basis of a universal curve (Seah and Dench 1979). In a related experiment, Getzlaff *et al* (1993a) measured the spin-dependent transport of photoemitted electrons from a W(110) substrate through deposited body-centred cubic (bcc) Fe and hexagonal close-packed (hcp) Co thin films. The authors found significantly larger mean free paths than the earlier study of Pappas *et al* (1991) and this they attributed to different packing densities and possibly different structural properties of the ferromagnetic films.

In another study, Vescovo *et al* (1995a) examined the spin-dependent electron scattering in ferromagnetic Co films deposited on a Cu(111) substrate. These authors also reported an asymmetry in the mean free paths, $\lambda^{\uparrow(\downarrow)}$, for the two spin states. Measuring the asymmetry

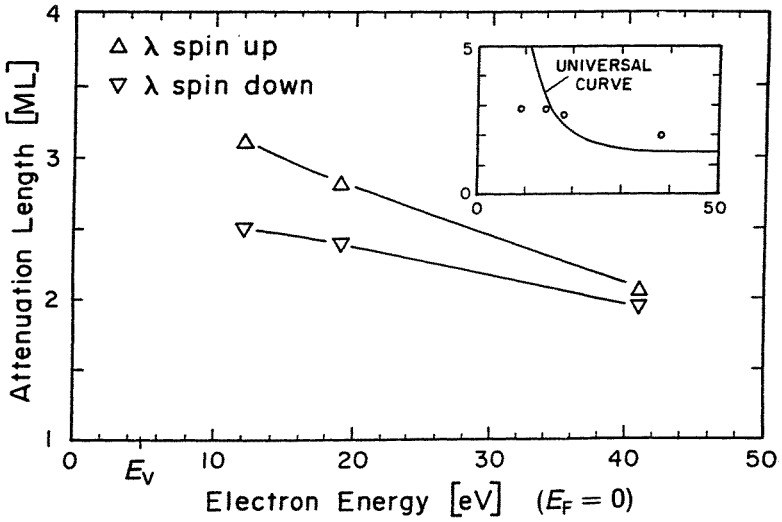


**Figure 5.** Spin-dependent inelastic mean free paths (IMFP) determined from the spin-polarized photoemission spectra. Values of the spin-averaged IMFP compared to the 'universal' mean free path curve. The electron energies are referenced to the Fermi energy. The error bars on the spin-averaged data reflect the error in the thickness calibration whereas the error bars in the spin-resolved data include only contributions from the polarization uncertainty.

$A_\lambda$ defined as

$$A_\lambda = \frac{(\lambda^\uparrow - \lambda^\downarrow)}{(\lambda^\uparrow + \lambda^\downarrow)} \tag{11}$$

as a function of transmission energy they reported a monotonic decrease as the energy increased until at energies above 30 eV it was unclear if any asymmetry existed at all.

Both elastic and inelastic scattering events have been cited as the source of asymmetry in spin-dependent mean free paths. Gokhale and Mills (1991) have examined the spin filtering solely in terms of elastic scattering. The calculations, which consider an electron beam transmitted through a ferromagnetic fcc Fe film deposited on a jellium substrate, yield both a strong energy and thickness dependence on the transmissivity. The authors conclude that it is the exchange asymmetry in this transmissivity rather than a spin dependence of the electron mean free path that is responsible for the effect reported by Pappas *et al* (1991).

A different approach is taken by Schonhense and Siegmann (1993) who have examined a number of experiments in detail. As shown in figure 6 they find that the total scattering cross section $\sigma(E) = 1/\lambda$ is well described by the expression

$$\sigma = \sigma_0 + \sigma_d(5 - n) \tag{12}$$

where $\sigma_d$ accounts for scattering into the d-holes and $\sigma_0$ is a constant accounting for other inelastic scattering events. They define a transport polarization $\boldsymbol{a}$ such that an electron beam with small initial polarization $P_0$ will acquire a polarization after travelling a distance $x$ such that

$$P(x) = P_0 + \boldsymbol{a}(\boldsymbol{x}). \tag{13}$$

The transport polarization $\boldsymbol{a}$ is given by

$$\boldsymbol{a} = \frac{[\exp(\sigma^- - \sigma^+)\boldsymbol{x} - 1]}{[\exp(\sigma^- - \sigma^+)\boldsymbol{x} + 1]} \tag{14}$$

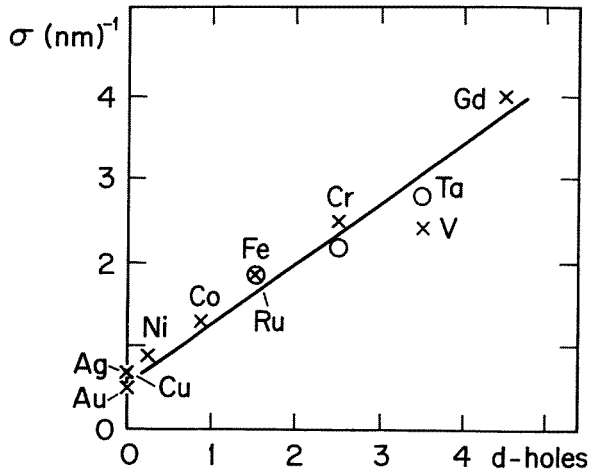


**Figure 6.** Total scattering cross section $\sigma = 1/\lambda$ in $nm^{-1}$ against the number of unoccupied d-orbitals for the transition metals indicated. The data are obtained by analysing the electron spin polarization in overlayer films and are valid for electron energies within 5 eV of the vacuum level.

with $\sigma^{(\pm)}$ representing the spin-dependent cross sections. In their picture the spin polarization is, therefore, dominated by the inelastic scattering involving unoccupied states above the Fermi level.

A similar idea had been discussed earlier by Penn *et al* (1985). The latter authors found that the scattering rate for minority spin electrons is enhanced with respect to that of the majority spin electrons because of the excess of minority spin holes. They found, however, that the effect only becomes significant for kinetic energies below 5 eV when the electrons scatter into the unoccupied d states.

Schonhense and Siegmann (1993) note that a spin polarimeter based on the use of spin-dependent transmission will have an FOM given by $\boldsymbol{a}^2 I$ where $I = 2\,\mathrm{e}^{-\sigma \cdot x}$ represents the total spin-integrated transmission through the film and $\sigma$ is the spin-averaged total cross section. On the basis of their experimental observations they show that the FOM for an iron film will peak at approximately $7 \times 10^{-2}$ for film thicknesses of approximately 1.0 nm. For Co they predict an FOM of $6 \times 10^{-2}$ for a film thickness of approximately 1.5 nm.

The possibility of such a spin polarimeter has been tested further in a series of studies of the spin-dependent transmission through a free standing Co film (Lassailly *et al* 1994, van der Sluijs *et al* 1994). In these studies a longitudinally polarized electron beam from a GaAs source was directed through a 10 nm thick Co film sandwiched between 210 nm Au film and a 20 nm Au film. At low energies, close to the surface vacuum level, the transmission coefficient for the minority spin electrons was found to be 0.7 that found for the majority spin electrons. The total transmitted current was of the order of $10^{-5}$ of the primary beam. By cesiating both sides of the film, this transmission ratio was increased to $3 \times 10^{-4}$ (van der Sluijs *et al* 1994). In this same experimental configuration, operating with an incident energy of 2.5 eV, the authors measured a Sherman function $S = 0.4$ and an increased transmission of $3 \times 10^{-4}$. Thus, as the authors note, the experimentally measured FOM for such a device is close to that of the Mott scatterers. The Sherman function is also consistent with the predictions of Schonhense and Siegmann (1993) suggesting that if the film can be made thinner, the FOM will be even higher.

### *3.2. The polarization measurement*

Before closing our discussion of the experimental details we offer a brief introduction to the practicalities of a spin-polarization measurement. A more detailed discussion can be found elsewhere (Kessler 1985).

In order to define a quantization direction for the spin of the electrons it is necessary that the sample under investigation is magnetically saturated. For elemental metals such as Fe, Co or Ni, a number of experiments have been successfully completed with the sample machined in the form of a picture frame. The magnetizing field is obtained from a solenoid wrapped around one arm of the frame. To minimize problems from stray magnetic fields, the magnetizing field is reduced to zero and the measurements are made with the sample in a remnant magnetic state. Evaporated thin films have also been successfully used in spin-polarized photoemission studies. Indeed, epitaxially grown thin films can be magnetized as a single Weiss domain. In the case of thin films the magnetizing field is obtained by discharging a current pulse through a small coil in close proximity to the film.

To avoid any error being introduced into the measurement by apparatus asymmetries it is necessary to make two measurements of the spin polarization, one with the sample magnetized 'up' ($I_{\mathrm{L}}^{+}$, $I_{\mathrm{R}}^{+}$) and one with the sample magnetized 'down' ($I_{\mathrm{L}}^{-}$, $I_{\mathrm{R}}^{-}$). Here $I_{\mathrm{L}}$ and $I_{\mathrm{R}}$ represent the number of electrons scattered from the target into the left and right channels, respectively. Assuming that the incident beam does not move between the '+' and '−' measurements, any instrumental asymmetry derived from a misalignment of the beam incident on the scattering target can then be removed by combining the four measurements such that the true spin polarization $P$ is given by

$$P = \frac{1}{S}\frac{\sqrt{I_{\mathrm{L}}^{+}I_{\mathrm{R}}^{-}} - \sqrt{I_{\mathrm{L}}^{-}I_{\mathrm{R}}^{+}}}{\sqrt{I_{\mathrm{L}}^{+}I_{\mathrm{R}}^{-}} + \sqrt{I_{\mathrm{L}}^{-}I_{\mathrm{R}}^{+}}} \tag{15}$$

where as before $S$ represents the Sherman function of the instrument. The measured intensities combined in this manner remove, to first order, any instrumental asymmetry. The two measurements, '+' and '−', may have different count rates without affecting the measured polarization. Assuming that there is not an asymmetry that changes with the two magnetization directions, the instrumental asymmetry $A$ is given by

$$A = \frac{\sqrt{I_{\mathrm{L}}^{+}I_{\mathrm{L}}^{-}}}{\sqrt{I_{\mathrm{R}}^{+}I_{\mathrm{R}}^{-}}}. \tag{16}$$

The individual spin-up and spin-down spectra are obtained from the polarization $P$ by

$$I^{\uparrow} = \langle I\rangle(1+P) \qquad I^{\downarrow} = \langle I\rangle(1-P) \tag{17}$$

where

$$\langle I\rangle = \frac{I_{\mathrm{L}}^{+} + I_{\mathrm{L}}^{-} + I_{\mathrm{R}}^{+} + I_{\mathrm{R}}^{-}}{4}. \tag{18}$$

### *3.3. The complete facility*

As in any electron spectroscopy, spin-polarized photoemission requires the use of an electron spectrometer. These instruments can take many different forms although, as illustrated in figure 7, the hemispherical analyser represents the most commonly used instrument in SPES at the present time. A more complete discussion of the properties of such an analyser can be found elsewhere (e.g. Roy and Carette 1977). Here we note that in such an instrument the

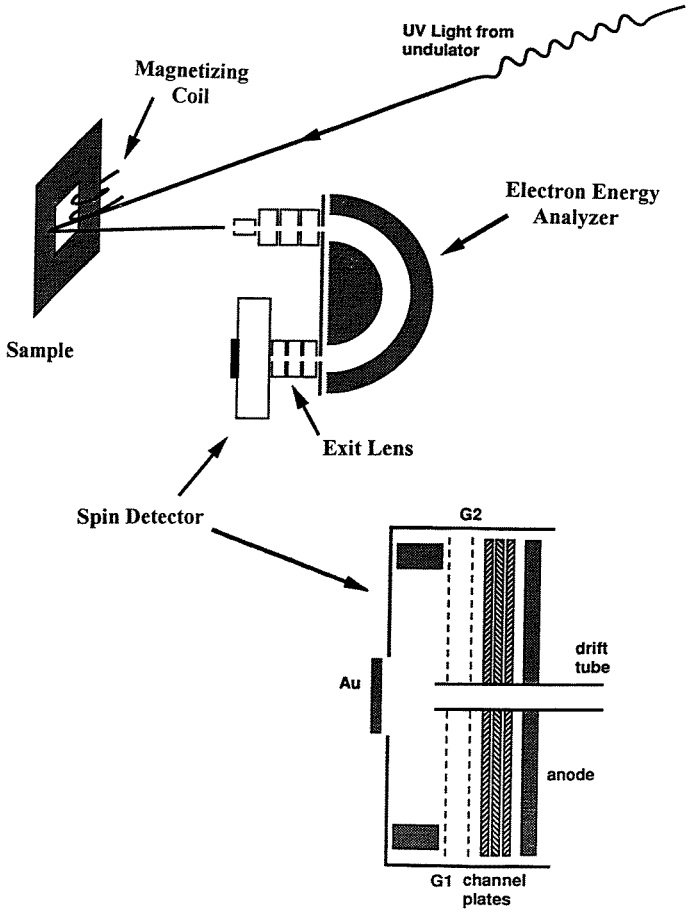


**Figure 7.** A schematic of a 'complete' experiment showing a hemispherical analyser backed by, in this case, a low-energy diffuse scattering spin polarimeter. In the latter device the incident electrons with energy 150 eV are back scattered by the gold target through energy filtering grids into discrete anodes. Photoelectrons are excited from a magnetized sample.

kinetic energy of the electron is measured by retarding electrostatic fields applied between the two hemispheres and the momentum is selected by defining a small angle of collection. As also illustrated in figure 7, some form of electrostatic lens is required to couple this analyser to whichever spin polarimeter is selected for the experiment.

An overview of the practicalities of coupling spin polarimeters to electron spectrometers has been given by Pierce *et al* (1988). In particular, these authors emphasize the requirement for optimizing the experiment by matching the phase space or acceptances of the source, the electron spectrometer and finally of the spin polarimeter itself. At any point on the pathway of the electron beam the Helmholz–Lagrange law states that there will be a conservation of the product $EA\Omega$, where $E$ is the energy, $\Omega$ the solid angle and $A$ the cross sectional area. In the optimum configuration this product will be matched to the acceptance phase space of the polarimeter. Pierce *et al* (1988) have tabulated the latter for a number of different spin polarimeters.

Whilst the FOM of spin detectors is slowly improving, a large photon flux is still required if a reasonable signal-to-noise ratio is to be achieved. Suitably high photon fluxes are now

routinely available from insertion devices, including both undulators and wigglers, that have been installed at a number of 'second and third' generation synchrotron radiation sources. The use of undulator radiation has resulted in the quality of spin-resolved spectra being comparable to that obtained in many non spin-resolved photoemission measurements. An example of a spin-polarized photoemission facility based on the use of undulator radiation has been described by Johnson *et al* (1992).

## 4. Bulk studies

### *4.1. Valence band studies*

*4.1.1. Elemental materials.* Spin-polarized photoemission studies of the elemental materials Fe and Ni have concentrated on the identification of exchange split bands at low or room temperature and the extension of these studies to the effects of high temperature. In the latter case it is hoped to study the ferromagnetic to paramagnetic phase transition. At low temperatures, the comparison between experiment and theory for Fe has been relatively easy. In the case of Ni, correlation effects have made the interpretation more difficult. To the author's knowledge there have been no detailed studies of hcp Co. However, as described later, fcc Co has been studied in thin film form.

Early spin-polarized photoemission studies were restricted to threshold studies to avoid the problems associated with stray magnetic fields. In agreement with the predictions of Wohlfarth (1971, 1977), an early study of the Ni(001) surface found a negative spin polarization at threshold (Eib and Alvarado 1976). However, Moore and Pendry (1978) were unable to reproduce these experimental observations in a photoemission calculation taking the local spin density functional (LSDF) value of 0.6 eV for the exchange parameter, $\Delta E_X$. Rather, they found that a value of 0.3 eV for $\Delta E_X$ gave a better description. The requirement of a reduced value for the exchange splitting was confirmed both in subsequent threshold photoemission studies of the Ni(111) surface (Kisker *et al* 1979) and in angle-resolved photoemission studies of the low index planes of Ni (Himpsel *et al* 1979, Eberhardt and Plummer 1980, Heimann *et al* 1981).

A spin-integrated, angle-resolved photoemission study of the Ni(110) surface by Heimann *et al* (1981) revealed a symmetry-dependent exchange splitting for the $e_g$ and $t_{2g}$ states of 0.18 and 0.3 eV, respectively. A reduced bandwidth for the d-bands was also observed. All of these results were confirmed in the first spin-, energy- and angle-resolved photoemission study of this surface by Raue *et al* (1983). Using an Ne resonance lamp (16.85 eV) as the excitation source, the latter authors identified the $X_2^{\downarrow}$ at $-0.06$ eV and $X_2^{\uparrow}$ the at $-0.24$ eV, respectively, giving an exchange splitting for these $S_4$ bands of 0.18 eV. They also located the $X_5^{\uparrow}$ at a binding energy of $-0.10$ eV.

The band narrowing and reduced exchange splitting of Ni are generally associated with the presence of a 6 eV satellite in the spectra. This satellite has in fact been observed in both the core levels (Hufner and Wertheim 1975) and the valence bands (Guillot *et al* 1982). Following a suggestion of Mott (1964) the satellite is generally associated with more localized or atomic-like effects (Penn 1979, Davis and Feldkamp 1979), particularly as the valence band satellite is known to undergo a resonance at photon energies corresponding to threshold excitation of the 3p core level. The satellite is seen as representing the $d^8$ configuration with the associated excitation route on resonance being

$$3p^6 3d^9 \rightarrow 3p^5 3d^{10} \rightarrow 3p^6 3d^8 + e^- \tag{19}$$

where $e^-$ represents the final-state continuum electron. Here the 3p core hole is thought

to have decayed via a super-Coster–Kronig-type transition. Feldkamp and Davis (1979) suggested that the Ni Auger electrons would carry very little spin polarization whereas the photoelectrons produced in the resonant mechanism would carry spin polarization because of the spin selectivity in the initial excitation at threshold. This prediction was verified in a spin-polarized photoemission study of the satellite on and off resonance by Clauberg *et al* (1981) who found that on resonance the satellite was spin polarized in excess of the average valence band polarization.

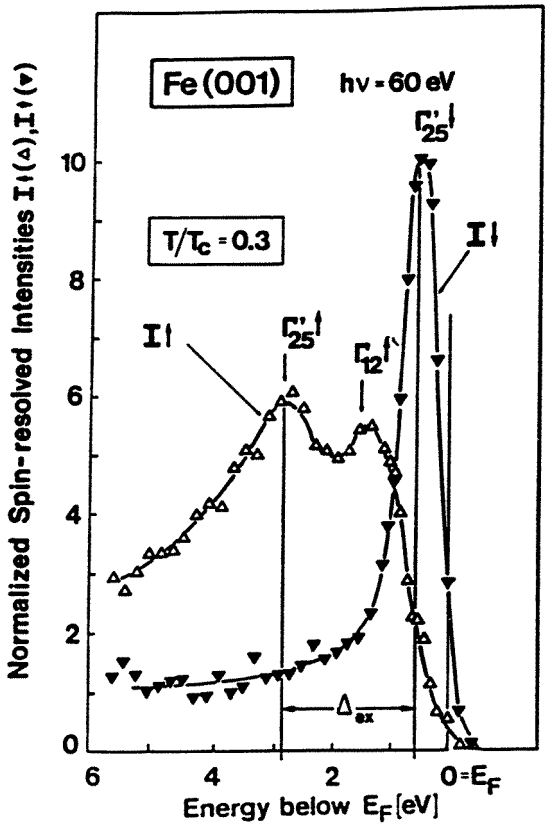


**Figure 8.** Spin-polarized photoemission spectra recorded along the surface normal from an Fe(001) surface at a temperature corresponding to $0.3T_c$. With an incident photon energy of 60 eV, the emission is primarily from the $\Gamma$ point in the Brillouin zone. The different critical points in the spectra are indicated.

Liebsch (1979, 1981) was able to explain the narrowing of the Ni d-band width in terms of self-energy corrections or correlations amongst the d-electrons. In essence, his model reflects the presence of a sum rule whereby spectral weight is transferred from the majority spin valence band to the satellite resulting in the narrowing of the d-bands and reduced exchange splitting. His theory was further able to explain the symmetry dependence of the exchange splitting observed in the experiments of Heimann *et al* (1981). In a later study, Victora and Falicov (1985a), taking full account of both bandstructure effects and electron–electron interactions, were able to calculate the exact density of emitted states and obtain good agreement with the photoemission experiments.

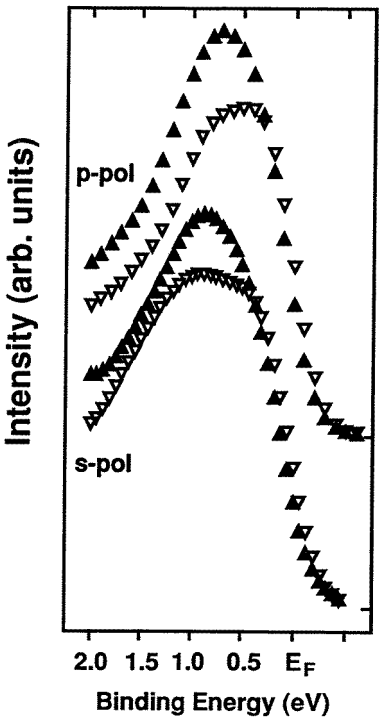


**Figure 9.** Light polarization dependence of the spin-polarized valence band spectra recorded from bcc nickel. The photon energy is $h\nu = 60$ eV. In this case s- and p-polarized light refers to the angles of light incidence $\theta_i = 35^\circ$ and $70^\circ$, respectively.

As in the case of Ni, the exchange split electronic structure of Fe was first examined along the high-symmetry directions using angle-resolved photoemission without recourse to the added complication of spin detection. These early angle-resolved photoemission studies with resonance lamps (Heimann and Neddermeyer 1978, Schultz *et al* 1979) found broad agreement with calculation but were unable to identify specific critical points. Indeed, the authors of these studies concluded that it was not possible to observe band dispersions in Fe. However, this latter objective was actually achieved in later studies using synchrotron radiation as the excitation source (Eastman *et al* 1980, Turner *et al* 1984, Sakisaka *et al* 1985). In particular, a study of all three low index crystal planes by Turner *et al* (1984) found good agreement with first-principles calculations by Callaway and Wang (1977). However, the experimental study indicated that the presence of surface states complicated the interpretation of spectra, particularly in the case of the (001) surface.

The first spin- and angle-resolved photoemission study of Fe was undertaken on the (001) surface. Using incident s-polarized synchrotron radiation of 60 eV energy, Feder *et al* (1983) were able to identify transitions from the $\Gamma_{25'}$ and $\Gamma_{12}$ majority spin critical points and from the $\Gamma_{25'}$ minority spin point. Shown in figure 8, the same group was subsequently able to obtain data from the same crystal with improved energy resolution (Kisker *et al* 1985). Because of the incident light polarization, the spectra are dominated by the transitions from the $\Gamma_{25'}$ points. The majority spin $\Gamma_{25'}$ and $\Gamma_{12}$ points are located at binding energies of $2.6 \pm 0.2$ eV and $1.2 \pm 0.2$ eV, respectively. The minority spin $\Gamma_{25'}$ point is located at a

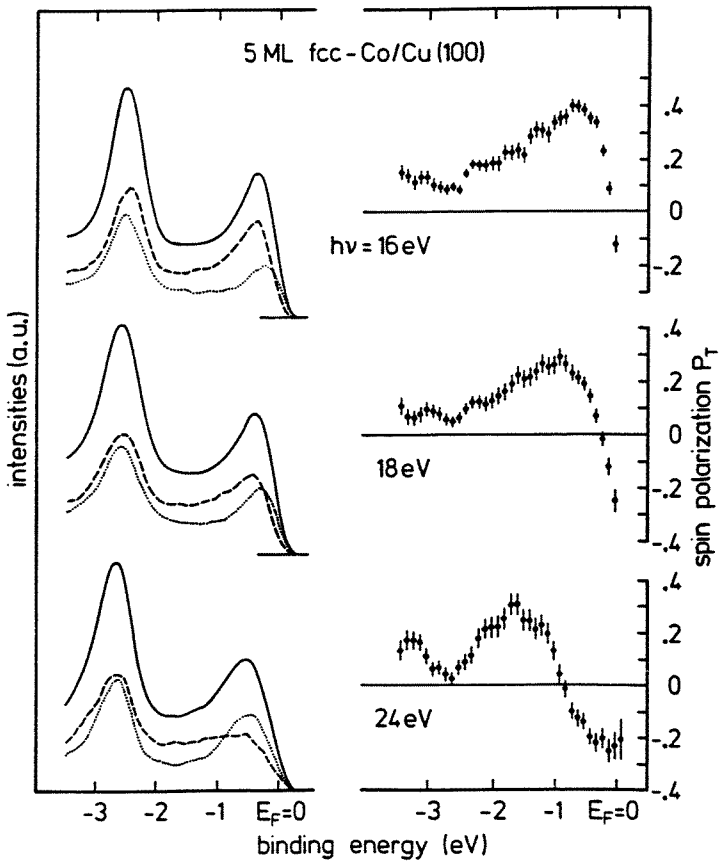


**Figure 10.** Energy distribution curves (left column) and the in-plane spin-polarization component $P_T$ (right column) obtained from five-monolayer (ML) films of fcc Co(100) in normal emission. From the total intensities (full curves) and the corresponding spin-polarization distributions the partial spin densities (left column) are calculated. These indicate directly the contributions of the majority (- - - -) and minority (· · · · · ·) spin electrons.

binding energy of $0.4 \pm 0.2$ eV. These binding energy values are uniformly higher than the values obtained in the spin-intgerated photoemission studies (Turner *et al* 1984) but this may simply reflect the choice of position for the Fermi energy. In fact the value obtained for the exchange splitting in the two studies is nearly identical. The experimental observations may be compared with the results of a theoretical study by Hathaway *et al* (1985), who predict binding energies of 0.69 eV and 2.51 eV for the two $\Gamma_{25'}$ critical points and 0.99 eV for the $\Gamma_{12}$ point. In a later spin-polarized photoemission study, Johnson *et al* (1992) were able to enhance the emission from the $\Gamma_{12}$ critical point by altering the angle of incidence of the light to increase the magnitude of the p-polarized component. However, the binding energy for the $\Gamma_{12}$ critical point in the latter study was essentially identical to that found in the earlier studies.

In a more detailed study Kisker *et al* (1985) measured the photon energy dependence of the spin-resolved spectra from the Fe(001) surface and interpreted their data in terms of direct interband transitions into a free-electron-like, final-state band. With incident s-polarized light, they found strong changes in the spectra between photon energies of

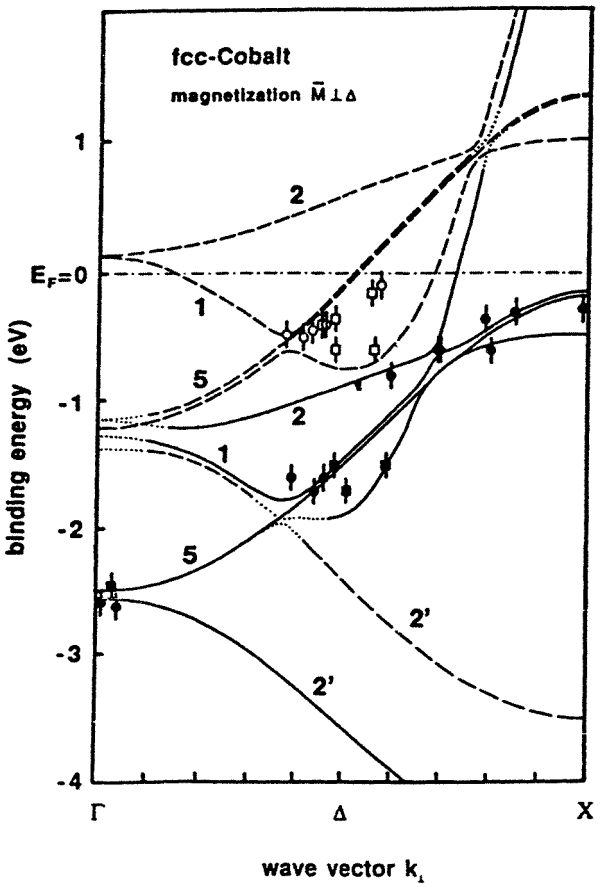


**Figure 11.** Comparison of a band structure calculation for bulk fcc Co (lattice parameter $a_0 = 3.51$ A) with experimental band mapping results for fcc Co. Note the change of the spin character within particular bands from majority (full) to minority (broken) via intermediate-character (dotted) hybridization points due to spin–orbit coupling. The circular symbols refer to normal light incidence, the square ones to oblique incidence.

20 and 60 eV. At a photon energy below 33 eV, the intensity of the minority spin peak immediately below the Fermi level suddenly dropped as the initial state $\Delta_5$ band crossed the Fermi level at the centre of the Brillouin zone. At lower photon energies the spectra were dominated by majority spin emission.

Schröder *et al* (1985) have reported a spin-polarized photoemission study of an Fe(110) film grown on a GaAs substrate. The films, which were not grown *in situ*, were cleaned by Ne ion sputtering. The authors concluded that their study showed good agreement with the results of first-principles calculations (Hathaway *et al* 1985). However, we note that because the experimental study was restricted to the single photon energy of 30 eV, the only new information was the identification of majority spin emission from the band running from $\Gamma_{12}$ to $N_4$.

*4.1.2. Novel phases stabilized by epitaxial growth.* The bcc phase of Ni may be grown epitaxially on Fe(001) substrates. Grown in this fashion it has been studied using low-energy

electron diffraction (LEED) (Marcus *et al* 1986, Wang *et al* 1987), reflection high-energy electron diffraction (RHEED) (Heinrich *et al* 1986a, 1987), polarized neutron reflection (PNR) (Bland *et al* 1991) and spin-polarized photoemission (Brookes *et al* 1992). The structural studies indicate that for films less than six layers the nickel grows in a bcc manner. Above this thickness it is thought that the strained overlayer relaxes by forming misfit dislocations (Heinrich *et al* 1986b).

Calculations for the bcc phase of nickel show that at the calculated equilibrium lattice spacing (2.773 Å) a non-magnetic state is favoured (Moruzzi 1986, Moruzzi *et al* 1986, Moruzzi and Marcus 1988). However, a magnetic phase transition is expected to occur for a 1.5% expansion. Hence, at the iron lattice 2.866 Å, bcc nickel should be ferromagnetic with a predicted moment of $0.5\mu_B$. In a PNR study of a Au/3ML bcc Ni/5ML bcc Fe/Ag(001) sandwich at 4 K, Bland *et al* (1991) reported a nickel magnetic moment of $0.55$–$0.80\mu_B$ and a moment of $2.2$–$2.4\mu_B$ for the Fe substrate. In the spin-polarized photoemission study (Brookes *et al* 1992), the authors measured the background spin polarization as a function of Ni thickness. With the assumption that this polarization $P$ scales with the magnetic moment $m$ such that

$$P = \frac{m}{n_d} \tag{20}$$

where $n_d$ represents the number of localized d electrons they concluded that the magnetic moment on the Ni sites was of the order of $0.4\mu_B$ in agreement with the calculations.

By varying the angle of incidence of the light, Brookes *et al* (1992) studied the light polarization dependence and related symmetry of the spin-polarized valence bands. Shown in figure 9, the spectra revealed the presence of minority spin peaks at 0.4 and 0.9 eV binding energy and majority spin peaks at 0.7 and 0.9 eV binding energy. As in the case of Fe, it was assumed that with an incident photon energy of 60 eV these peaks correspond to transitions around the $\Gamma$ point. Thus the peaks at 0.4 eV and 0.7 eV were identified as the exchange split $\Gamma_{12}$ pair and the peaks at 0.9 eV binding energy as the $\Gamma_{25}$ pair. In the latter case the exchange splitting was unresolvable.

The study also revealed the presence of a 6 eV satellite identical to that observed for fcc Ni. At a photon energy of 68 eV the satellite was found to resonate and show a spin polarization of $\sim 25\% \pm 9\%$, an observation that was a further indication of long-range ferromagnetic order existing in bcc nickel at room temperature.

The stable structure of bulk Co at room temperature is the hcp structure. However, the fcc phase, which in the bulk occurs at a temperature only above 750 K, may be stabilized through epitaxial growth on Cu(001) (Gonzalez *et al* 1981, Miranda *et al* 1983). LEED studies (Clarke *et al* 1987) indicate that a tetragonal distortion exists in very thin Co films.

A spin-polarized photoemission study of a 5 ML thick fcc Co film grown in this manner found that the electronic structure was already bulk-like (Schneider *et al* 1990). The experiment, using incident circularly polarized light, was carried out in a geometry that restricted the initial states to bands of $\Delta_5$ symmetry. In this way it was determined that the exchange splitting of the $\Delta_5$ bands, shown in figure 10, was $1.4 \pm 0.2$ eV, which is less than the 1.8 eV given by a non-relativistic band structure calculation. However, in a later paper the same authors (Schneider *et al* 1991b) reported that the experimental observations were in reasonable agreement with the results of a spin-polarized relativistic Korringa–Kohn–Rostoker (KKR) band structure calculation. We reproduce this comparison as an example of band mapping in figure 11. Without performing an explicit spin analysis but still using incident circularly polarized light, the same group was able to show experimentally that the spin–orbit interaction introduces an extra splitting $\Delta E_{so} \sim 0.1$ eV over that reflecting the

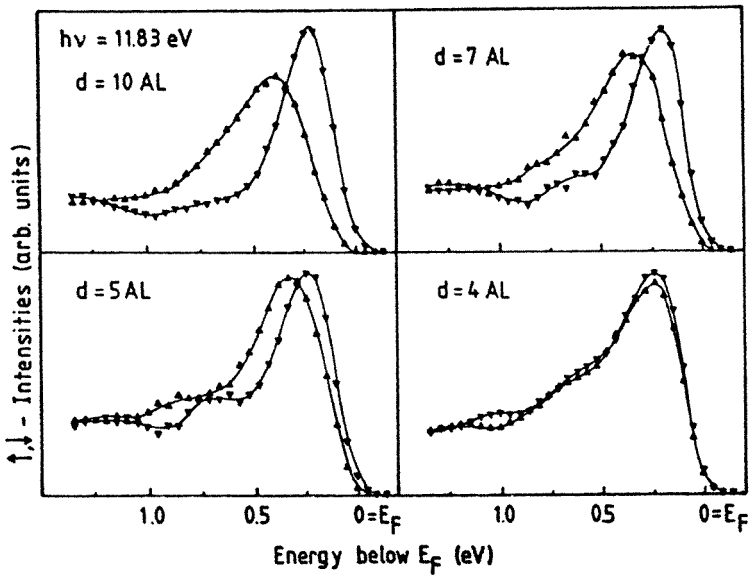


**Figure 12.** Spin-resolved spectra of epitaxial Ni(111)/W(110) layers with varying thickness recorded in normal emission with $h\nu = 11.85$ eV. For this photon energy the initial state corresponds to the point 2/3(Γ–L). Majority spin electrons are indicated by the upward pointing arrows and minority spin electrons are indicated by downward pointing triangles.

exchange interaction (Schneider *et al* 1991a).

The bcc phase of Co has been grown on (110) GaAs substrates. A spin-polarized photoemission study (Prinz *et al* 1985) using incident photons of 30 eV energy identified a much larger minority spin emission from bcc Co than from bcc Fe. In agreement with spin-polarized full-potential linearized augmented plane wave (FLAPW) band structure calculations (Jansen *et al* 1984), this observation was interpreted in terms of a rigid band shift between the two systems with the extra electron in Co going into the minority-spin d-band in the Γ-N region of the Brillouin zone. The magnetic moment of the Co films was measured to be $1.5\mu_B$ per atom.

It is clear from studies of thin films of Fe and Co that the experimentally measured exchange splitting in these materials appears to scale with the magnetic moment on the atom. Indeed, it has been suggested that for the 3d elements simply measuring the exchange splitting will provide a measure of the moment through the linear relationship that the exchange splitting is 1 eV/$\mu_B$ (Himpsel 1991). A similar idea has also been used in the interpretation of spin-flip transitions in electron energy loss studies (Walker *et al* 1992). That such an approximate relationship exists relates to the fact that if we polarize the valence bands in the ferromagnetic material the relative shift of the two spin components is given by (Ziman 1972)

$$E_\sigma = E_0 \pm U n_{\sigma'} \tag{21}$$

where $E_0$ is the binding energy in the unpolarized band, $U$ is the Coulomb or exchange potential and $n_{\sigma'}$ is the number of electrons of the opposite spin. From equation (21) we see that the splitting between the two spin components $\Delta$ is given by

$$\Delta = Um \tag{22}$$

where now we have introduced the magnetic moment $m = n_\sigma - n_{\sigma'}$.

The relationship expressed in equation (22) has been successfully used as a self-consistency condition in tight-binding calculations allowing a determination of the magnetic ground state in both ferromagnetic and antiferromagnetic systems (Heine *et al* 1981, Johnson *et al* 1993, Stoeffler and Gautier 1993, Weinert and Blugel 1994). $\Delta$ is taken as the on-site splitting between the two spin components in the d-block and $U$ is taken as the local spin density approximation (LSDA) Stoner parameter which is related to the susceptibility of the material $\chi$ through the relationship

$$\chi = \frac{\chi_0}{1 - \frac{1}{2}UN(E_F)}. \tag{23}$$

Here $N(E_F)$ represents the density of states at the Fermi level and $\chi_0$ is the Pauli susceptibility. The susceptibilities and related Stoner parameters have been calculated by Janak (1977). From that study we note that for Fe and Co, $U$ has the value 0.93 eV which results in an exchange splitting of approximately 1 eV/$\mu_B$. However, this only applies to elements near the centre of the 3d row. For the centre of the 4d row the typical value of $U$ falls to 0.6 eV and in the centre of the 5d row the value is approximately 0.3 eV. Any scaling rule will therefore change accordingly.

*4.1.3. Studies at elevated temperatures.* It is well known that the long-range magnetic order in a ferromagnet disappears as the temperature is raised above the Curie temperature $T_c$. This leads to an obvious question 'by what mechanism is the long-range order lost?' Do the local magnetic moments disappear or do these moments fluctuate randomly with increasing temperature? Spin-polarized photoemission is an ideal technique for the study of such phenomena. It is sensitive to the degree of short-range order because its characteristic measuring time ($10^{-14}$ s) is considerably less than the time scale of the local magnetic moment fluctuations ($10^{-13}$ s).

It is clear that the Stoner model, a mean-field approximation to the Hubbard model, provides a perfectly adequate description of ferromagnetism at lower temperatures. In the Stoner model the spin polarization scales linearly with the magnetization. It would, therefore, be anticipated that the exchange splitting and associated local moments would disappear as the temperature is raised. However, at higher temperatures this mean-field approach fails. In fact, attempts to model the Curie temperature using such a model have resulted in excessively high predictions (Gunnarsson 1976).

A number of experiments have suggested that a degree of short-range order may exist above $T_c$. These observations have led to the development of alternative models which include the local-band model (Korenman 1986) and the disordered local moment model (Durham *et al* 1984). In the former, above $T_c$, a degree of short-range spin order exists over a length scale of approximately 20 A, whereas in the latter model no short-range order exists. In the local-band model the exchange splitting observed at elevated temperatures will depend on the ratio of the localization of the states under investigation to the degree of short-range magnetic order. A measure of the degree of localization is given by the rate of dispersion of the relevant band. Thus spin-polarized cluster calculations of the temperature dependence define a parameter $B$ such that

$$B = \frac{v\hbar}{\Delta\Lambda} = \frac{1}{\Delta\Lambda}\frac{\delta E}{\delta k} \tag{24}$$

where $v$ is the group velocity of the electronic state under investigation, $\Delta$ is the exchange splitting and $\Lambda$ reflects the magnetic correlation length (Haines *et al* 1985b, 1986). States with a small value of $B$ will show a temperature-independent behaviour in their splitting,

whereas states with a large value of $B$ may be expected to show a temperature dependence. In the former case, however, there will still be a loss of spin polarization due to spin mixing.

Temperature-dependent experimental studies have been carried out on Fe, Ni, Co and Gd. The first spin-polarized photoemission study of the ferromagnetic to paramagnetic transition was made in a study of the Ni $S_4$ bands close to the $X_2$ point by Hopster *et al* (1983). The photoemission spectra recorded along the surface normal of Ni(110) show the exchange splitting disappearing as the temperature is increased through the range $0.55 \leqslant T/T_c \leqslant 0.94$. However, the interpretation of the spectra was complicated by the fact that the lineshapes were of the same order as the exchange splitting. In a subsequent analysis of the data, Haines *et al* (1986) concluded that the temperature dependence was consistent with short-range order with a correlation length parameter $\Lambda = 5.4$ Å.

A subsequent study of the Ni(111) surface (Kamper *et al* 1990) found a temperature-independent exchange splitting at the Brillouin zone points corresponding to $1/3d$ (Γ–L) and $1/2d$ (Γ–L). In the latter case the authors observed the appearance of extra intensities at the binding energies of the opposite spin direction. In contrast, in the same study a temperature-dependent splitting was observed at the point corresponding to $2/3d$ (Γ–L) as shown in figure 12. The authors felt unable, on the basis of these observations, to draw any conclusions between the different models. However, examination of the relevant band does in fact show that its rate of dispersion or group velocity does increase as one moves out beyond $1/2d$ (Γ–L). The observation of a temperature dependence farther out in the zone might therefore be taken as being consistent with the local-band model.

Interestingly, in an earlier study, the same group observed identical behaviour in Ni(111) thin films grown on a W(110) surface (Kamper *et al* 1989). However, rather than raising the temperature of the crystal as in the bulk study the authors recognized that the Curie temperature scales with the thickness of the film. Indeed, when a system approaches the two-dimensional limit from three dimensions the Curie temperature $T_c$ follows the power law

$$\frac{T_c^{\text{bulk}} - T_c(d)}{T_c^{\text{bulk}}} = C_0 d^{1/\nu}. \tag{25}$$

The critical exponent $\nu$ is generally found to be $\nu = 0.63$ for the Ising model and $\nu = 0.59$ for the Heisenberg model (Yeomans 1992).

A recent valence band study using a modification of the standard angle-resolving method, scanned angle photoemission, examined the three-dimensional Fermi surface below and above $T_c$. (Aebi *et al* 1996). Such a study allowed a direct comparison of different points in the Brillouin zone under the same conditions. The authors again found that different points in the Brillouin zone displayed different temperature-dependent behaviour and, in agreement with earlier studies, concluded that a Stoner model did not provide an adequate description of the high-temperature behaviour.

A study of the temperature dependence of the Ni(110) 6 eV satellite found that its spin polarization decreased with increasing temperature (Kakizaki *et al* 1994). As we have noted earlier, this satellite may be viewed as a local or site specific phenomenon. Thus the observation of a loss of spin polarization was interpreted as evidence for the presence of fluctuating magnetic moments in ferromagnetic Ni.

A number of studies of the temperature dependence of the exchange splitting in Fe have also been made. A study of the exchange splitting observed at Γ, the centre of the Brillouin zone found no change in the magnitude of the splitting on increasing the temperature from $0.3T_c$ to $0.85T_c$ (Kisker *et al* 1984). However, as shown in figure 13, the intensities of the different peaks in the spectra did show a variation with temperature. As in the case of Ni,

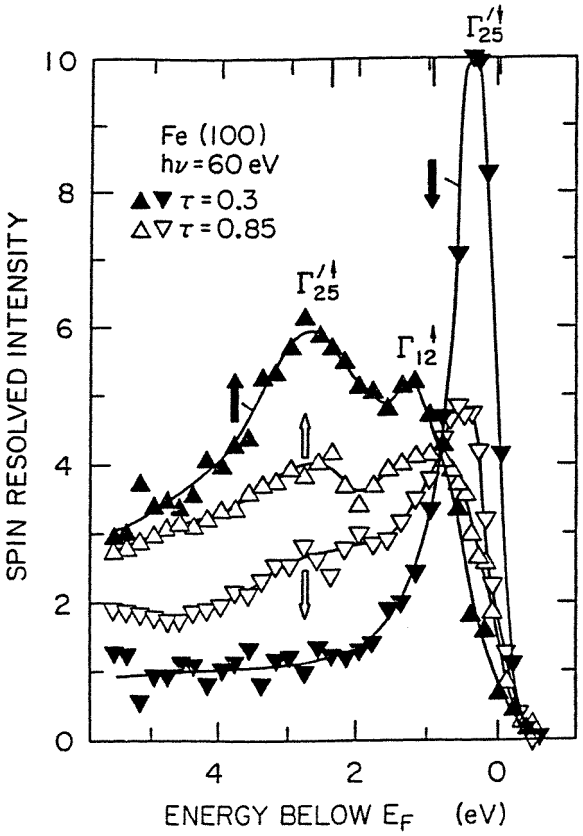


**Figure 13.** Spin-resolved photoemission spectra recorded along the surface normal of Fe (001) at two temperatures ($T = 0.3T_C$ and $T = 0.85T_C$). The incident photon energy is 60 eV and the angle of incidence corresponds to s-polarization. The two spin components are indicated.

modelling of this data lead to the conclusion that short-range order existed and that the spin correlation length $\Lambda$ must be larger than 4 Å (Haines *et al* 1985a). The calculations and comparison with experiment for $\Lambda = 5.4$ Å are reproduced in figure 14.

A similar type of behaviour has been observed in a temperature-dependent inverse photoemission study of the P point in the Fe Brillouin zone (Kirshner *et al* 1984). With increasing temperature, no change was observed in the exchange splitting. In contrast, however, in the same study, it was found that the exchange splitting of a pair of unoccupied states near the Γ–H line collapsed as the temperature was raised towards $T_c$. These observations are again consistent with our discussion of the local-band model. The Fe bulk bands at both the Γ and P points show little dispersion. However, the unoccupied bands in the Γ–H direction show considerably more dispersion reflecting the hybridization of the d-bands with the s–p bands.

A study of the temperature-dependent spin-polarized photoemission spectra recorded along the surface normal from Fe films grown on a W(001) substrate has been reported by Mulhollan *et al* (1991). Here the authors questioned whether or not the degree of short-range order found in bulk Fe above $T_c$ persists in the films or whether the hybridization with the substrate modifies it. The study was made on a 1.5 ML thick Fe film with a measured $T_c$ of $330 \pm 20$ K determined from surface magneto-optic Kerr-effect (SMOKE) studies. From

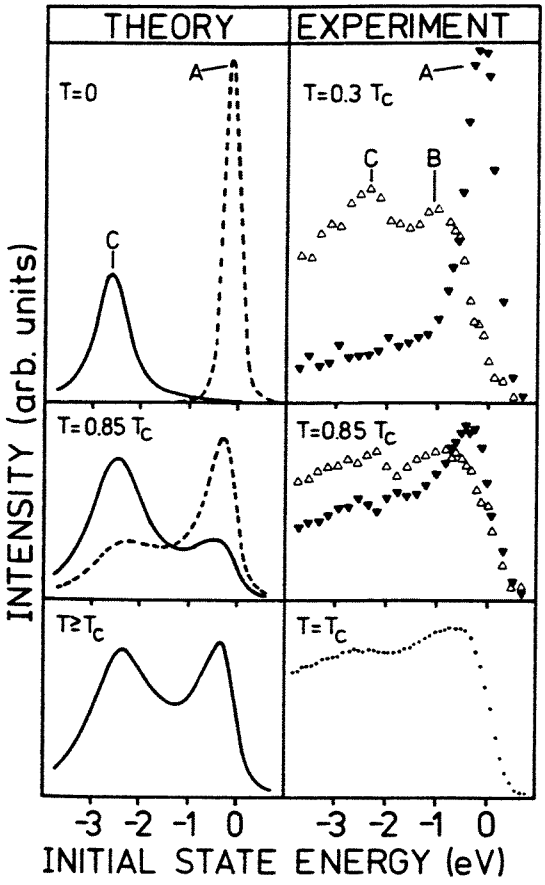


**Figure 14.** Theoretical spin-up (full curves) and spin-down (dashed curves) spectra for photoemission from the $\Gamma_{25}$ with $\Lambda = 5.4$ A at the temperatures indicated. An energy-dependent initial-state lifetime is convoluted with a Gaussian of 0.35 eV full width half maximum. For a more direct comparison the experimental spectra of figure 13 are reproduced in the right-hand panel.

the complete lack of any temperature dependence in the spectra, the authors concluded that a short-range order of ~4 Å did indeed persist above $T_c$ and consequently that the substrate hybridization had no effect.

There have been no studies to date of the temperature dependence of spin-polarized photoemission spectra recorded from bulk hcp Co. In part this lack of study reflects the high $T_c$ (1388 K) for this material and also the observation that a structural phase transition from hcp to fcc occurs at a temperature of 750 K. However, a study of the temperature-dependent photoemission from a thin fcc Co film deposited on a Cu(001) substrate has been reported (Schneider *et al* 1991c). Using incident circularly polarized light and vectorial spin analysis the authors examined the spin polarization of the photoemission spectra obtained from a 1.8 ML Co film at a temperature of 350 K corresponding to $1.1T_c$. They made the observation that whilst the spin polarization, indicative of long-range order, disappeared above $T_c$ the spin-integrated spectra remained the same. They concluded that the Stoner model failed to explain their observations and that some degree of short-range ferromagnetic order existed above the Curie temperature.

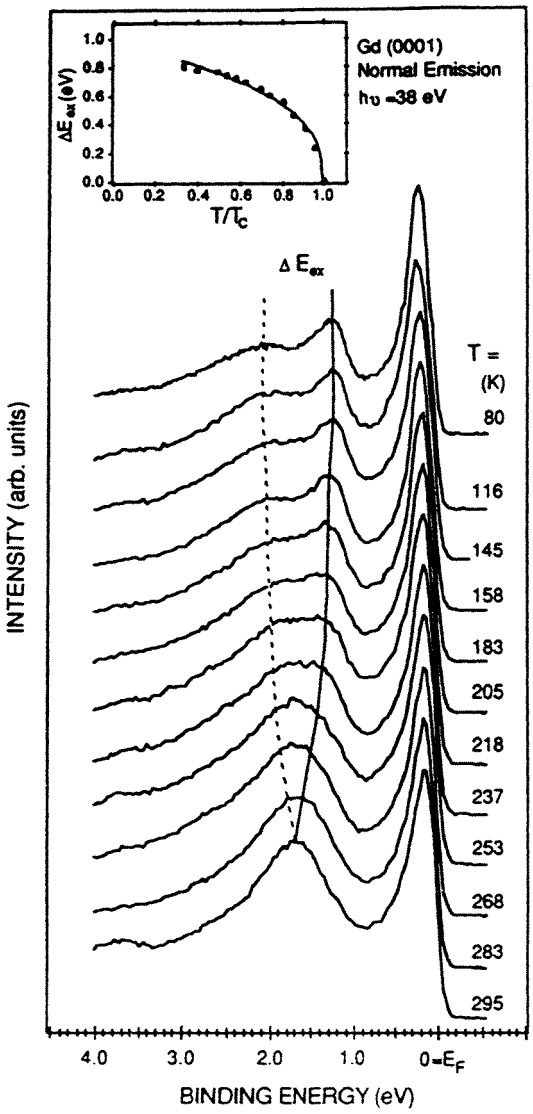


**Figure 15.** Temperature dependence of the exchange splitting for the $\Delta_2^{\uparrow}$ and $\Delta_2^{\downarrow}$ energy bands between $T = 0.27T_c$ and $T = T_c$ and fixed $k_\perp$ for the photon energy $h\nu = 38$ eV. The inset shows a plot of peak positions against reduced temperature, and a curve fitted using a power law of the form $E_{ex} = (1 - T/T_c)^{\beta}$. The value obtained for the critical exponent $\beta$ is 0.378, a value close to the exponent predicted by the Heisenberg model ($\beta \sim 0.35$) and also close to the experimental result ($\beta \sim 0.40$) for Gd obtained from magnetization measurements.

Several temperature-dependent studies have been carried out on the rare-earth Gd where the half-filling of the 4f bands results in a large local magnetic moment of $7\mu_B$. These local moments are coupled via an Ruderman–Kittel–Kasuya–Yosida (RKKY)-type interaction through polarization of the more itinerant 5d, 6s conduction bands. As shown in figure 15, a spin-intgerated study of the temperature-dependent exchange-splitting of these conduction bands near the $\Gamma$ point found a 'Stoner-like' behaviour with the exchange splitting disappearing at $T_c$ (Kim *et al* 1992). Fitting the measured exchange splitting to a

conventional power law $\Delta E_{ex} = (1 - T/t_c)^{\beta}$, the authors obtained a value of $\beta = 0.378$ for the critical exponent, close to the value of 0.35 predicted by the Heisenberg model. Similar 'Stoner-like' behaviour was also reported in an inverse photoemission study of the unoccupied bulk bands (Federov *et al* 1994). An important consideration in all of these studies and one not really fully explored in Gd is that, as we have seen for both Fe and Ni, different parts of the Brillouin zone can show very different behaviour. Indeed, the reduction in the exchange splitting observed for the Gd conduction bands was reproduced in a theoretical calculation by Nolting *et al* (1994), who found a 'Stoner-like' temperature dependence for the weakly correlated 's-like' dispersions, but a different behaviour for the more strongly correlated 'd-like' dispersions.

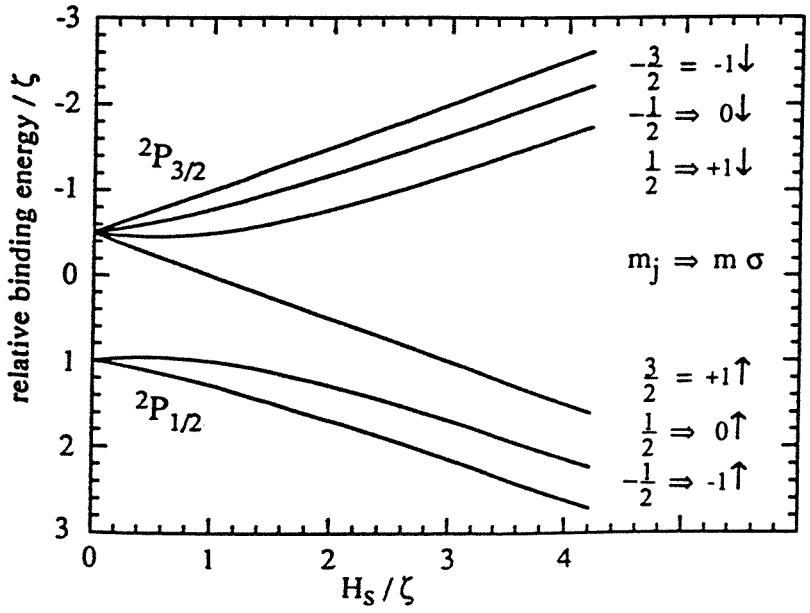


**Figure 16.** Energy levels of the core p sublevels as a function of the spin field $H_S$ in units of the spin–orbit parameter $\zeta$.

An alternative picture emerged in a theoretical study by Sandratskii and Kubler (1993). These authors argued that the local magnetic moment of the 5d electrons would always exist due to the strong polarization from the local 4f moment. They further suggested that the spin polarization and magnetization of the conduction bands would be lost at finite temperature due to global spin-hybridization effects.

A number of experimental studies have shown that the $T_c$ for the surface layer of Gd is enhanced by up to 60° over the 293 K characteristic of bulk Gd (Weller *et al* 1985, Rau and Robert, 1987, Tang *et al* 1993). Discussed further in the next section, the surface electronic structure is characterized by a well defined surface state immediately below the Fermi level (Li D *et al* 1991). Spin-polarized photoemission studies of this state have shown it to have majority spin character (Mulhollan *et al* 1992b). A spin-polarized photoemission study of the temperature dependence of this state (Li *et al* 1995a) reported evidence of a temperature-independent exchange splitting suggesting a spin-mixing behaviour characteristic of fluctuating local moments. In contrast, a spin-integrated inverse photoemission study of the same surface (Federov *et al* 1994) produced spectra that appeared

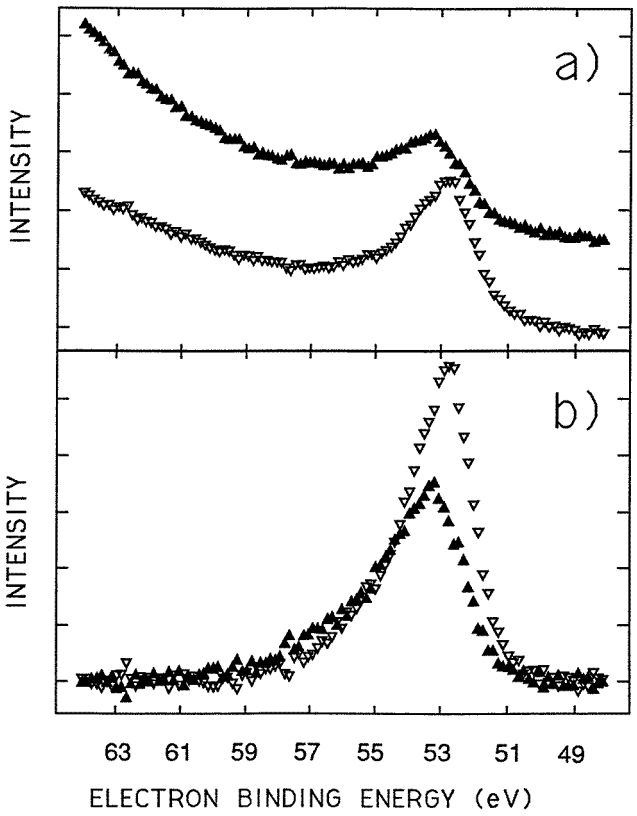


**Figure 17.** (a) Spin-resolved Fe 3p photoemission spectra recorded from clean Fe(001) with 90 eV photons. Upward triangles indicate majority spin, downward triangles indicate minority spin. (b) The same as in (a) but with the background subtracted.

to indicate that the unoccupied component of the surface state shifts towards the Fermi level with increasing temperature which would again be suggestive of 'Stoner-like' behaviour even for the surface layer. Thus at the present time it would appear that the exact mechanism leading to the loss of long-range order in the surface region remains an open question. Interestingly, in a related temperature-dependent photoemission and inverse photoemission study of the partially filled surface state on Tb(0001), the authors found no evidence of Stoner-like behaviour (Hubinger *et al* 1995).

### *4.2. Core level studies*

Magnetic core level spectroscopies offer the possibility of deriving site-specific or local magnetic information. Indeed it has already been demonstrated that information on both the spin and the orbital moments can be obtained from magnetic circular dichroism (MCD) studies (Chen *et al* 1995). Spin-polarized core level photoemission is a technique that also has the potential for providing such information. To this end there have been an increasing number of studies aimed at elucidating the factors which determine the spin polarization in the photoelectrons excited from the initially closed-shell core levels. The picture, however, is unclear and the question remains as to whether, for the 3d ferromagnets, the excitation

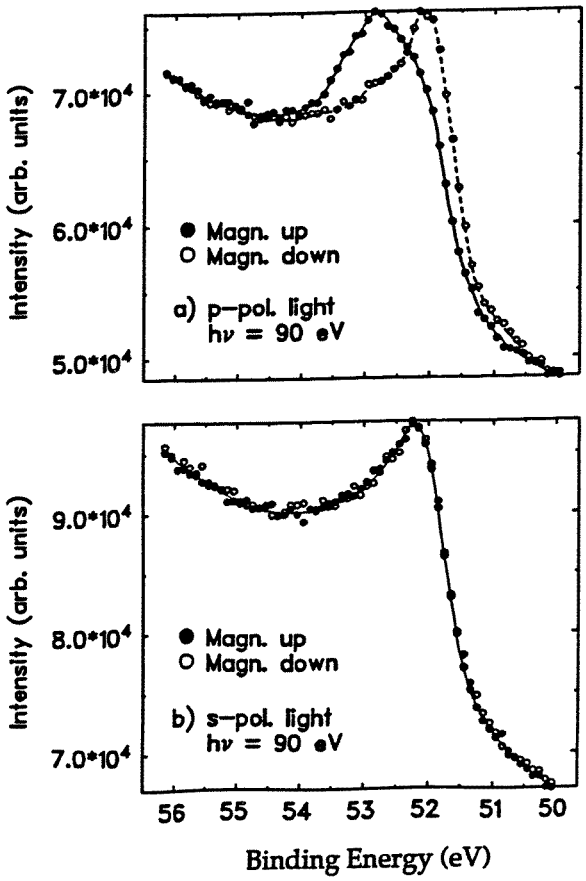


**Figure 18.** Spin-intgerated Fe 3p photoemission spectra recorded at 90 eV photon energy. In (a) the spectra are excited with p-polarized light with the magnetization $M$ up and $M$ down. In (b) the spectra are excited with s-polarized light under the same geometry as in (a) and for the same magnetization directions.

process can be treated as a localized atomic phenomena or does the itinerant nature of the valence electrons have to be recognized.

Early non-spin-resolved studies of the 3s photoemission from ferromagnetic systems identified a satellite that was not present in studies of non-magnetic systems (Shirley 1978). The satellite was interpreted as evidence of a final-state interaction between the spin of the final-state core hole and the net spin of the valence bands. In a simple model due to Van Vleck (1934), the splitting, $\Delta E$, between the satellite and main peak will reflect the net spin in the valence bands, $S$, such that

$$\Delta E = \frac{2S+1}{2l+1} G^l(3s, 3d). \tag{26}$$

Here $G^l(3s, 3d)$ represents the appropriate exchange integral between the 3s and 3d level. However, the early spin-integrated studies found that the experimentally determined splitting was smaller than that predicted by equation (26), and this led to the suggestion that configuration interactions between different multiplets in the final state play an important role (Fadley *et al* 1969).

Whilst these effects were first discussed in connection with emission from the 3s level, the first spin-polarized studies were carried out on the 3p levels which have a higher photoionization cross section. In the following we will, therefore, first discuss the different studies of the 3p and 2p core levels of the elemental materials, Fe Co and Ni, and then return to a discussion of studies of the 3s and 2s levels. We will defer until later a discussion of the results of several studies where core level spectroscopies have been used to examine specific problems in thin-film magnetism.

*4.2.1. The 3p and 2p core levels.* Emission from core levels with $l > 0$ is complicated by the fact that both spin–orbit and exchange effects may play a role in determining the measured spin polarization. Figure 16 shows the relative binding energies of the different sublevels of p-type core level as a function of the spin field or exchange interaction $H_S$ in units of the spin–orbit parameters $\zeta$. To the left of the figure the splitting is dominated by the spin–orbit interaction, to the right, the exchange interaction. In that the spin–orbit interaction becomes more dominant as the binding energy of the core level increases, moving from right to left of the figure is equivalent to moving to deeper binding energy. As a specific example, for Fe, emission from the 2p level would correspond to a ratio $H_S/\zeta = 0.1$, whereas emission from the 3p level is represented by a ratio $H_S/\zeta = 1.37$ (Van der Laan 1995). The former is close to the limit of $jj$ coupling, the latter falls within the regime of intermediate coupling.

The first experimental studies of the Fe 3p core level found a strong spin polarization, typically $-30\%$, even though the 3p level was completely filled in the initial state (Carbone and Kisker 1988, Sinkovic *et al* 1990). The spin-resolved spectra were characterized by a minority spin component at low binding energy and a less intense majority spin peak at higher binding energy. Example spectra from a study by Sinkovic *et al* (1990) are shown in figure 17. The 'exchange splitting' between the two spin components in the figure is 0.5 eV. The splittings observed in other studies have ranged from 0.26 eV (Van Campen *et al* 1993) through less than 0.5 eV (Carbone and Kisker 1988), 0.5 eV (Mulhollan *et al* 1992a) to 0.7 eV (Jungblut *et al* 1992).

The dominance of the minority spin emission is clearly evident in figure 17 where the spectra are shown with an appropriate background subtracted. The intensity loss in the majority spin channel has been attributed to spin-dependent filtering effects in the transmission of the photoelectrons to the surface (Van der Laan 1995), to multiple-scattering data events in the final state (Tamura *et al* 1994) and to configuration interactions involving other configurations at higher binding energies (Bagus and Mallow 1994). In the latter mechanism it would be expected that intensity will be redistributed from the higher binding energy components to more tightly bound configurations. As we have already noted and will be discussed in more detail later, such configuration interactions had previously been invoked to explain the small exchange splitting observed in emission from the 3s core levels (Fadley *et al* 1969).

The presence of the spin–orbit interaction in the Fe 3p level leads to strong dichroic effects. Thus both magnetic linear dichroism (MLD) in angle-integrated photoemission (Roth *et al* 1993b) and magnetic linear dichroism in angle-resolved photoemission (MLDAD) (Roth *et al* 1993a, Sirotti and Rossi 1994, Rossi *et al* 1994) have been demonstrated. In the studies of MLDAD, it has been shown that the photoemission spectrum recorded with linearly polarized light changes upon reversal of the magnetization direction. Shown in figure 18 this observation requires the plane containing the incident light polarization and the electron emission direction to be perpendicular to the magnetization

direction. The same effect is not observed with s-polarized light. Magnetic linear dichroism on the other hand may be observed with s-polarized light in angle-integrated photoemission. Here a strong change is observed in the angle-integrated spectrum depending on whether the magnetization of the sample is parallel to the light polarization vector or perpendicular to it. A number of theoretical treatments have subsequently shown that MLDAD is in fact equivalent to magnetic circular dichroism in angular distributions (MCDAD) whereby the photoelectrons are initially excited by circularly polarized light (Cherepkov 1994, Venus 1993, 1994, Van der Laan and Thole 1994, Thole and van der Laan 1994a). The experimental demonstration of this equivalence has recently been presented by Hillebrecht *et al* (1995).

Several attempts have been made to unravel the relative spin–orbit and exchange contributions to the Fe 3p spectra. Tamura *et al* (1994) have analysed the MLD and photoemission spectra with full multiple scattering using a layer KKR Green function method. In their approach an exchange interaction couples the core hole spin to the average magnetization of the valence band. They conclude that a spin–orbit splitting of $1.1 \pm 0.1$ eV and an exchange splitting of $0.95 \pm 0.05$ eV provides the best description of the experimental spectra. In a different study, Van der Laan (1995), using an Anderson impurity approach, has analysed the same spectra and concluded that reasonable agreement is obtained with the spin–orbit parameter $\zeta = 0.95$ eV and the exchange field $H_S = 1.3$ eV. The latter parameter was taken directly from the results of a study based on the spin-polarized Dirac equation (Ebert 1989).

Huang *et al* (1995) have analysed the 3p core level spectra obtained in a spin-resolved photoemission study of a series of Fe films grown on a W(110) substrate. They use a simple photoemission model that simultaneously includes core-valence exchange and core-hole spin–orbit interactions. As in the earlier study of Tamura *et al* (1994) the exchange interaction reflected the mean magnetization in the valence bands. The authors calculated the relative intensities of the different components within the dipole approximation for the matrix elements. They found that the spin–orbit splitting, which is of the order of $0.67 \pm 0.02$ eV, is constant for all film thicknesses as would be expected for an on-site atomic property. They found that the exchange splitting increases with film thickness to a value of 0.42 eV in films thicker that 3 ML. A value of 0.42 eV is smaller than the separation observed between the two main components in the experimental spectra. However, the authors note that this is a reflection of the relative intensities in the different sublevels. In fact the exchange splitting represents the difference in binding energy between two opposite pure spin states.

Whilst their model appeared to provide a reasonable description of the different interactions, Huang *et al* noted that it failed to account for the relative intensity of the majority and minority spin components. Indeed their model found a relative ratio between the two spin components of 1.0, whereas in the thicker films they experimentally found a ratio of 1.5. Other experimental studies have found values for this ratio of 1.0 (Carbone and Kisker 1988) 1.25 (Van Campen *et al* 1993), 1.3–1.4 (Sinkovic *et al* 1990) and 2.6 (Jungblut *et al* 1992). If all of the emission is detected the experimental ratio should be 1.0, reflecting the fact that the initial excitation is from a closed shell. This amounts to the zeroth moment sum rule as discussed by Thole and van der Laan (1994b). Huang *et al* obtain a ratio of 1.0 in their model because they use a single configuration. It remains a problem as to whether the 'missing' information in the experiment reflects interactions with other configurations or losses due to other effects as discussed earlier.

There have been three spin-resolved studies of the Co 3p emission. In a study of fcc Co grown on a Cu(001) substrate, Clemens *et al* (1992a) reported an exchange splitting of $0.3 \pm 0.15$ eV. In a study of thick Co films deposited on an Fe single crystal Kachel *et al*

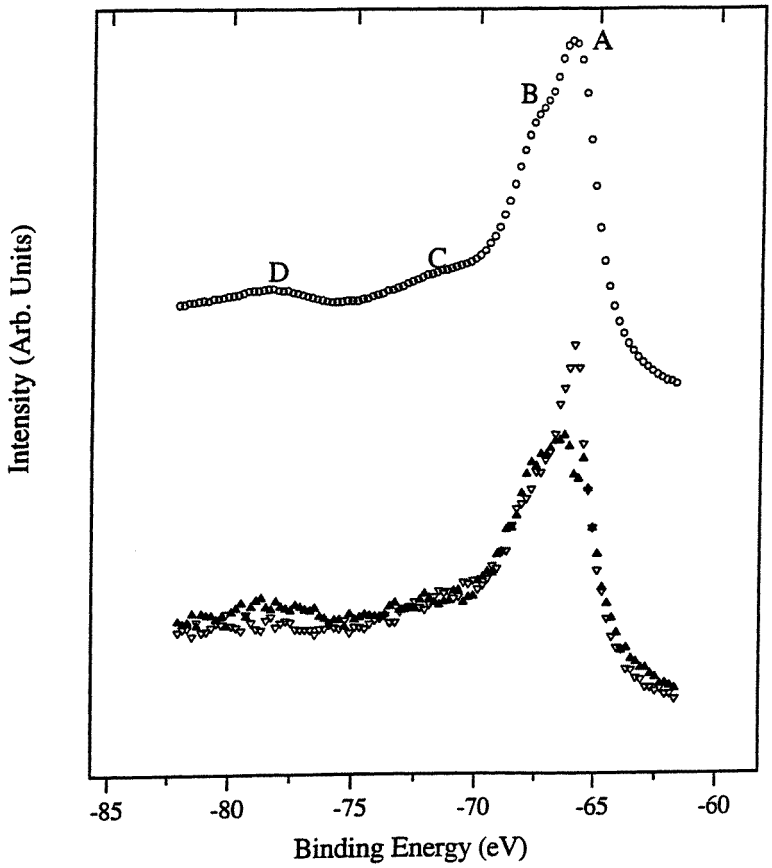


**Figure 19.** Spin-intgerated (upper spectrum) and spin-resolved (lower spectrum) photoemission spectra of the Ni 3p core level. A and B indicate 'spin–orbit'-derived features in the main line and C and D indicate satellite features. In the lower panel the minority spin electrons are indicated by the open triangles and the majority spin electrons are indicated by the full triangles. The incident photon energy is 248 eV.

(1993) reported a splitting for the Co 3p level of 0.15 eV. The latter authors interpreted both the majority and minority spin peaks observed in the spectra as representing emission from the high spin state alone. In a later study of metallic Co deposited on glass, Klebanoff *et al* (1994) reported a splitting between the two spin components of only $0.1 \pm 0.05$ eV.

As we have already noted, early spin-integrated studies of the Ni 3p core level identified a satellite at 6 eV binding energy with respect to the main 3p line (Hufner and Wertheim 1975). A second satellite was observed at a relative binding energy of 14.0 eV with respect to the main line. Hufner and Wertheim assign these satellites to the $3p^5 3d^9$ configuration and the main line to emission from the $3p^5 3d^{10}$ configuration.

The first spin-polarized photoemission study of this system reported the observation of a spin polarization in the main 3p emission (Kachel *et al* 1993). The authors attributed the main peak to the $3p^5 3d^{10}$ configuration and proposed a model whereby the spin polarization reflected the presence of spin-polarized multiplets. In a second spin-resolved study by See and Klebanoff (1995a), spin polarization was again observed in the main Ni 3p level. These authors noted that such an observation points to the presence of some mixture of the $3p^5 3d^9$

and $3p^5 3d^{10}$ configurations in the main line because the $3d^{10}$ configuration with a filled d-band will not, by itself, lead to any spin polarization. See and Klebanoff further proposed that extra-atomic screening involving hybridized 3d–4sp states would lead to a final-state 3d valence configuration of ∼50% $3d^9$ and ∼50% $3d^{10}$. In a separate study (See and Klebanoff 1995c) the same authors sought to explain the spin polarization observed in the satellites within the same model. They concluded that both satellites represented emission from the $d^8$ configuration.

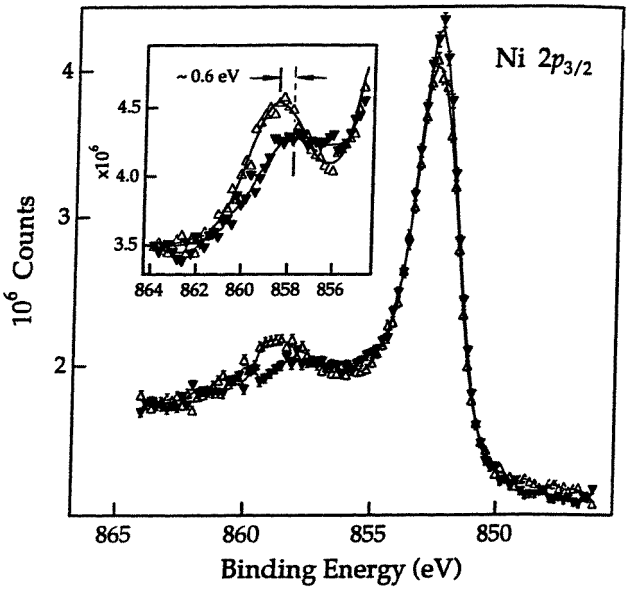


**Figure 20.** Majority and minority spin spectra showing excitation of the Ni $2p_{3/2}$ level with incident unmonochromatized Mg K$\alpha$ radiation ($h\nu = 1253.6$ eV). The full curves through the data reflect the application of a five-point smoothing routine. The inset displays a separate spectrum of the $2p_{3/2}$ satellite. In the latter case the full curves reflect the application of a 13-point smoothing routine.

Two further studies have also observed the presence of spin polarization in the main line and the more deeply bound satellites (Liu *et al* 1995, Saitoh *et al* 1995). The spin-integrated and spin-resolved spectra obtained by Liu *et al* are shown in figure 19. The spin-intgerated spectra are identical to those obtained in the earlier studies by Hufner and Wertheim (1975). The main peak shows the characteristic 'spin–orbit splitting', A and B, and the satellites, represented by C and D, lie at higher binding energies. The spin-resolved spectra now show that the minority spin polarization in the main peak is strongly concentrated in the leading edge. Satellite C shows a mixed polarization and satellite D shows majority spin polarization. These observations have been made in all studies; the interpretations, however, differ.

Liu *et al* (1995) interpret their spectra in terms of an Anderson impurity model which predicts a ground state for Ni of 14% $d^8$, 48% $d^9$ and 38% $d^{10}$. Differing from the $d^8$ assignment of See and Klebanoff (1995c), Liu *et al* associate the 14 eV satellite with $^1$F and $^1$P states of the $d^9$ configuration and the 6 eV satellite with $^3$D and $^3$P states from the $d^9$ configuration. In the spin–orbit split main peak they show that the lower binding energy peak represents the $^1$D and $^3$F states of the $d^9$ configuration while the higher binding energy partner represents the $d^{10}$ configuration. This assignment explains the high spin polarization

observed in the leading edge as a reflection of the strong mixing between the $d^9$ and $d^{10}$ configurations. Saitoh *et al* (1995) have identical assignments for the two satellites but, following an earlier calculation (Thole and van der Laan 1991a), reverse the assignment in the main peak. Thus, they identify the leading edge with the $d^{10}$ configuration and the shoulder with the $d^9$ configuration.

It is clear from these Ni studies that it is important to take account of term splitting hybridization, exchange interaction and spin–orbit coupling when interpreting the 3p core level spectra from 3d transition metals. Indeed the observed spectra may reflect an interplay of all of these different effects.

Turning to the more deeply bound core levels, there have recently been several studies of the 2p levels. For these core levels the spin–orbit interaction is an order of magnitude larger than the exchange interaction. Baumgarten *et al* (1990) reported a study of the spin polarization observed in the Fe 2p level as a result of excitation by incident circularly polarized light. They found that the $2p^{3/2}$ level showed an 'exchange splitting' between minority and majority spin components of $0.5 \pm 0.2$ eV. The $2p^{1/2}$ level on the other hand was split by $0.3 \pm 0.2$ eV. This data has been analysed by both Thole and van der Laan (1994b) and by Huang *et al* (1995). In the former case the exchange parameter was set at 0.4 eV and the spin–orbit parameter at 8.0 eV. In the latter case the exchange parameter was found by fitting to be $0.9 \pm 0.05$ eV and the spin–orbit parameter was set at 13.4 eV, the experimentally observed splitting between the two spin–orbit components. Surprisingly the latter exchange parameter of 0.9 eV obtained by Huang *et al* for the splitting in the 2p core level is larger than the exchange parameter that the same authors obtained in fitting the 3p level even though the 2p3d exchange integral is smaller than the 3p3d exchange integral.

In a subsequent spin-polarized photoemission study, Van Campen *et al* (1993) report an 'exchange splitting' of $0.48 \pm 0.05$ eV for the $2p^{3/2}$ level. They show the minority spin component in this level to be the more intense with a ratio between the two components, majority to minority, of 0.81. For the $2p^{1/2}$ level the majority spin component at higher binding energy is the more intense although they were unable to report an exchange splitting. In a separate spin-polarized photoemission study of the same levels, Sinkovic and Sheckel (1994) report an exchange splitting in the $2p^{3/2}$ level of $0.42 \pm 0.05$ eV and a similar magnitude in the $2p^{1/2}$ level. They also reported the reversal of intensities with the minority peak the more dominant in the $2p^{3/2}$ level and the majority spin peak the more dominant in the $2p^{1/2}$ level. This reversal of intensities or polarization reflects the different spin polarization in the $3/2$ and $1/2$ levels.

See and Klebanoff (1995a, c) have also studied the emission from the Ni $2p^{3/2}$ and $2p^{1/2}$ core levels. They observe a reasonable spin polarization in the main $2p^{3/2}$ component consistent with the presence of a $d^9$ contribution to the final state as discussed earlier in connection with the Ni 3p emission. The spin polarization observed in the main $2p^{1/2}$ emission is considerably smaller.

For both the $2p^{3/2}$ and $2p^{1/2}$ core lines, a satellite dominated by majority spin emission is observed at 6 eV higher binding energy. In the case of the $2p^{3/2}$ satellite, the authors report an 'exchange splitting' of 0.6 eV as shown in figure 20. They assign the satellites to emission from the $(2p^{3/2})^3 3d^8$ configuration and suggest that their experimental results are in contrast to the findings in a calculation of Thole and van der Laan (1991a) who assign the satellites to the $(2p)^5 3d^9$ configuration. However, it is interesting to note that the latter study produces many features in common with the experiment. These include a minority spin polarization in the main $2p^{3/2}$ line, little or no polarization in the main $2p^{1/2}$ line and an exchange splitting in the $2p^{3/2}$ satellite which is absent in the $2p^{1/2}$ satellite. The latter observation reflects the fact that the exchange interaction of the $p^{1/2}$ level with

the valence electrons is weak. The spin polarization of the Ni 2p level has also been studied theoretically by Menchero (1996) who concluded that hybridization resulted in the satellites having approximately 65% $3d^9$ and 35% $3d^{10}$ character.

The Co 2p emission has been studied in both metallic Co and Co glass (Klebanoff *et al* 1994). Here we will restrict our discussion to the results observed for the former. The authors report an 'exchange splitting' of $0.18\pm0.05$ eV in the $2p^{3/2}$ level and $0.07\pm0.05$ eV in the $2p^{1/2}$ level. As in the case of Fe (Van Campen *et al* 1993), the minority spin component is the more dominant in the $2p^{3/2}$ level and the majority spin more dominant in the $2p^{1/2}$ level. Interestingly, these results are again consistent with CI calculations (Thole and Van der Laan 1991b) where it was shown that the $p^{3/2}$ peak has both a high and low spin component but the $p^{1/2}$ peak has only the low spin component.

*4.2.2. The 3s and 2s core levels.* With the increased intensity now available from photon sources in the soft x-ray range, there have recently been a number of spin-polarized photoemission studies of the 3s core levels. Hillebrecht *et al* (1990) were the first to show that the Fe 3s spin-polarized spectra were, as in the case of the 3p emission, characterized by a strong minority spin feature at low binding energy and a majority spin feature at higher binding energy. These two peaks were interpreted as the exchange-split singlet and triplet states with the high spin triplet state at lower binding energy.

A simple analysis via the use of Clebsch–Gordon (CG) coefficients provides some measure of the relative intensities to be expected in the different components (Alvarado and Bagus 1978, Rothberg 1980, Sinkovic *et al* 1991). The photoelectron carries away spin 1/2 so that if $S$ represents the net spin of the atom in the initial state, the ion in the final state will be left in either a high spin state with total spin $S+1/2$ or in a low spin state with total spin $S-1/2$. The high spin final state may have $z$-components $S_z$ equal to $S+1/2$ or $S-1/2$. The wavefunction for this state $\Psi_{\mathrm{HS}}$ is then

$$\Psi_{\mathrm{HS}} = A|S+1/2, 1/2|S+1/2, -1/2\rangle + B|S+1/2, 1/2|S-1/2, 1/2\rangle \tag{27}$$

where we recognize that to conserve the spin $S$ the photoelectron carries spin $-1/2$ if the ion final state corresponds to $S+1/2$ and *vice versa*. In such a model we are neglecting any orbital angular momentum of the valence electrons. Analysis of the CG coefficients yields

$$A = \sqrt{\frac{2S+1}{2S+2}} \qquad \text{and} \qquad B = \sqrt{\frac{1}{2S+2}} \tag{28}$$

resulting in a spin polarization $P$ for the high spin state given by

$$P = \frac{B^2 - A^2}{B^2 + A^2} = -\frac{S}{S+1}. \tag{29}$$

The low spin state has only one $z$-component $S = S-1/2$ with wavefunction $\Psi_{\mathrm{LS}}$ given by

$$\Psi_{\mathrm{LS}} = C|S-1/2, 1/2|S-1/2, 1/2\rangle. \tag{30}$$

Here the photoelectron carries spin $+1/2$ resulting in 100% spin polarization for the low spin state at higher binding energy.

The model described above predicts that the majority spin channel should have two separate peaks reflecting the presence of the high and low spin states. In a second spin-polarized photoemission study of the Fe 3s level Carbone *et al* (1991) interpreted their spectra as providing evidence for these two components. More recent studies with improved signal to noise have clearly resolved the different components (See and Klebanoff 1995b,

Xu *et al* 1995b). While the spectra in these latter experiments are nearly identical, the interpretations differ. Xu *et al* (1995b) assume that all of the peaks observed in their spectra, which are reproduced in figure 21, are derived from either the low spin or high spin final states. They interpret the majority spin peak at lower binding energy as the majority spin component of the high spin final state and analyse their data accordingly. The relative intensities of the two spin components in the high spin state are then in approximate accord with the model presented above. However, these latter two components are separated in energy. The question therefore arises as to the origin of this splitting. Does it reflect a splitting in the initial state or is there some additional splitting in the final state?

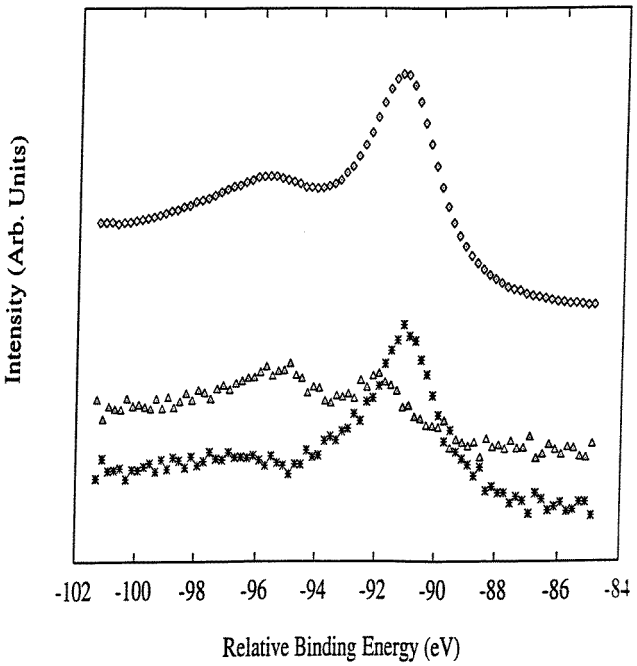


**Figure 21.** Spin-resolved photoemission spectra from the Fe 3s level recorded at a photon energy of 250 eV. The upper spectrum represents the spin-intgerated spectrum, the lower spectra represent the majority (open triangles) and minority (asterisks) spin-resolved spectra.

See and Klebanoff (1995b) take a different approach. They interpret the lower binding energy majority spin peak as reflecting the coupling of the final-state electron to the excited $^1$G state of the valence configuration to give a $^2$G state. They suggest through comparison with the earlier data of Hillebrecht *et al* (1990) that this state shows a strong photon energy dependence. However, the study by Xu *et al* (1995b) was carried out at the same photon energy as that of Hillebrecht *et al*, clearly showing that the proposed photon energy dependence is less marked than See and Klebanoff suggest.

In a series of papers, Thole and Van der Laan (1991a, 1991b, 1994b) have analysed in detail the spin-polarization effects that would be expected in photoemission studies of different core levels. They analyse the different excitation spectra in terms of the fundamental spectra which represent linear combinations of polarized spectra directly connected to physical properties. In particular, they show that in order to obtain information on the spin-polarization characteristics of the valence band it is necessary to complete an analysis of the first and higher moments of the intensity in the spin spectra.

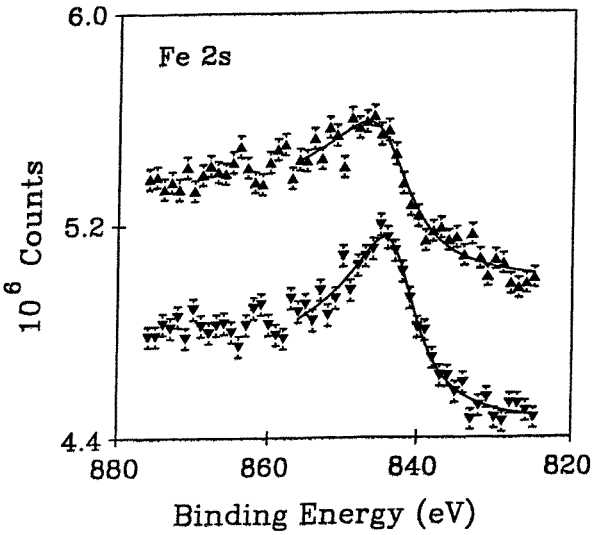


**Figure 22.** Majority and minority spin spectra showing excitation of the Fe 2s level with incident unmonochromatized Mg K$\alpha$ radiation ($h\nu = 1253.6$ eV). The full curves through the data represent a lineshape fitting using a single Doniach–Sunjic lineshape convoluted with a Gaussian.

In the case of 3s emission, the first moment of the spin spectrum normalized to the isotropic intensity $\int E \cdot I(E)\,\mathrm{d}E$ will be given by

$$\int E \cdot I(E)\,\mathrm{d}E = \frac{-SG^l(3s, 3d)}{(2l+1)} \tag{31}$$

where as before $G^l(3s, 3d)$ represents the exchange integral between the 3s core electron and the valence 3d electron, $I(E)$ represents the intensity in the spin spectrum and $S$ represents the net spin in the valence band. An identical expression has also been derived by Kakehashi (1985). Johnson *et al* (1995) have applied such a first moment analysis to a simple model represented by two states, low and high spin, of equal and opposite magnitude, separated in energy according to equation (26). Removing intensity from the low spin state at higher binding energy, the conservation as defined by equation (31) results in a reduction of the separation between the two components as observed experimentally and the emergence of a new satellite at much higher energy.

The satellite, which represents emission from the $3s^2 3p^4 3d^{n+1}$ configuration as opposed to the main peak $3s^1 3p^6 3d^n$ configuration (Bagus and Mallow 1994), has been observed in a number of studies of ionic compounds and the gas phase of these elemental materials. Johnson *et al* (1995) claim the first observation of the satellites in metallic chromium through nickel. Their results show that as one progresses from left to right across the periodic table the separation of the satellite from the main peak becomes increasingly larger. This observation reflects the relative shift in binding energies of the 3s and 3p levels with the 3p level becoming more tightly bound at a faster rate than the 3s levels as the row is crossed. The intensity of the satellite proved too weak to allow spin-polarized studies. However, from the first moment analysis described above and a theoretical analysis of the configuration interactions it is clear that the satellite should have majority spin. Johnson and co-workers concluded that in the event that the intensity and binding energies of the satellites are measured and further that a spin analysis is made of the high and low spin

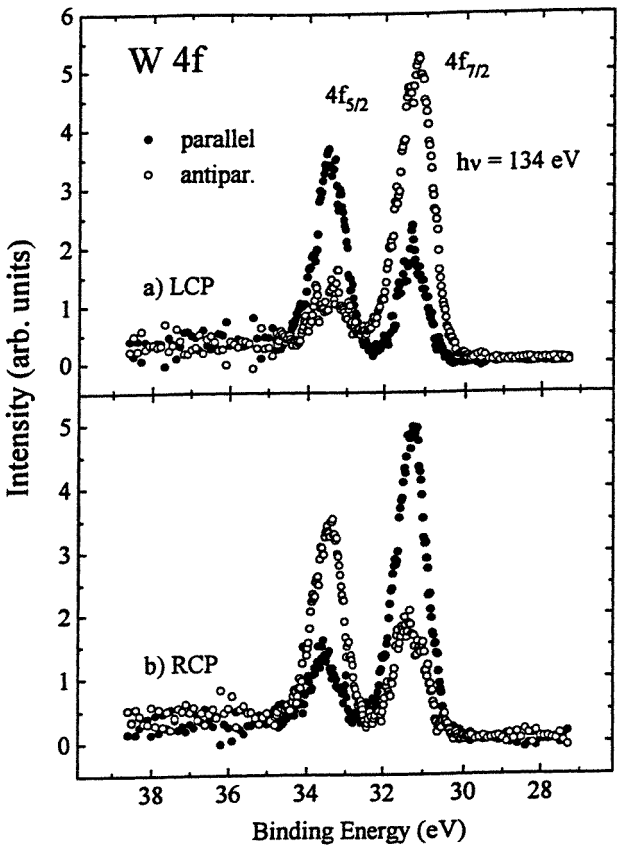


**Figure 23.** Spin-resolved photoemission spectra of the W 4f spin–orbit doublet excited at $h\nu = 134$ eV with (a) left circularly polarized light and (b) right circularly polarized light. Full and open symbols give the intensities for electrons with spin parallel and antiparallel to the light propagation direction.

states in the main peak, it should be possible to obtain a reasonable estimate of the local magnetic moment from studies of the 3s level.

One potential complication in such studies is that a plasmon loss occurs in the same energy range, particularly for Fe. However, rather than showing an increase in relative binding energy on moving across the 3d row, the plasmon loss is typically of the order of 20 eV with a slight decrease on crossing the row (Egerton 1986).

Photoemission from the Co and Ni 3s core levels has also been studied. Van Campen and Klebanoff (1994) have studied the spin-polarized photoemission from the 3s core level of a polycrystalline Co film. They reported an exchange splitting of $3.3 \pm 0.3$ eV between the high and low spin components and compared this with the exchange splittings of 5.0 and 6.0 eV observed in $CoF_2$ and $CoF_3$, respectively (Carver *et al* 1972). They noted that these measured splittings appeared to scale linearly with $2S + 1$ as defined in Van Vleck's model, equation (26). However, a later study of fcc Co with higher energy resolution reported an exchange splitting of 4.5 eV for the same 3s level (Johnson *et al* 1995) a result that would argue against the straightforward application of the Van Vleck model. Johnson *et al* (1995) also reported the observation of a satellite at a relative binding energy of 29.0 eV which, as in the case of Fe, they attributed to the $3s^2 3p^4 3d^{n+1}$ configuration.

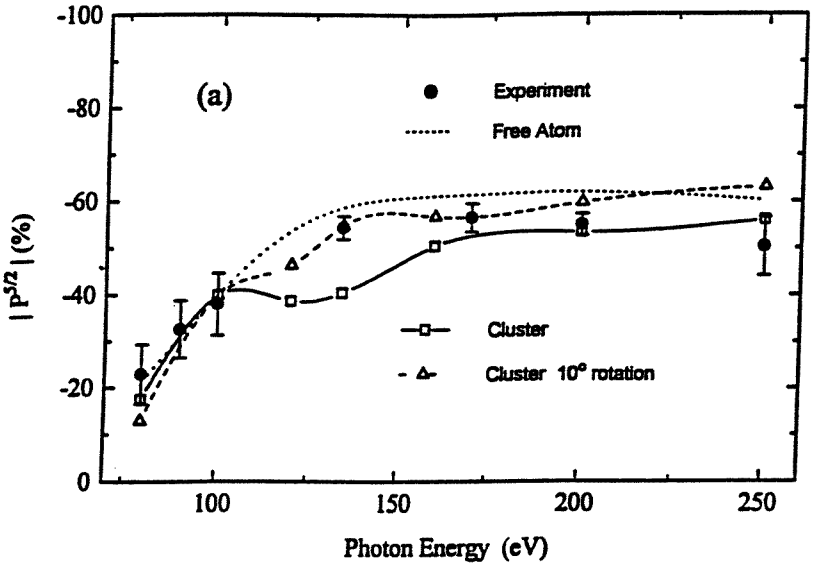


**Figure 24.** (a) Energy dependence of the W $4f_{5/2}$ spin polarization. The experimental data (full circles) are compared to free-atom theory based on equation (1) (dotted curve), and large-cluster multiple-scattering photoelectron diffraction calculations (full curve and open squares), and with the crystal rotated 10° about the surface normal (dashed curve and open triangles).

The spin polarization of the Ni 3s photoemission has been studied by See and Klebanoff (1995a, c). These authors report an exchange splitting of 0.38 eV for the main line which they attribute to the presence of a mixture of 50% $d^9$ and 50% $d^{10}$ configurations. They also report that the 6 and 14 eV satellites show almost 100% majority spin polarization and associate them with the $^2$G and $^2$S final state terms of the $d^8$ configuration, respectively.

Saitoh *et al* (1995) have also examined the Ni 3s core level spectrum. They again measure a spin polarization in the main peak which they attribute to a mixture of $d^9$ and $d^{10}$ configurations. They also measure a majority spin polarization in the 6 eV satellite. Unlike the study of See and Klebanoff (1995c), however, they suggest that the satellite is derived from the $d^9$ configuration with the spin polarization reflecting the larger $^1$D component.

Before leaving our discussion of the 3s core levels we turn briefly to an examination of the linewidths. The early SPES studies of the Fe 3s level were unable to resolve the two distinct peaks representing the low and high spin states in the majority spin channel (Hillebrecht *et al* 1990). This resulted in the majority spin 'peak' being considerably broader than the minority spin peak and lead naturally to the idea that the lifetime of the majority spin core hole was less than that of the minority spin core hole. The explanation offered for this was simply that the lifetime reflects the density of states in the valence band and there are more majority spin than minority spin valence electrons.

With increased intensity and resolution Johnson and coworkers (1995) have re-examined this question. They find that for both Fe and Co 3s emission, the low spin final state is broader by a factor of approximately three than the majority spin component of the high spin final state. In particular, for Fe, the full width half maximum (FWHM) of the former is 3.72 eV and that of the latter 1.5 eV. Furthermore, the minority spin component is broader than the majority spin component in the high spin final state, 2.38 eV and 1.5 eV FWHM, respectively, for Fe. It is clear that these lifetimes, reflecting Auger decay, are not

determined simply by the spin of the core hole but rather by the configuration of the final state of the ion.

There have also been a few studies of the more deeply bound 2s core levels. To date, the polarized spectra have been characterized simply by exchange split majority and minority spin peaks. Unlike the 3s emission described above, the majority spin emission has not been resolved into two distinct peaks. The measured exchange splittings between the two spin components are $0.65 \pm 0.3$ eV for the Co 2s level (Van Campen and Klebanoff 1994) and $1.2 \pm 0.3$ eV for the Fe 2s levels (Van Campen *et al* 1993). The latter spectra are reproduced in figure 22. The much smaller splittings observed in the 2s levels when compared with the 3s levels are consistent with the reduction in the associated Slater exchange integrals by a factor of approximately three (Watson 1959).

*4.2.3. Non-magnetic solids.* Before closing our discussion of spin-polarized core level photoemission we briefly review two studies of the spin-polarized photoelectrons emitted from the core levels of non-magnetic solids.

Roth *et al* (1994) have reported the observation of spin polarization in the 2p and 3p core levels of Cu when excited by linearly polarized radiation. In the case of the 3p core levels they found that with the spin quantization axis orthogonal to the reaction plane, defined by the directions of light incidence and electron emission, strong polarization was observable in the spin–orbit split $p^{1/2}$ and $p^{3/2}$ levels. The polarization was opposite for the two components and approximately twice as strong in the $p^{1/2}$ level. They also observed a reversal of the spin polarization for the two spin–orbit split components of the 2p level.

In agreement with free-atom theory (Cherepkov 1983), the authors suggested that their observations were consistent with the spin polarization being induced by an interference between the dipole allowed final-state continuum wavefunctions with angular momentum $l + 1$ and $l - 1$ in the presence of the spin–orbit interaction for a bound state with $l > 0$. They noted that without experimentally resolving the spin–orbit splitting, it would not be possible to observe any polarization in the spectrum.

In a subsequent paper Starke *et al* (1996) reported the observation of a strong spin polarization in the W 4f core levels when excited by circularly polarized light. Shown in figure 23, the spin–orbit split 4f levels show a spin polarization of approximately 55% for the $f_{5/2}$ line and $-40\%$ for the $f_{7/2}$ line when excited by left circularly polarized light of energy in the range 130–250 eV. Upon reversal of the light helicity the polarization of both lines changes sign but remains constant in magnitude. When using linearly polarized light with the electric-field vector in the interaction plane along the $y$-axis, the authors reported a vanishing spin polarization in both lines in agreement with the theory of free atoms.

Starke *et al* also compared the experimentally measured energy dependence of the $4f_{5/2}$ spin polarization with both a free-atom calculation and a multiple-scattering calculation taking full account of photoelectron diffraction. These comparisons are reproduced in figure 24, where the spin polarization is defined with respect to the incident light polarization axis. The authors noted that the 4f levels are particularly suited for comparison with free-atom theory because there is no Cooper minimum in the photoemission cross section and the spin polarization originates from the core level spin–orbit splitting itself. In the free-atom case, the spin polarization $P_z^J$ of the photoelectron emitted from a core level of total angular momentum $J$ is given by

$$P_z^J = \frac{S_3(A^J + \frac{1}{2}\gamma^J) + S_2\eta^J}{1 + \frac{1}{4}\beta(1 + 3S_1)} \tag{32}$$

where the Stokes parameters $S_1$, $S_2$ and $S_3$ are known for the incident light, $\beta$ is the normal

asymmetry parameter and $A^J$, $\gamma^J$ and $\eta^J$ are spin-polarization parameters adopted from the review of Cherepkov (1983). It is clear from the comparison in figure 24 that this approximation provides a good description of the observed energy dependence. However, the comparison with multiple-scattering calculations also pointed to the possibility of strong modulations in the spin polarization resulting from scattering and diffraction effects.

## 5. Surface studies

### *5.1. Clean surfaces*

First-principles calculations predict that the clean surfaces of many materials will have enhanced magnetic moments in the surface region (Freeman and Wu 1991). This enhancement reflects the reduced coordination number or reduction in the number of nearest neighbours as the dimensionality is reduced. The same calculations predict that the moments will increase still further as one proceeds from the two-dimensional surface through the linear one-dimensional chain to the free atom.

As a particular example, the magnetic moment at the surface of an Fe crystal cut in the (001) plane is predicted to be $2.96\mu_B$ as opposed to the $2.2\mu_B$ characteristic of the bulk. On the (110) surface, where the coordination number is six rather than the four of the (001) surface, the moment is predicted to be $2.6\mu_B$. Moving to the linear chain the magnetic moment is calculated to be $3.4\mu_B$ and that of the free atom, $4.0\mu_B$. These theoretical predictions for the surface region have never been directly verified experimentally although several studies of magnetic thin films appear to indicate that the average magnetic moment increases as the film becomes thinner and two-dimensional behaviour is approached (Clemens *et al* 1992a).

Although it is not possible to determine the magnitude of the magnetic moment from angle-resolved photoemission studies, it is possible to verify many other aspects of the calculation. In particular, it is possible to identify and characterize the surface states that are responsible in part for the surface magnetic structure. A surface state represents an electronic state that is localized within the surface region. d-derived surface states tend to be more localized in the outer surface layers than the s–p derived states which may have wavefunctions decaying over several layers away from the surface. A true surface state must lie within a gap that is formed when the bulk bands are projected onto the two-dimensional surface Brillouin zone. Outside of these bulk bandgaps there may also exist states which resonate in the surface region. These latter states, referred to as surface resonances, have many characteristics in common with surface states. Figure 25 shows the results of a spin-polarized electronic structure calculation for a 49-layer Fe slab (Stroscio *et al* 1995). The figure shows both majority and minority spin surface states of even symmetry as defined by the mirror plane in the $\bar{\Gamma}\bar{X}$ azimuth.

Experimentally, an electronic state is identified as a surface state if it fulfils two criteria. First, the state will often show a strong sensitivity to the level of surface contamination. Adsorbate atoms on the surface will have little affect on the bulk states, but will considerably reduce and may completely remove any surface related features from the photoemission spectrum. Second, if the state is two-dimensional, then for a given $k_\parallel$, it will show no dispersion with $k_\perp$. That is, a peak reflecting emission from a surface state will remain at the same binding energy as the incident photon energy is varied.

There have been an extensive number of spin-integrated photoemission studies of surface states on both Fe and Ni surfaces. In a study of the Ni(001) surface a majority spin $\bar{\Gamma}$ surface state with sensitivity to s-polarized light was identified near the centre of the surface

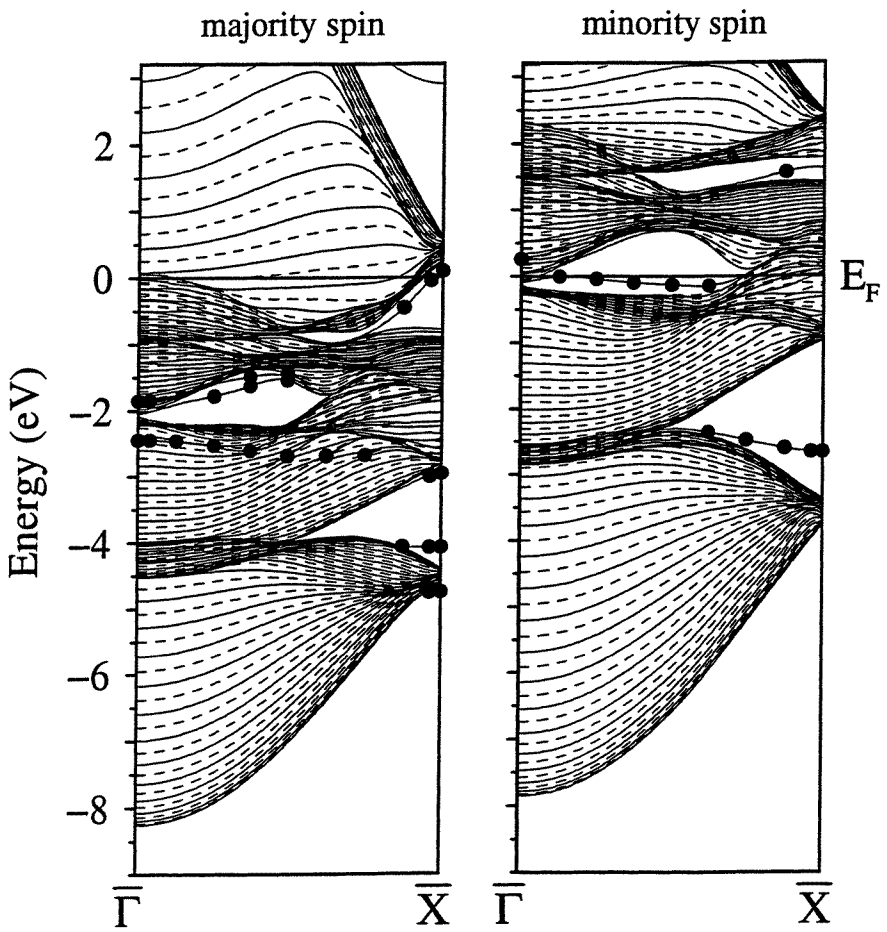


**Figure 25.** Band structure of majority and minority spin even symmetry states along $\bar{\Gamma}$–$\bar{X}$ for a 49-layer Fe film in the left and right panels, respectively. States with high localization in the surface region are marked with circles.

Brillouin zone (Erskine 1980). The spin assignment was made through comparison with calculation. However, a subsequent spin-polarized photoemission study indicated that the correct spin assignment should be minority rather than majority spin and further suggested that the emission reflected off-normal $\Delta_2$ bulk band contributions rather than a surface state (Clauberg *et al* 1984). Other surface states on the Ni(001) surface were identified in symmetry gaps of the two spin subsystems (Plummer and Eberhardt 1979). In particular, a state of odd symmetry was identified in the majority spin gap around the $\bar{M}$ point and a state of even symmetry was found in the minority spin gap around the $\bar{X}$ point.

To date there have been no surface states examined in spin-polarized photoemission studies of any of the low-index nickel surfaces. However, there have been a number of spin-polarized inverse photoemission studies of both crystal-derived and image-derived unoccupied surface states on all three low-index nickel surfaces (Donath 1994). States derived from the sp-bands have been identified in the vicinity of the $\bar{X}$ point on both the Ni(110) (Donath *et al* 1990) and Ni(001) (Starke *et al* 1992) surfaces. An exchange splitting of the order of 170 meV was observed for the former and a splitting of the order of 180

meV for the latter. In a study of the Ni(111) surface (Donath *et al* 1993) a surface state was identified immediately above the Fermi level at the centre of the zone. The authors of the study noted that the state was derived from the p-like $L_2'$ point rather than the d-like $L_3$ point. They further suggested that the state contributed to the surface moment present at the (111) surface.

Turning to Fe early spin-integrated angle-resolved photoemission studies of the Fe(001) surface revealed a number of surface states and resonances along the $\Sigma$ and $\Delta$ symmetry lines (Turner *et al* 1982, Turner and Erskine 1983, 1984). The authors assigned spin labels to these states again by comparing with different slab calculations. Later spin-polarized studies have confirmed the surface character of many of these states but have modified some of the spin assignments.

The first spin-polarized study using p-polarized light identified, through its sensitivity to oxygen contamination, figure 26, a minority spin surface resonance at a binding energy of 2.3 eV at the centre of the Brillouin zone (Brookes *et al* 1990). As we noted earlier, the parallel momentum, $k_\parallel$, is conserved on crossing the vacuum–solid interface. Thus, measuring the dispersion of a feature with respect to $k_\parallel$ outside in the vacuum allows a direct mapping onto the dispersion as a function of $k_\parallel$ inside the crystal potential. Brookes *et al* (1990) were able to follow the dispersion of the minority spin surface state out along the $\bar{\Gamma}\bar{\mathrm{X}}$ azimuth to the zone boundary at $\bar{\mathrm{X}}$. At the latter point the state falls within a projected bulk bandgap and becomes a true surface state localized in the surface layers. The experimentally determined dispersion is in excellent agreement with the results of the first-principles calculation shown in figure 25. Further experimental agreement with the latter calculation was provided in the accompanying tunnelling spectroscopy study (Stroscio *et al* 1995). Examining the unoccupied electronic states the authors observed an intense sharp feature in their spectra in agreement with the minority spin surface state predicted to lie 0.2 eV above the Fermi level.

However, a different conclusion regarding the accuracy of the FLAPW calculation was reached in the second spin-polarized photoemission study of the Fe(001) surface by Vescovo *et al* (1993b). These authors used s-polarized rather than p-polarized incident light, which for normal emission, changes the sensitivity from $\Delta_1$ to $\Delta_5$ like bands. The study revealed a majority spin state with the latter symmetry immediately below the Fermi level. The same surface state had previously been identified in earlier spin-integrated photoemission studies (Turner *et al* 1982, Turner and Erskine 1983, 1984). Vescovo *et al* (1993b) in their study noted that such a state was not predicted in the FLAPW calculation of this surface but that a majority spin surface resonance was predicted to lie just below the Fermi level in a separate calculation (Feder *et al* 1984) analysing the Fe(001) spin-polarized photoemission data of Kisker *et al* (1985). The assignment of majority spin again represented a reversal of spin assignment from that suggested by the authors of the spin-intgerated photoemission studies.

A study of the Fe(110) surface (Vescovo *et al* 1993a) using s-polarized incident light identified a surface state of minority spin character midway along the $\bar{\Gamma}\bar{\mathrm{H}}$ azimuth. The authors noted that a LSDF calculation (Wu and Freeman 1992) using the FLAPW method for a seven-layer slab points out the importance of minority spin surface states near the Fermi level for this surface. The decreased symmetry at the surface results in the valley between the bonding and antibonding states becoming less pronounced in the surface-projected density of states due to filling with minority spin states. Furthermore, for this particular surface, the surface band narrowing results in an appreciable reduction in the majority spin surface density of states at $E_\mathrm{F}$.

A recent angle-integrated spin-resolved photoemission study of polycrystalline Fe at higher photon energies has also reported the observation of surface related emission

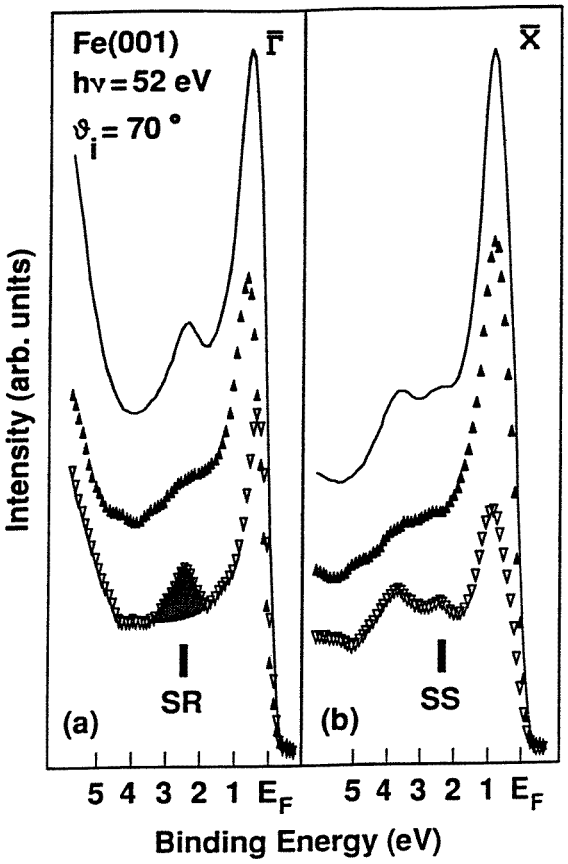


**Figure 26.** Spin-resolved photoemission spectra recorded from clean Fe (001) at the (a) $\bar{\Gamma}$ and (b) $\bar{X}$ points of the Brillouin zone. The associated spin-intgerated spectra are indicated by the full curve. SR and SS mark the minority spin surface resonance and surface state, respectively. The attenuation of the minority spin surface resonance following 0.1 L oxygen exposure (where 1 L = $10^{-6}$ Torr s) is shown by the hatched region.

(Sinkovic *et al* 1995b). Such an experiment differs from the angle-resolved studies in that now the experiment is sampling the surface emission integrated across the surface Brillouin zone. The authors identified the latter contribution to the spectra by subtracting a theoretical bulk component obtained from a first-principles calculation.

Studies have also been carried out on the rare-earth Gd(0001) surface. As we have already noted a spin-intgerated photoemission study identified a surface state of $d_{z^2}$ character 2 eV below the Fermi level (Li D *et al* 1991). Shown in figure 27, a subsequent spin-polarized photoemission study found that this state carried majority spin suggesting that the surface magnetic moments were ferromagnetically aligned with the substrate (Mulhollan *et al* 1992b). Such an observation disagreed both with the results of an earlier spin-polarized photoemission study of the Gd core levels (Weller *et al* 1985) and with a subsequent first-principles total-energy calculation which favoured an antiferromagnetic alignment of the surface and bulk moments (Wu *et al* 1991). Further spin-polarization studies of the secondary electrons and the Gd 4f core levels confirmed the ferromagnetic alignment but suggested the possibility of a small canting of the surface moments with a component

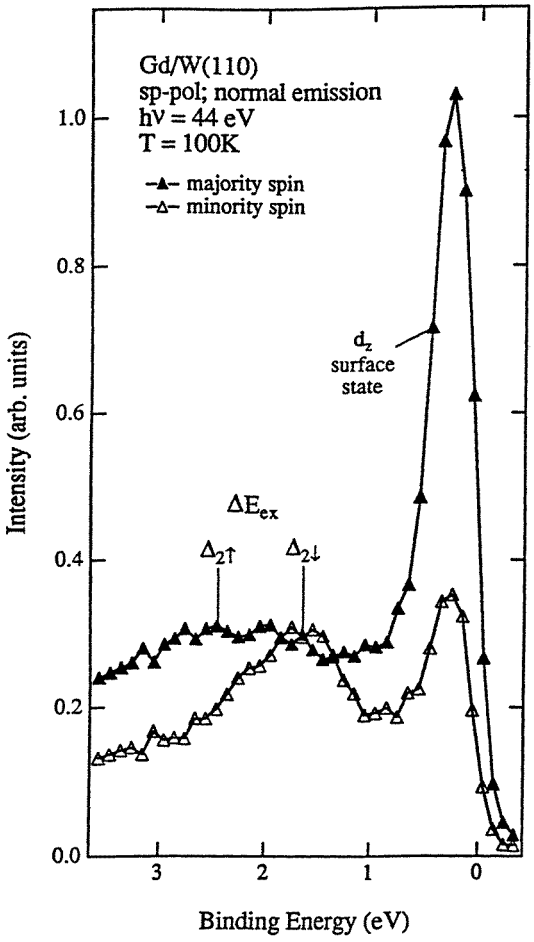


**Figure 27.** Spin-resolved photoemission spectra recorded along the surface normal from a Gd film grown on a W(110) substrate. The strong majority spin surface state sitting immediately below the Fermi level is clearly visible.

sticking out of the surface (Tang *et al* 1993, Li *et al* 1993). A ferromagnetic alignment of the surface and bulk moments has also been suggested for Tb (Arenholz *et al* 1995).

More recent theoretical studies appear to have resolved the discrepancy between the earlier first-principles calculations and the experimental observation of ferromagnetic alignment between the surface and bulk moments for Gd(0001). Bylander and Kleinmann (1994) argue that the discrepancy can be traced to the LSDA approach treating the core and valence electrons together. By allowing the valence electrons to see a Hartree–Fock potential from the core electrons and the LSDA potential amongst themselves and by introducing an additional parameter to correctly adjust the LSDA exchange potential the authors were able to obtain ferromagnetic alignment as the lowest energy configuration.

The question of whether the reduced coordination in the surface region of a paramagnet will lead to a ferromagnetic surface has been investigated in the case of the Rh(001) surface. Indeed magnetic surface layers have been invoked (Li H *et al* 1991) as a possible explanation of the surface expansion $(+0.5 \pm 1)\%$ found in LEED studies of the (001) surface (Oed *et al* 1988).

An *ab initio* pseudopotential calculation by Morrison *et al* (1993) did indeed predict a large surface moment of the order of $1.8\mu_B$. This surprisingly large moment has been challenged in two subsequent calculations. Weinert *et al* (1993) using the LSDA found that the surface was non-magnetic. However, they found that by modifying the calculation so that the magnetic contributions were determined by the valence charge alone they were able to reproduce the earlier results of Morrison *et al*. A second calculation again using the pseudopotential method but now treating the core levels in a more realistic fashion also found a non-magnetic surface (Cho and Kang 1995).

The conclusions of the calculations of Weinert *et al* were supported by a spin-polarized photoemission study of the Rh(001) surface (Wu *et al* 1994). In the latter study a very small spin polarization was observed in a surface resonance located at the $\bar{M}$ point in the surface Brillouin zone. However, the authors concluded that the spin polarization, measured at room temperature, would point to a surface moment of the order of $0.1–0.2\mu_B$ at most, i.e. an order of magnitude less than the original calculation.

### *5.2. Adsorbate covered surfaces*

Chemisorption of foreign atoms on magnetic surfaces represents a research area of interest both to the surface science community and the magnetism community. Studies of the electronic structure combined with spin analysis provide, on the one hand, a more detailed test of different adsorption models and, on the other, as we shall see later, a test of the effectiveness of different spin-dependent calculations.

Assuming that adsorption or contamination of a surface lead to the formation of magnetic 'dead' layers, early studies concentrated on changes to the substrate electronic structure (Schmitt *et al* 1985, Seiler *et al* 1985). Indeed, in an early study of oxygen adsorbed on Ni(110) the exchange splitting of the substrate $S_4$ bands was observed to disappear upon adsorption of 1 L of O although interestingly no reduction in the substrate exchange splitting was observed upon adsorption of 1 L of CO (Schmitt *et al* 1985). In contrast a later study of the ordered $(2 \times 1)$ O and $c(2 \times 2)$ S structures on Ni(110) found no change in the exchange splitting of the substrate $S_4$ d-bands (Schmitt *et al* 1987). The overall conclusion from this later study was that adsorption had no strong affect on surface magnetism.

Theoretical studies at this time predicted the presence of induced magnetic moments on the adsorbates themselves. Indeed, several calculations of the adsorption system oxygen on Fe(001) concluded that hybridization with the spin-polarized bands of the substrate resulted in the presence of a small magnetic moment on the oxygen site of the order of $0.24\mu_B$ (Huang and Hermanson 1985, Chubb and Pickett 1987). Theoretical studies of sulphur adsorbed on Fe(001) found a similar result with a moment of $0.14\mu_B$ being induced on the sulphur site (Chubb and Pickett 1988a, b).

The predictions of induced magnetic moments on the adsorbate were confirmed in a series of experimental studies of oxygen and sulphur adsorption on Fe(001) (Johnson *et al* 1988, Schonhense *et al* 1988a, b, Clarke *et al* 1990). The first study of the $Op(1 \times 1)$/Fe(001) system found clear evidence of exchange split adsorbate bands (Johnson *et al* 1988). The results are reproduced in figure 28. The oxygen derived bands located 6 eV below the Fermi level show a strong spin polarization indicative of a moment on the oxygen site. Similar evidence had also been obtained in an earlier spin-polarized Auger electron spectroscopy study of this system where the authors found a spin polarization in the oxygen KLL Auger line (Allenspach *et al* 1985).

The symmetries of the adsorbate derived bands shown in figure 29 are determined by the sensitivity to the incident light polarization. Thus excitation of the $p_z$ orbital is favoured

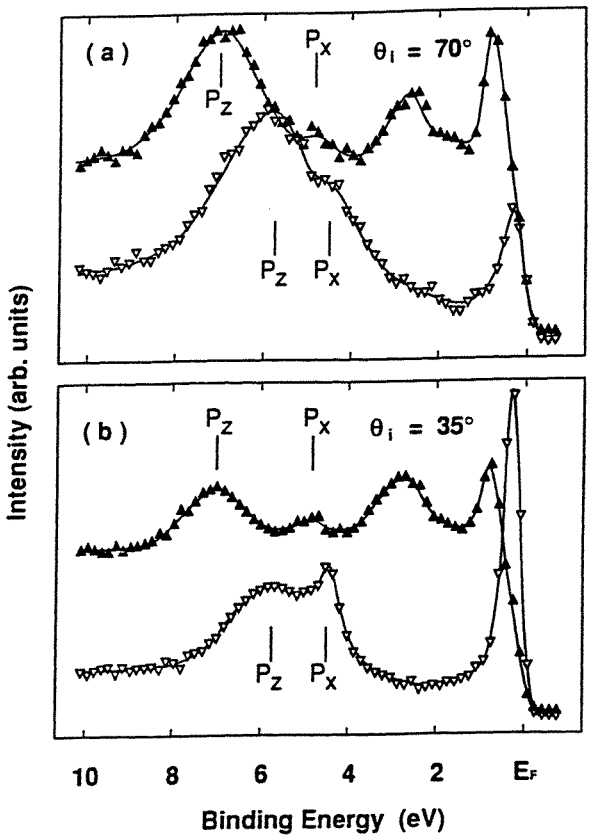


**Figure 28.** Spin-resolved photoemission spectra for normal emission from Fe(001)–p(1 × 1) O. Full upward pointing triangles correspond to majority spin and open downward pointing triangles correspond to minority spin. (a) Angle of light incidence $\theta_i = 70^\circ$ corresponds to p-polarized light; (b) $\theta_i = 35^\circ$ results in a larger proportion of s-polarization. The symmetry of the different oxygen derived features is indicated.

by grazing incidence light and excitation of the $p_{xy}$ orbital is favoured by more normally incident light. At the centre of the surface Brillouin zone the O $2p_z$ bands are shown to be exchange split by 1.3 eV and the $2p_x$ bands by 0.35 eV. A later study of oxygen adsorption on Fe films grown on a W(001) substrate (Fink *et al* 1992) found a similar result with the $2p_z$ orbital at the centre of the zone having a larger exchange splitting than the O $2p_x$ orbital. However, in the latter case, the $2p_z$ splitting was 0.6 eV and the O $2p_{xy}$ splitting was 0.1 eV. Interestingly, in both studies it was found that a marked anisotropy existed in the exchange splitting observed for the $2p_z$ on moving out to the edge of the zone. Indeed, in the earlier study it was found that the exchange splitting was reduced from 1.3 eV at the centre of the zone to 0.25 eV at the $\bar{X}$ point on the zone boundary (Johnson *et al* 1988).

As shown in figure 29 the marked difference in the exchange splitting for the different symmetry orbitals at the centre of the zone and the strong variation of the $2p_z$ exchange splitting across the zone were not predicted in the first-principles calculations (Huang and Hermanson 1985, Chubb and Pickett 1987). LEED studies indicate that the oxygen atoms in the p(1 × 1) structure on Fe(001) sit in the hollow site with the adsorbate almost coplanar

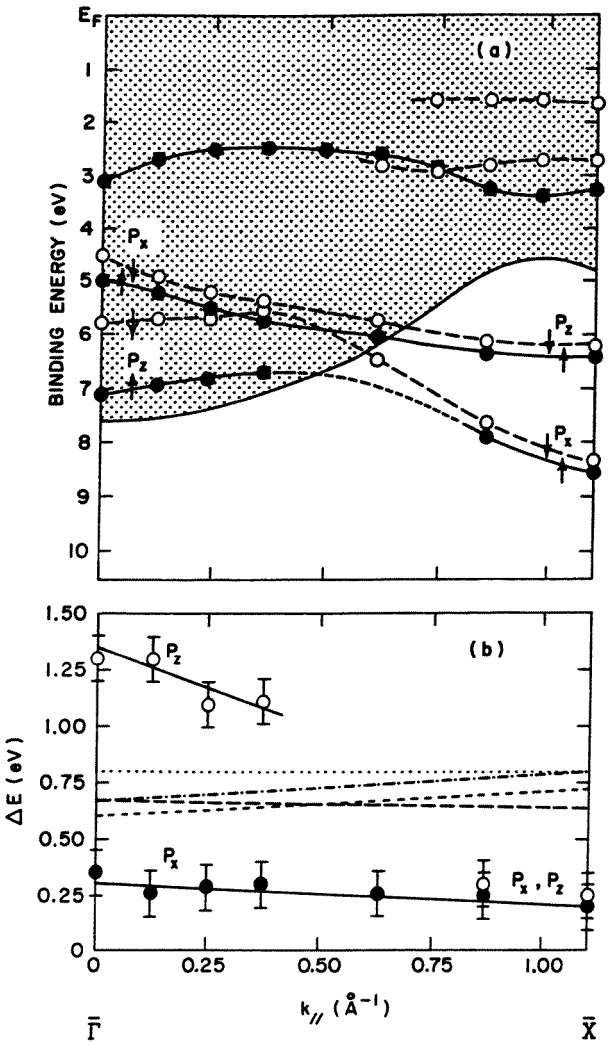


**Figure 29.** (a) Spin-resolved $E(k_{\|})$ dispersion curves for oxygen-induced features on Fe(001)–p(1 × 1) O; data points are given as full (open) circles for the majority (minority) spin systems; the smooth curves represent guides to the eye. (b) Comparison between the experimentally-derived exchange splittings and those generated for $p_x$ and $p_z$ components in the calculations of Huang and Hermanson (1985) and Chubb and Pickett (1987).

with the surface Fe layer (Legg *et al* 1977a). Thus, the exchange splitting of the $2p_z$ orbital reflects the vertical bonding of the oxygen atom to the subsurface Fe atom sitting vertically below. The splitting of the $2p_{xy}$ orbitals, on the other hand, derives from the 'horizontal' bonding to the adjacent atoms in the surface layer. In both cases the bonding involves the substrate d-orbitals and the exchange splitting reflects the level of hybridization with these orbitals throughout the zone.

Further evidence for the strong 'vertical' hybridization may be found in the individual peak linewidths which are much larger for the $2p_z$ orbital than the $2p_{xy}$ orbitals. Interestingly

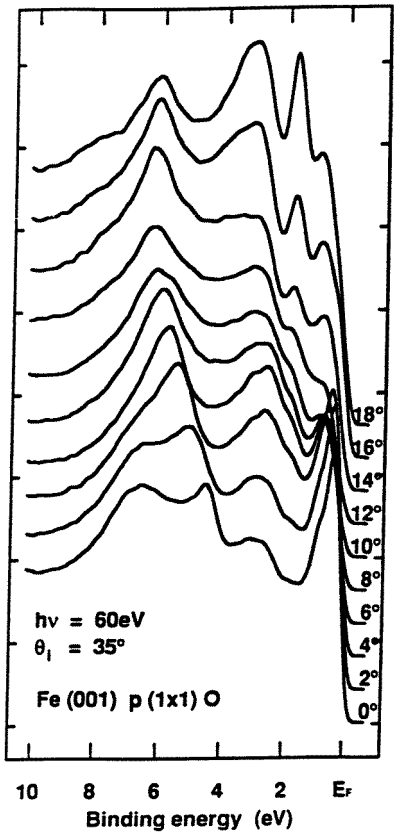


**Figure 30.** Spin-intgerated spectra recorded from the p(1 × 1) oxygen overlayer on an Fe(001) substrate in the $\bar{\Gamma}$–$\bar{X}$ azimuth. The oxygen-induced features at binding energies of 1.7 and 3.0 eV have minority and majority spin, respectively.

in both studies described above the $2p_z$ minority spin linewidth is larger than that of the majority spin. At the centre of the zone the Fe minority spin $\Gamma_{12}$ point derived from the $d_{z^2}$ orbital lies above the Fermi level. Thus a larger linewidth in the adsorbate minority spin peak suggests that the bonding primarily involves an interaction with the unoccupied Fe $d_{z^2}$ orbital.

Clarke *et al* (1990) were able to reproduce the anisotropic exchange splitting observed in the O $2p_z$ orbital in a tight-binding simulation. The authors noted that the oxygen exchange splitting at the centre of the zone primarily reflected the pd$\sigma$ interaction between the oxygen $p_z$ orbital and the substrate $d_{z^2}$ orbital on the Fe atom in the site immediately below. However, starting from a parameter set based on the approach of Harrison (1980) they noted that the best agreement was achieved by reducing both the pd$\sigma$ and the pp$\sigma$ interactions but leaving the $\pi$ interactions alone except for the pd$\pi$ interaction with the Fe atom below. Leaving all of the interactions alone resulted in an isotropic exchange splitting as found in the LSDA calculations. In the latter first-principles approach, all spin effects are included via an effective local magnetic field $B(\boldsymbol{r})$ that acts on all states of a given spin regardless of their orbital character. Clarke *et al* point out that this may be a reasonable assumption for homogeneous systems such as elemental Fe because all

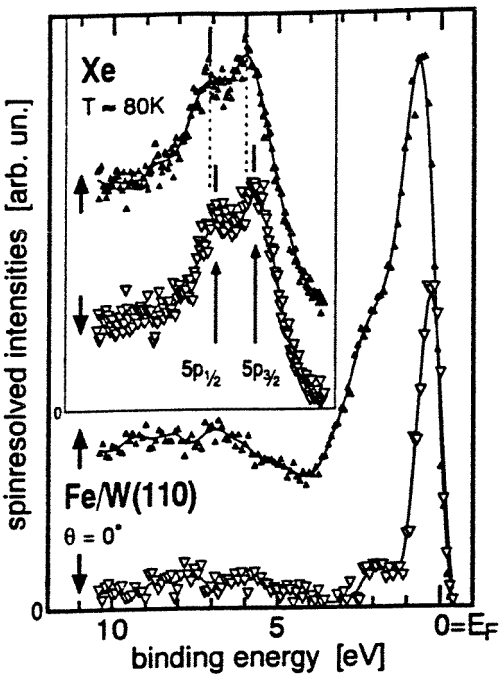


**Figure 31.** Spin-resolved photoelectron spectrum of a thin Fe(110) film (25 A) epitaxially grown on W(110). The inset shows the corresponding energy range for Xe physisorbed on the same film at $T = 80$ K. The spectra were taken at $h\nu = 21.2$ eV (He1) and normal emission. Full symbols denote the majority spin channel, open symbols the minority channel. The two peaks observed belong to the spin–orbit split Xe $5p_{1/2}$ and $5p_{3/2}$ orbitals. Both peaks show a significant difference of the energetic positions in the majority and minority spin spectra, indicated by the bars and dashed lines.

states that are participating in the magnetization are of similar character. For an adsorbate system, however, the orbital character of the adsorbate and substrate are different and the approximation may no longer be valid.

The studies of oxygen adsorption on Fe(001) may be compared with studies of oxygen adsorption on Fe(110). Theoretical studies (Wu and Freeman 1992) indicate that a considerably larger magnetic moment is induced on the oxygen atom when adsorbed in the p(1 × 1) structure on the Fe(110) surface than on the Fe(001) surface. They calculate a moment of $0.7\mu_B$ on the oxygen site for the Op(1 × 1)Fe(110) structure which is to be compared with an oxygen moment of $0.24\mu_B$ calculated for the Op(1 × 1)Fe(001) system (Huang and Hermanson 1985, Chubb and Pickett 1987). In an experimental study of Op(1 × 1)Fe(110), Vescovo *et al* (1993a) measured an exchange splitting for the oxygen $2p_x$ orbital of 0.5 eV, larger than the 0.35 eV reported in the earlier study of adsorption on the Fe(001) surface (Clarke *et al* 1990). The experiment of Vescovo *et al* was not sensitive to the $p_z$ orbitals and so it is not possible to make a direct comparison between the two adsorption systems for this particular orbital. At higher oxygen exposures Vescovo *et al* noted that the chemisorbed phase was followed by the formation of an FeO(111) thin overlayer after flashing the sample to $T > 600\,^{\circ}$C.

Other oxygen adsorption systems that have been studied include oxygen adsorption on fcc Co(001) (Clemens *et al* 1992b), and hcp Co(0001) (Getzlaff *et al* 1994). In the former

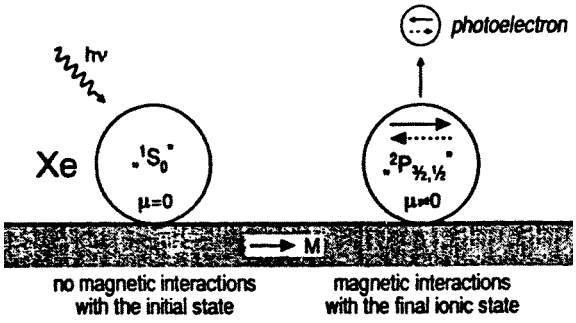


**Figure 32.** In the ground state, Xe atoms possess saturated spin and orbital moments and, therefore, cannot carry a magnetic moment (left). After the 5p-photoemission process there is a non-vanishing magnetic moment of the ionic hole states leading to a magnetic interaction between substrate and adsorbate (right).

study Clemens *et al* report an exchange splitting of 0.2 eV for the O $2p_{xy}$ orbital. In the later study of oxygen adsorption on hcp Co(0001) films grown on a W(110) substrate Getzlaff *et al* (1994) reported exchange splittings for the O $2p_z$ and $2p_{xy}$ orbitals of 0.35 eV and 0.3 eV, respectively. In a later study Getzlaff *et al* (1996) reported a reduction in these exchange splittings as one moved away from the centre of the zone. This is consistent with the observations made in the earlier studies of the p(1 × 1) oxygen overlayer on Fe(001) (Johnson *et al* 1988, Clarke *et al* 1990).

Studies of sulphur adsorption on different surfaces have found similar results. A spin-polarized inverse photoemission study of S adsorbed on Ni(110) identified exchange split sulphur derived bands (Schonhense *et al* 1988b). A spin-polarized photoemission study of S adsorbed on Fe(001) in the c(2 × 2) structure found an exchange splitting of 0.5 eV for the S $3p_z$ bands at the centre of the zone (Clarke *et al* 1990). As in the case of the oxygen $2p_z$ bands, this exchange splitting was reduced to a value of 0.2 eV at $\bar{M}$, the zone boundary. These observations are to be compared with theoretical studies of this system, which found an average exchange splitting of 0.5 eV throughout the zone (Chubb and Pickett 1988a, b). The smaller exchange splitting, 0.5 eV, of the S $3p_z$ bands at the centre of the zone as opposed to the 1.3 eV observed for the O $2p_z$ bands reflects the difference in height of the two adsorbates above the surface plane of the Fe. Indeed LEED studies indicate that the oxygen atoms are 0.48 A above the surface layer (Legg *et al* 1977a) and the sulphur atoms 1.0 A above the surface (Legg *et al* 1977b).

In the case of O and S adsorption on Fe(001) adsorbate-induced features have also been identified in the substrate d-bands (Clarke *et al* 1990). For the S c(2 × 2) overlayer, a new minority spin feature was observed at the centre of the zone at a binding energy of 1.4 eV. For the p(1 × 1) oxygen overlayer, new minority spin features at binding energies of 1.7 and 2.8 eV were identified near the $\bar{X}$ point in the surface Brillouin zone as shown in figure 30. These same features were also identified in an accompanying first-principles calculation. The peak at a binding energy of 2.8 eV was shown to reflect the bonding between the O $p_z$ orbital and the minority spin surface state that characterizes the clean surface. The latter state we have previously discussed in section 5.1. The oxygen-induced peak at lower binding energy, on the other hand, reflects bonding between the O $p_x$ orbital and Fe states of appropriate symmetry.

Sinkovic *et al* (1989) have also identified the substrate d-bands involved in the bonding in a spin-polarized Auger electron study of the c(2 × 2)S/Fe(001) system. In a separate study

of the diffraction effects observed in the S Auger line Sinkovic *et al* (1995a) concluded that the sulphur adsorption resulted in a reduction of the surface iron moments in qualitative agreement with calculations of Chubb and Pickett (1988a, b).

To date there has only been one study of halogen adsorption on a ferromagnetic surface reported in the literature. A study of iodine dissociatively adsorbed in the c($3 \times 1$) structure on Fe(110) films (Getzlaff *et al* 1993b) again found evidence of exchange split adsorbate bands, in this case the I $5p_{xy}$ and $5p_z$ bands. In normal emission, the exchange splitting of the $5p_{xy}$ orbitals was determined to be $0.35 \pm 0.1$ eV and $0.15 \pm 0.1$ eV for the $5p_z$ orbitals. Thus, unlike the chalcogens discussed previously, the $p_z$ splitting for this system is now smaller than the $p_x$ splitting.

Oxygen, sulphur and iodine all represent strongly bonded or chemisorbed systems. Xenon adsorption, on the other hand, represents an example of a weakly bonded or physisorbed system. Getzlaff *et al* (1993c) report a spin-polarized photoemission study of Xe adsorbed on Fe(001). Xenon is an inert gas with a filled 5p band. Its bonding to the substrate is, therefore, driven by a Van der Waal like polarization and one anticipates no spin polarization of the valence electrons in the ground state. However, as shown in figure 31, Getzlaff *et al* find a spin polarization in both the Xe $5p^{3/2}$ and $5p^{1/2}$ emission. They interpret the observation of a spin polarization as a final-state effect as in the case of excitation from a filled core level. However, in the case of Xe the spin-polarized photohole presumably couples to the local spin derived from the neighbouring substrate as illustrated in figure 32.

The spin-polarized photoemission studies of oxygen, sulphur and iodine adsorption have clearly revealed evidence of the bonding of the atom to the surface via the interaction of the p-orbitals with the substrate d-orbitals. Interestingly, a subsequent study of carbon monoxide adsorption on an Fe(001) surface (Brookes *et al* 1989) found no spin-polarization evidence for the interaction of the equivalent molecular orbital, the $5\sigma$ level, with the substrate d-orbitals even though this is a frequently cited mechanism for the CO bonding (Blyholder 1964). In the latter model, the bonding of the $5\sigma$ level, the highest occupied CO orbital, to the substrate $d\sigma$ or $d_{z^2}$ levels is compensated by 'backdonation' into the molecular $2\pi$ level from the substrate $d\pi$ level.

At room temperature, carbon monoxide initially bonds to the Fe(001) surface in the fourfold hollow site, tilted 55° to the surface normal. At low temperatures a second CO species adsorbs on the surface in a vertical geometry. Brookes *et al* (1989) found no spin polarization in the molecular $5\sigma$ level in either geometry. They did, however, observe the emergence of a new spin-polarized feature in the vicinity of the substrate d-bands for the tilted species. They interpreted this observation as evidence for the interaction of the molecular $2\pi$ level with the substrate Fe d-bands. The lack of any spin polarization in the $5\sigma$ level suggests that the interaction of the latter is more likely to be with the sp levels rather than the more polarized d-bands. The lack of any observable spin polarization could also be due to the quenching of the surface magnetization by the adsorbed molecules. However, by monitoring the spin polarization of the Fe 3p core level Brookes *et al* (1989) concluded that the reduction in the surface magnetization was minimal. A similar result was found in a study of CO adsorbed on an Fe(110) film (Getzlaff *et al* 1992). Again no spin polarization was found in the molecular $5\sigma$ level. Finally, in a study of benzene adsorbed on Fe(110) and Co(0001) films, (Getzlaff *et al* 1995) no spin polarization was observed in either the $\sigma$ or $\pi$ molecular levels even though the spectra provided clear evidence of a chemisorbed bond to the substrate.

Before closing our discussion of absorption studies, we will review some studies of the oxidation of different surfaces following exposure to heavier doses of oxygen. A

spin-polarized core level photoemission study of the oxidation of Fe(001) was reported by Sinkovic *et al* (1990). These authors demonstrated the possibility of combining spin polarization analysis with studies of the chemically shifted core levels to provide site-specific magnetic information. The study concluded that the initial chemisorption phase with the oxygen atoms sitting in the fourfold hollow sites on the surface is followed by oxidation with the oxygen atoms tunnelling under the surface.

This process is highlighted in figure 33 which shows the spin-resolved Fe 3p photoemission spectra obtained by Sinkovic *et al* following exposure of the Fe(001) surface to 16 L of $O_2$ and after annealing the latter surface to 650 °C. The main substrate iron emission is represented by the minority spin feature at a binding energy of 52.9 eV. As in the clean Fe 3p spectrum shown earlier in figure 17, the majority counterpart is at a binding energy 0.5 eV higher. With the initial oxidation, figure 33(a), we identify a new majority spin peak shifted to higher binding energy with respect to the clean surface peak by 4.5 eV. The shift in binding energy for this peak suggests that it is derived from a site with $Fe^{3+}$ valency (Brundle *et al* 1977). This, together with the observation that it is spin polarized, further suggests that the initial oxide is of the ferrimagnetic form $\gamma$-$Fe_2O_3$. The observation that the substrate Fe emission is dominated by minority spin electrons but the initial oxide is dominated by majority spin emission suggests that the moments on the outer Fe ions associated with the oxide are antiferromagnetically coupled to the moments of the substrate. One explanation for this coupling is proposed by the authors who propose a superexchange mechanism involving subsurface oxygen atoms.

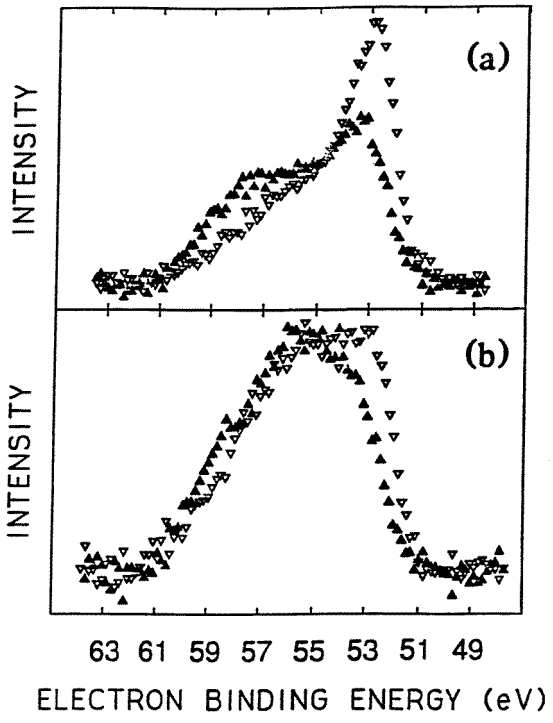


**Figure 33.** (a) Spin-resolved Fe 3p spectra showing the initial oxidation of Fe after exposure to 16 L of $O_2$ with the background subtracted (1 L (Langmuir) = $10^{-6}$ Torr s). (b) The same as in (a) but after annealing to 650 °C. The photon energy used in the studies was 90 eV.

Following annealing, figure 33(b), it is still possible to identify emission from the substrate but now the spectra are dominated by unpolarized emission shifted approximately 2.0 eV from the main peak. The latter shift in binding energy is now indicative of an $Fe^{2+}$ phase (Brundle *et al* 1977). These observations taken together suggest that the oxide following annealing is most probably the antiferromagnetic form $Fe_xO$.

Clemens *et al* (1992b) have reported a study of the oxidation routes for fcc Co. Exposing the surface to oxygen at room temperature they observed that, following the initial chemisorbed phase, an antiferromagnetic CoO surface phase began to form with exposures greater than 7 L. This they were able to demonstrate by comparing the valence band spectra with spectra recorded from bulk CoO. In particular, they were able to identify a correlation satellite in the photoemission spectrum at a binding energy of 10 eV. The presence of such a satellite may be taken as evidence of increased localization of the 3d electrons. Again by comparison with bulk valence band spectra the authors were able to show that exposure of the surface to oxygen at low temperatures (150 K) resulted in the formation of a $Co_3O_4$ phase.

Similar results were reported in a study of the oxidation of hcp Co(0001) films grown on a W(110) substrate by Getzlaff *et al* (1994). At room temperature the oxygen diffuses into the bulk to form antiferromagnetic CoO. By examining the spin polarization in the valence bands and in a satellite associated with the oxide the authors were able to demonstrate the co-existence of chemisorbed 'magnetized' oxygen and antiferromagnetic CoO near the surface. With higher exposures a $Co_3O_4$ layer forms. However, no spin polarization or peak separation associated with this latter oxide was observable.

## 6. Thin-film studies

Thin films are particularly interesting because they offer the possibility of studying a range of new phenomena in magnetism. As an example, ferromagnetic films may show marked anisotropies as the film thickness is varied. Indeed, the very first spin-polarized photoemission study of Fe films deposited on a Ag(100) substrate (Jonker *et al* 1986) found that the anisotropy resulted in the magnetic moments of the Fe orienting perpendicular to the surface for the thinnest films. More detailed SMOKE studies of this system (Qiu *et al* 1993) have shown that as the Fe films become thicker the moments align in the plane of the film. This spin reorientation represents a competition between the magnetic shape anisotropy and the surface anisotropy. In thin films it is the dominance of the latter that leads to the perpendicular orientation. Whilst such effects have been studied using a number of other techniques, there has been very little study using spin-polarized photoemission. This reflects the observation that the energy differences involved in the reorientation tend to be on a much smaller scale than those currently probed in SPES.

In SPES studies of thin films the emphasis has been on the identification of states specifically associated with the interface and with the evolution of the electronic structure from the ultrathin regime through to the thicker films. These thicker films may represent possible new phases of the material (i.e. bcc Ni or fcc Fe) as we have already discussed in section 4.1.2. In the following we divide our discussion into different subsections representing studies of the 3d–3d, the 3d–4d and the 3d–5d interfaces. We then turn our attention to the detailed studies of the development of quantum well states in the thicker films. As we will see, these studies are particularly relevant to the complex magnetic behaviour observed in the related magnetic multilayers.

### *6.1. The 3d–3d interfaces*

Chromium films deposited on Fe(001) substrates have been extensively studied in thin-film magnetism. The interest stems largely from the oscillatory exchange coupling (Grunberg *et al* 1986, Parkin *et al* 1990, Parkin 1991, Unguris *et al* 1991) and giant magneto-resistance (Baibich *et al* 1988) that has been observed in the related Fe/Cr multilayers. The study of Unguris *et al* (1991) is shown schematically in figure 34. The authors measured the relative direction of magnetization in an Fe film deposited on a Cr wedge previously deposited on an Fe(001) substrate. The study provided evidence of the oscillatory exchange coupling but also clearly demonstrated the role of interfacial roughness in determining the period length.

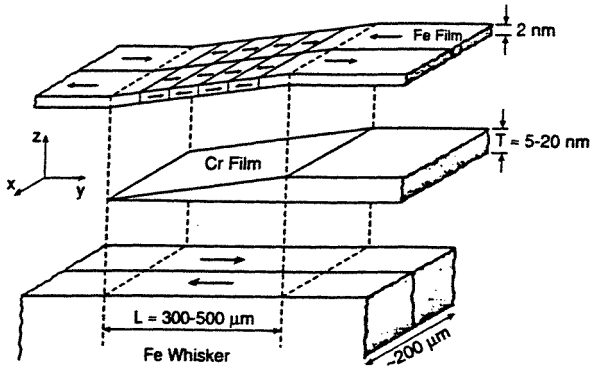


(a)

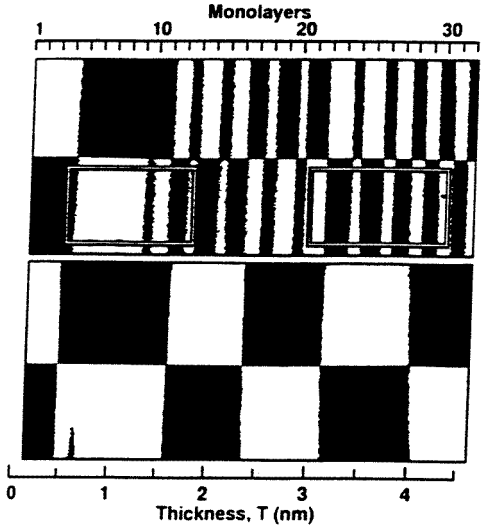


(b)

**Figure 34.** (a) A schematic view of the sample structure used in the experiment of Unguris *et al* (1991). An Fe overlayer was deposited on a Cr wedge that had previously been evaporated on an Fe(001) single-crystal whisker. The arrows in the Fe show the direction of magnetization in each domain. (b) SEMPA images showing the difference in the magnetic coupling of the Fe layers in the Fe/Cr/Fe sandwich for the Cr wedge grown at room temperature (lower panel) and at elevated temperatures (upper panel).

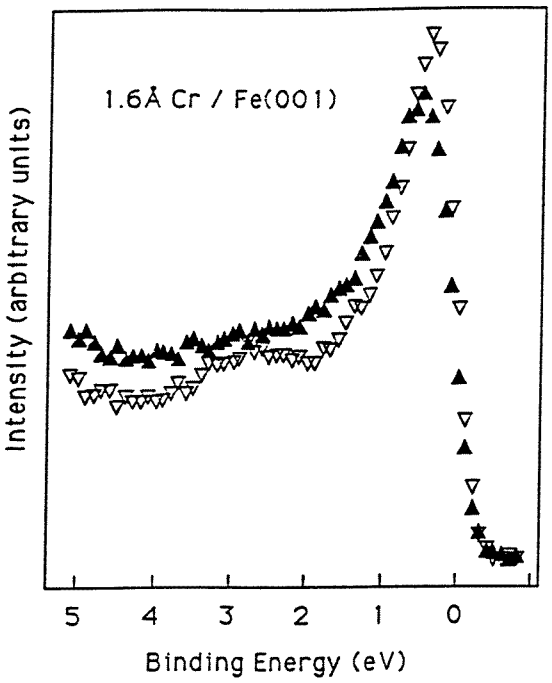


**Figure 35.** Spin-polarized spectra recorded from approximately one monolayer (1.6 A) Cr deposited on an Fe(001) substrate. The incident photon energy is 52 eV, an energy at which a local minimum occurs in the Fe 3d cross section.

Chromium has an identical lattice structure to Fe but its half-filled d-band results in the antiferromagnetic rather than ferromagnetic state representing the lowest energy configuration. In the bulk crystal each atom is antiferromagnetically coupled to its nearest neighbour so that every (001) plane is ferromagnetically aligned within the plane but antiferromagnetically aligned to neighbouring (001) planes. Calculations indicate that a Cr monolayer deposited on an Fe(001) substrate will also be ferromagnetically aligned within the plane but antiferromagnetically aligned to the substrate (Victora and Falicov 1985b, Fu *et al* 1985, Johnson *et al* 1993). The calculations also predict that the moment on the Cr site is considerably enhanced $3.1\mu_B$ as opposed to the $0.6\mu_B$ characteristic of bulk Cr.

In a separate tight-binding study of the development of thicker Cr films Xu *et al* (1995a) found that the growth of chromium proceeded with each new Cr layer aligning antiferromagnetically with respect to the preceding one. This result is consistent with experimental studies that have shown antiferromagnetic layer-by-layer growth (Unguris *et al* 1992). The study of Xu *et al* (1995a) found that throughout the growth of the film the surface layer of Cr always supports an enhanced moment of the order of $2.1\mu_B$ and that the inner layers have a moment that slowly relaxes towards a value characteristic of bulk Cr as the films become thicker. An almost identical result has been reported in another tight-binding study by Stoeffler and Gautier (1995).

Spin-polarized photoemission studies have in part confirmed these theoretical predictions. A valence band study was unable to conclude anything about the size of the moments, but did confirm the prediction of a Cr derived interface state at a binding energy close to the Fermi level for the monolayer coverage (Johnson *et al* 1993). As shown

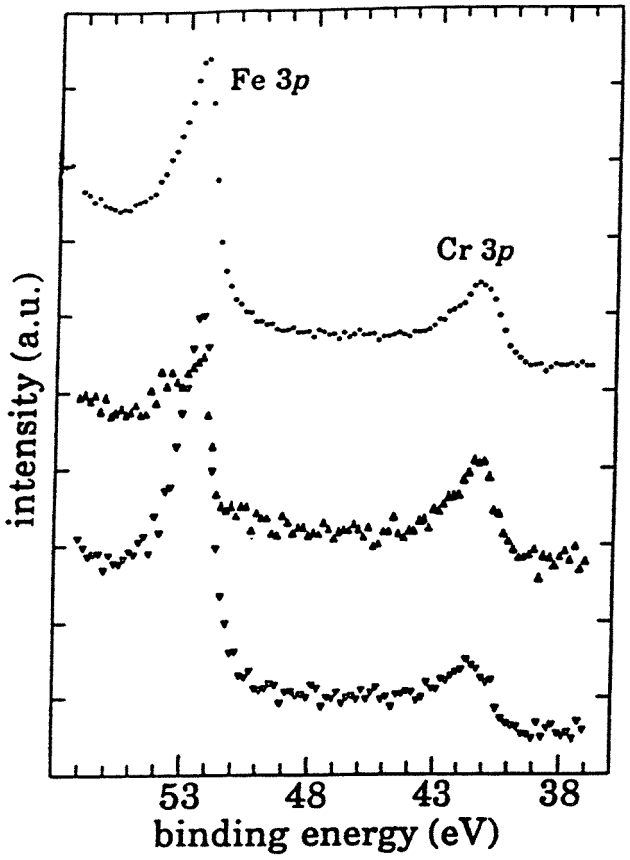


**Figure 36.** Spin-integrated and spin-resolved photoemission spectrum recorded from 1.5 A Cr deposited on Fe(001) showing the Fe 3p and Cr 3p core levels. The incident photon energy for these spectra was 117 eV.

in figure 35 this minority spin state of $d_{z^2}$ character has its charge density split equally between the Cr overlayer and the Fe surface layer. For comparison these spectra recorded from the Cr monolayer may be compared with the spectra from the clean Fe(001) surface that were reproduced earlier in figure 26(a). In both cases the spectra were recorded under nearly identical conditions.

Two spin-polarized core level photoemission studies of the Cr 3p level have shown that the initial monolayer is indeed ferromagnetically aligned within the layer and antiferromagnetically aligned with respect to the substrate (Hillebrecht *et al* 1992, Xu *et al* 1995a). Both of these studies were carried out on Cr films deposited on a thick Fe(001) film that had previously been grown on a Ag(001) substrate. Shown in figure 36, the core level study of Hillebrecht *et al* (1992) concluded that the magnetic moment on the initial layer was in the range 0.6–1.0$\mu_B$. A similar result was obtained in a MCD study where it was concluded that in the submonolayer range the magnetic moment on the Cr site was identical to that for bulk Cr, 0.6$\mu_B$ (Idzerda *et al* 1993). Unfortunately structural studies indicate that at room temperature the growth of Cr on Fe(001) does not proceed in a simple layer-by-layer fashion. Rather, in a recent scanning tunnelling microscopy (STM) study,

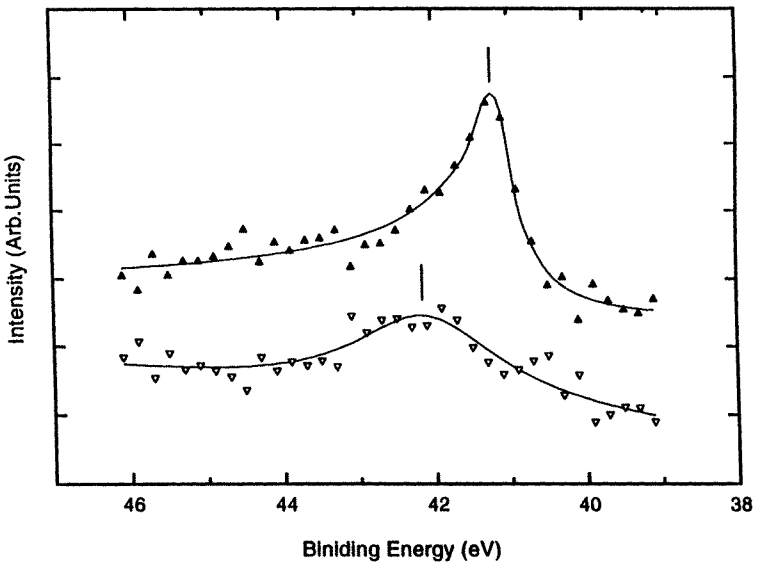


**Figure 37.** Spin-resolved Cr 3p spectra recorded from 0.6 ML of Cr deposited on Fe(001). The incident photon energy is 250 eV.

Pierce *et al* (1994) were able to demonstrate that the initial growth proceeded with the formation of islands. By increasing the substrate temperature the size of the islands or platelets increased but at temperatures above 300 °C interdiffusion of Cr and Fe occurs at the interface.

Reproduced in figure 37, the second spin-polarized photoemission study of Xu *et al* (1995a) was able to obtain a measure of the Cr 3p spin polarization at a lower coverage corresponding to 0.6 ML. For this coverage it was concluded on the basis of island growth that the magnetic moment on the Cr site was at least $1.8\mu_B$, a result that was in good agreement with the findings of studies of this system using spin-polarized electron-loss spectroscopy (Walker *et al* 1992) and energy-resolved spin-polarized secondary-electron emission (Fuchs *et al* 1996). It is clear that the growth of Cr on Fe represents a complex system and that more studies will be helpful. Indeed, Stoeffler and Gautier (1995) have recently considered the role of a monatomic step on the Fe substrate. They find that the influence of the step is limited to its own immediate vicinity with a small extension in the plane of the Cr layers. However, a wall that is generated in the Cr by the step splits the Cr layer into two domains thereby frustrating the antiferromagnetic ordering and reducing the average magnetic moment on the Cr site. Such effects combined with island formation will clearly add complexity to any experimental measurement.

Mn films grown on Fe(001) are predicted to show extremely complex magnetic behaviour (Wu and Freeman 1995). These authors find that for submonolayer coverage the moments on the manganese sites are aligned antiparallel to those of the iron substrate. As the coverage approaches one monolayer, antiferromagnetism within the Mn layer itself becomes the lowest energy configuration. This antiferromagnetic structure is predicted to drive a c(2 × 2) buckling reconstruction within the overlayer. With the formation of a Mn bilayer the moments on the Mn layer closest to the interface now align parallel to those of the substrate. The two Mn layers are coupled antiferromagnetically as found for adjacent

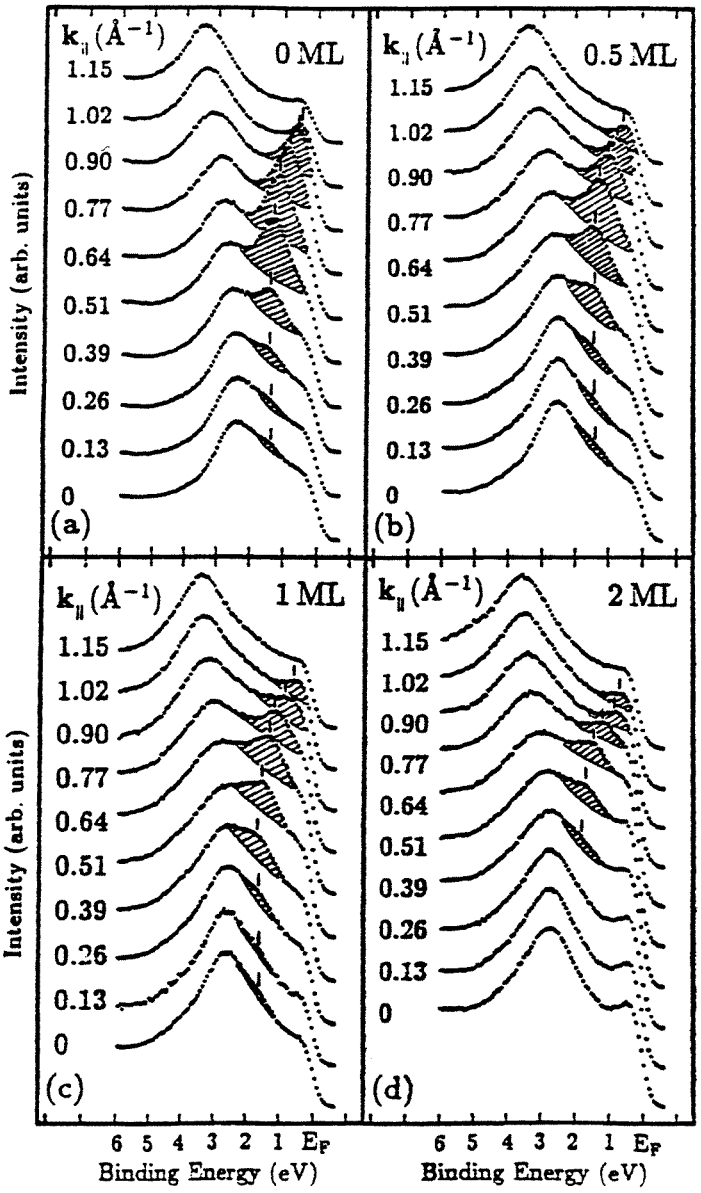


**Figure 38.** Spin-intgerated spectra recorded as a function of $k_{\|}$ from Fe films of different thickness deposited on a Pd(001) surface. The hatched area indicates the surface state on the clean surface that evolves into an interface state.

layers in the Cr films. The parallel alignment in the interface has also been predicted in calculations of the magnetic configuration in FeMn multilayers (Purcell *et al* 1992, Stoeffler and Gautier 1993).

Several aspects of these calculations have been supported by experiment. A SPEELS study (Walker and Hopster 1993) found that initially the Mn aligns antiferromagnetically with respect to the substrate and beyond 5 ML each Mn layer is antiferromagnetically

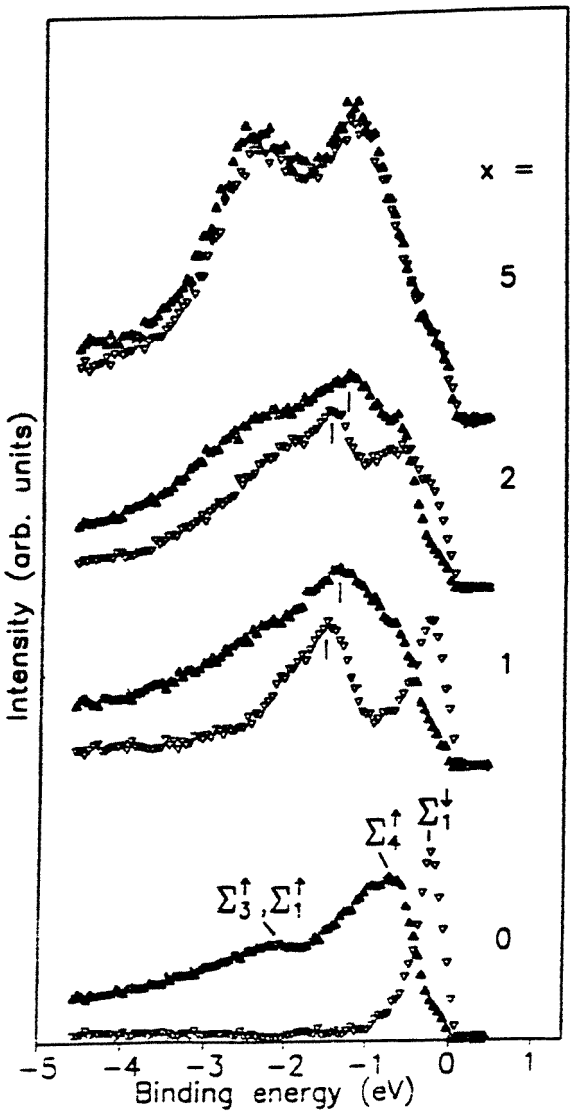


**Figure 39.** Spin-resolved spectra recorded from different thicknesses ($x$ atomic layers) of Pd deposited on an Fe(110) surface. The majority and minority spin spectra are indicated by the full up triangles and open down triangles, respectively. The incident photon energy is 21.2 eV.

coupled to the previous layer. For thicknesses less than 5 ML the authors concluded that the outer Mn layer was antiferromagnetically aligned with respect to the substrate.

In a spin-polarized core level photoemission study Roth *et al* (1995) found a net majority spin polarization in the Mn 3p core level for submonolayer coverage. This observation is again a clear indication that in this regime the Mn aligns antiferromagnetically with respect to the Fe substrate. At a film thickness close to one monolayer the authors claim, on the basis of a local minimum in the measured spin polarization, to have found evidence for the predicted antiferromagnetic ordering within the Mn layer. Measuring the spin polarization in the Fe 3p level Roth *et al* further concluded that at the monolayer coverage, the Fe

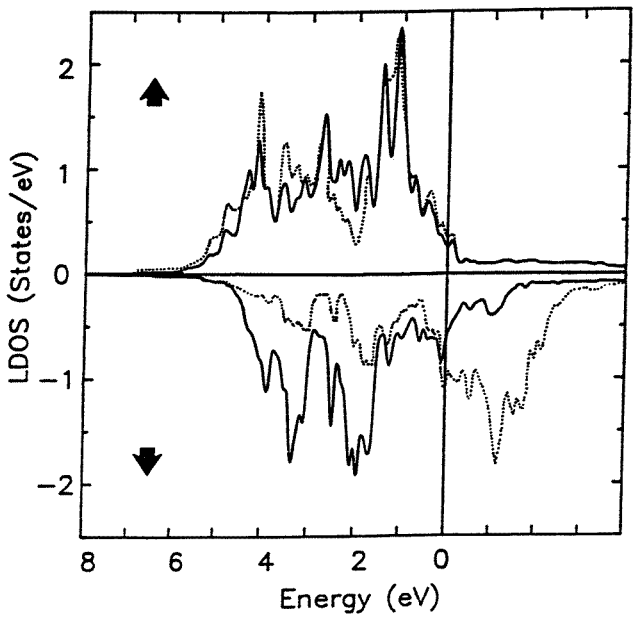


**Figure 40.** FLAPW calculation for a Pd/7Fe(001)/Pd slab. Layer-resolved majority spin (↑) and minority spin (↓) density of states of the Pd overlayer on Fe(001) (full curve) and of the topmost Fe layer underneath the Pd (dotted curve).

interfacial moment did indeed decrease as predicted in the calculations. However, they did not observe the anticipated increase in the Fe moment with the formation of the Mn bilayer.

Co films grown on both Cu and Ni substrates have been studied. In a SPES study of Co films grown on a Cu(001) substrate Clemens *et al* (1992b) found that the exchange splitting of the Co $\Delta_5$ bands increased as the films became thinner. As we noted earlier, such an observation is consistent with the idea that the magnetic moment increases as the dimensionality of the system decreases (Freeman and Wu 1991). Some insight into the Cu/Co(001) interface also comes from MCD studies of copper films deposited on a Co(001) substrate (Samant *et al* 1994, Held *et al* 1996). Here the authors were able to demonstrate that a small magnetic moment of the order of $0.05\mu_B$ exists on the copper interfacial site. However, on moving away from the interface the copper moments rapidly decrease.

An inverse photoemission study of Co films grown on a Ni(001) substrate reported the possibility of an unoccupied interface state existing 0.55 eV above the Fermi level (Hwang and Himpsel 1995). This conclusion was based on the observation that the intensity in this part of the spectrum builds up on a length scale of 2.4 A, a value which is considerably shorter than the 4–5 A that might characterize the mean free path of the electrons at the incident energies used. Unfortunately no calculations currently exist that might support this experimental observation.

We have already discussed the study of bcc Ni films grown on Fe(001) by Brookes *et al* (1992). In the same study the authors examined the evolution of the electronic structure from the ultrathin regime through to the thicker films. They reported that in the thinnest films (<4 ML) the photoemission spectra showed distinct characteristics suggestive of unique interfacial properties. Indeed, a first-principles FLAPW calculation for one- and two-layer Ni films on Fe(001) (Lee *et al* 1993) shows that there are strong hybridization

effects between the iron and nickel d-bands which lead to an interfacial iron moment that is enhanced slightly with respect to the bulk but lower than that characteristic of the clean Fe(001) surface. They report interfacial moments of $2.65\mu_B$ on the iron site and $0.86\mu_B$ on the nickel site for the one-monolayer film and $2.59\mu_B$ on the iron site and $0.69\mu_B$ on the nickel sites for the two-monolayer film. Interestingly both the experiment and calculation place even symmetry states exchange split by approximately 0.5 eV immediately below the Fermi level for the two-monolayer film.

### *6.2. The 3d–4d interfaces*

The Pd/Fe interface has been the subject of a number of studies both with Fe as the substrate (Weber *et al* 1991, Rader *et al* 1992, Hartmann *et al* 1993) and with Pd (Rader *et al* 1994) as the substrate. In both cases, if we consider the (001) direction, calculations predict that the Pd atoms in the interface will have a local moment of the order of $0.3\mu_B$ (Huang *et al* 1986, Rader *et al* 1992, 1994).

Liu and Bader (1991) have studied the temperature dependence of the magnetization of Fe films deposited on Pd(001). They report that samples grown at 100 °K have a vertical easy axis, samples grown at 300 °K have an in-plane easy axis. However, the thickness dependence of the Curie temperature $T_c$ is independent of the spin orientation of the sample.

As shown in figure 38, a spin-polarized photoemission study of Fe films deposited on Pd(001) at room temperature by Rader *et al* (1994) revealed that a non-magnetic surface state associated with the Pd surface evolved into a magnetic interface state localized in the interface between the Fe and Pd. As a working definition the authors chose to define a state as an interface state if it has approximately 50% of its charge density located on the atoms either side of the interface. The Pd surface state of even symmetry had previously been investigated in a separate spin-intgerated photoemission study (Elliot *et al* 1991). An accompanying first-principles calculation of Rader *et al* (1994) shows this state to be more than 50% localized in the surface layer. However, with the deposition of Fe the state does not disappear, a behaviour characteristic of surface states as discussed earlier, but rather evolves into the interface state at slightly higher binding energy. The calculation shows this new interface state, which has majority spin character, to be equally distributed between the Fe layer in the interface and the Pd surface layer reflecting the hybridization between Pd 4d and Fe 3d states. In fact the presence of a bandgap in the substrate helps to localize the state in the interface. The authors concluded that the interface state contributed to the development of the magnetic moment on the interfacial Pd which they calculated to be $0.32\mu_B$/atom.

There have also been studies of the reverse case, Pd films deposited on Fe substrates. In figure 39 we show an example of spin-polarized interface states observed in a study of Pd deposited on an Fe(110) surface (Weber *et al* 1991). Pd grows epitaxially on the Fe(110) surface until at a coverage close to one monolayer a phase transition results in the overlayer adopting the (111) structure. Subsequent growth proceeds epitaxially in (111) planes. In the study of Weber *et al* which represents a study of the Pd(111)/Fe(110) interface, the authors identified an interface state at a binding energy of 1.5 eV with respect to $E_F$. The interfacial character was confirmed by its lack of dispersion with $k_\perp$ as the incident photon energy was varied and the observation that its intensity saturated at 1.5 ML. The authors interpreted the spin-resolved spectra shown in figure 39 for the one- and two-monolayer coverage as an inverted exchange split pair. However, the complete identification of an exchange split pair requires the demonstration that the two spin components, majority and minority, have the same symmetry. Weber *et al* did not report such an observation in their study.

In a separate study of a Pd monolayer deposited on Fe(001) (Rader *et al* 1992), it was again shown that spin-polarized features characterizing the Pd overlayer were evident in the spectra. By examining the spin polarization as a function of coverage, these authors were able to confirm the observation made in the earlier study (Weber *et al* 1991) that the polarization of the Pd was confined to the interfacial layer. In fact the spin-polarized spectra indicated that in a 2.1 ML thick Pd film the surface layer had a moment that was already reduced with respect to that characterizing the monolayer. Through comparison with calculation, it was further determined that the magnetization induced in the Pd reflected a strong Pd–Fe interaction rather than a lateral Pd–Pd interaction. Interestingly, a monolayer of Pd on non-magnetic Ag(001) has been predicted to be paramagnetic even though the expansion of the Pd lattice is larger than that associated with Pd on Fe(001) (Blugel 1992). Because of the large exchange splitting in the substrate, the authors found that the interaction of the Pd is stronger in the majority spin channel than the minority spin channel. This in turn results in the majority spin states in the overlayer being distributed over a larger range in binding energy than those states of minority spin character. Shown in figure 40 their first-principles calculation indicated that the Fe interface moment for this system was $2.69\mu_B$, significantly larger than the bulk value of $2.15\mu_B$. A moment of $0.29\mu_B$ was calculated on the Pd sites for the monolayer coverage.

A similar result was found in a study of a Rh monolayer on Fe(001) (Kachel *et al* 1992). Here, because of the atomic size mismatch between Rh and Fe (7.7%), the growth mode is layer by layer but not epitaxial. However, from the observation of spin polarization it was concluded that the Rh was ferromagnetic as suggested in the authors' first-principles calculations which indicated a moment of $0.82\mu_B$ on the Rh site. Kachel *et al* concluded that, as in the case of Pd, the spin polarization reflected the strong hybridization between the Rh 4d bands and the substrate 3d bands.

An interaction of the overlayer 4d bands with the substrate 3d bands was also identified in a study of Ag films grown on an Fe(001) substrate (Brookes *et al* 1994). Here it was shown that a spin polarization was observable in the Ag 4d bands at the monolayer limit, but that this spin polarization disappeared with the development of the second layer. The authors concluded, however, that some interfacial interaction probably remained even in the thicker silver films. In the case of Ag, the d-bands are essentially full and any induced magnetic moment due to the interfacial hybridization will be small. Indeed, at the monolayer coverage, calculations predict a moment on the silver site of only $0.08\mu_B$ (Ohnishi *et al* 1984).

The studies of Ag on Fe(001) also revealed evidence of a well defined minority spin interface state reflecting the interaction of the silver s–p bands with the Fe d-bands (Brookes *et al* 1991, Vescovo *et al* 1995b). Brookes *et al* suggested that this interface state, shown in figure 41, evolved from the Fe(001) minority spin surface state at a binding energy of 2.4 eV that we have previously discussed in section 5.1. As we have already noted the idea of a surface state evolving into an interface state has also been discussed in connection with the Fe/Pd(001) interface (Rader *et al* 1994). Calculations indicate that the Ag/Fe(001) interface state is more than 67% localized in the interface with almost equal weight on the interfacial Fe and the silver layer. Brookes *et al* found that with the deposition of a second layer of Ag the interface state at a binding energy of 1.7 eV disappeared and a new state appeared at a binding energy of 1.0 eV. Discussed in more detail later, this new state represents the development of a quantum well state with significant weight in the silver layers.

Vescovo *et al* (1995b), who produce a Ag monolayer by annealing an Fe film deposited on a Ag substrate, have identified a second minority spin interface state at the point in the substrate surface Brillouin zone corresponding to the $\bar{X}$ point and a third minority spin

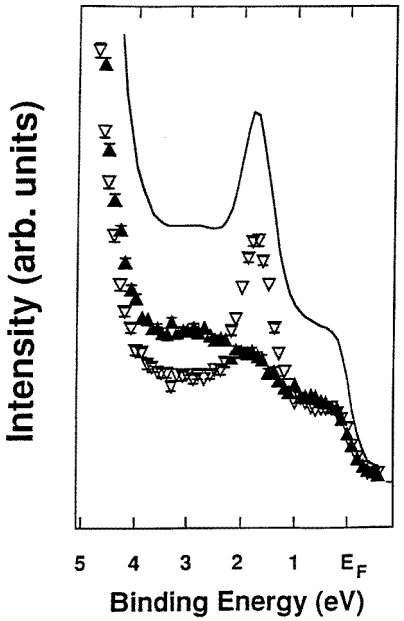


**Figure 41.** Spin-polarized photoemission spectra recorded along the surface normal for one monolayer of Ag deposited on Fe(001). The spin-intgerated spectrum is indicated by the full curve; the majority and minority spin components by full and open triangles, respectively.

feature localized around $\bar{\Gamma}$ the centre of the zone. By comparison with calculation they show that the state at $\bar{X}$, derived from a clean Fe surface state, again has significant weight within the interface. The third state at $\bar{\Gamma}$ is reported to be strongly localized in the Fe interface layer. However, we note that the latter state is not observed in the earlier study of Brookes *et al* where the silver monolayer is produced by evaporation on an Fe substrate.

### *6.3. The 3d–5d interfaces*

There have been a few studies based on 3d–5d interfaces. We have already discussed in section 4.1.3 a study by Kamper *et al* (1989) of the thickness dependence of the spin- and angle-resolved photoemission from Ni(111) films deposited on W(110). By varying the incident photon energy the authors monitored the behaviour at different points along the Γ–L line running normal to the surface. At points corresponding to $k \sim 1/3$(Γ–L) and $1/2$(Γ–L) they found little variation in the exchange splitting as the thickness of the film was reduced. However, at the point corresponding to $k \sim 2/3$(Γ–L) they found that the exchange splitting showed a continuous reduction with film thickness. Indeed, for a film thickness of $d = 4$ ML the exchange splitting had practically vanished. As we noted earlier these observations were consistent with the fact that the Curie temperature of thin films scales with the thickness of the film. Thus in this picture the magnetic disorder introduced by the reducing Curie temperature as the film thickness decreases results in $k$-dependent behaviour similar to that observed in bulk Ni(111) as the temperature is raised.

A similar result has been obtained in studies of the development of the spin-polarization properties of one- to three-monolayer films of p(1 × 1) Fe on W(001) (Fink *et al* 1991).

LEED studies of this system indicate that the growth is epitaxial. In the thinnest films corresponding to submonolayer coverage no in-plane remanent spin polarization was observed at a temperature of 115 K. However, SMOKE studies of this system indicated that for a 1.5 ML thick film $T_c$ had risen to approximately 320 K. Thus at a coverage of two monolayers and again at a temperature of 115 K the authors observed an exchange splitting of 2.15 eV for the $\Gamma'_{25}$ states similar to that observed for bulk Fe(001). A follow-up study examined the spin polarization in the Fe 3p core levels for this system (Mulhollan *et al* 1992a). In the thinnest films the spin polarization was again observed to vanish. Thus unlike the observations in the study of Co films deposited on Cu(001) (Clemens *et al* 1992a) in the case of the Fe films on W(001) the hybridization with the broad substrate bands outweighs the effects of the reduced dimensionality in the overlayer. This in turn results in the magnetic moments in the overlayer being reduced rather than enhanced in the thinnest films.

### *6.4. Rare-earth thin films*

Carbone and Kisker (1987) have studied the Gd/Fe(001) interface. They found that the Gd $4f^7$ emission was predominantly in the minority spin channel, an indication that the Gd spin moments were antiferromagnetically coupled to the Fe substrate. This observation had previously been made in a separate study of the same system using spin-resolved Auger electron spectroscopy (Taborelli *et al* 1986). A second spin-polarized photoemission study (Carbone *et al* 1990) reported antiparallel coupling of Gd, Tb, Dy and Nd monolayers deposited on Fe(001).

A spin-polarized photoemission study of the Sm/Fe(001) interface (Vescovo *et al* 1992) found that up to the monolayer coverage the Sm is trivalent with the in-plane spin moment of the 4f electrons antiparallel to the Fe 3d majority spin direction. To maximize the sensitivity to the 4f levels at low coverage, the authors used photon energies in the vicinity of the 4d→4f giant resonance close to the Sm 4d core level threshold. With increasing coverage the study indicated that the Sm develops a divalent surface layer with the underlying layers remaining trivalent. However, the in-plane ferromagnetic ordering was observed to rapidly decrease with increasing overlayer thickness and to vanish three atomic layers from the interface.

### *6.5. Non-magnetic thin films*

The previous discussion has considered systems where the spin polarization results from the exchange interaction either in the substrate or in the overlayer itself. In this section we will briefly examine studies of thin films where the spin polarization in the film reflects the spin–orbit interaction.

In a series of papers, Heinzmann and co-workers (Schmiedeskamp *et al* 1988, Stoppmanns *et al* 1991, Schmiedeskamp *et al* 1992) have examined the electronic structure of an Au monolayer deposited on Pt(111) using incident circularly and linearly polarized light. The observation of spin-polarized photoelectrons for incident s-polarized light is predicted only if the surface possesses a threefold rotational axis (Tamura *et al* 1987). Experimentally, this prediction was verified in a study of the Pt(111) surface by Schmiedeskamp *et al* (1988). These authors observed a spin polarization of more than 30% parallel to the surface. The polarization displayed a sinusoidal behaviour with the rotation angle $\omega$ about the Pt(111) surface normal and a 120° periodicity according to the threefold symmetry of the surface.

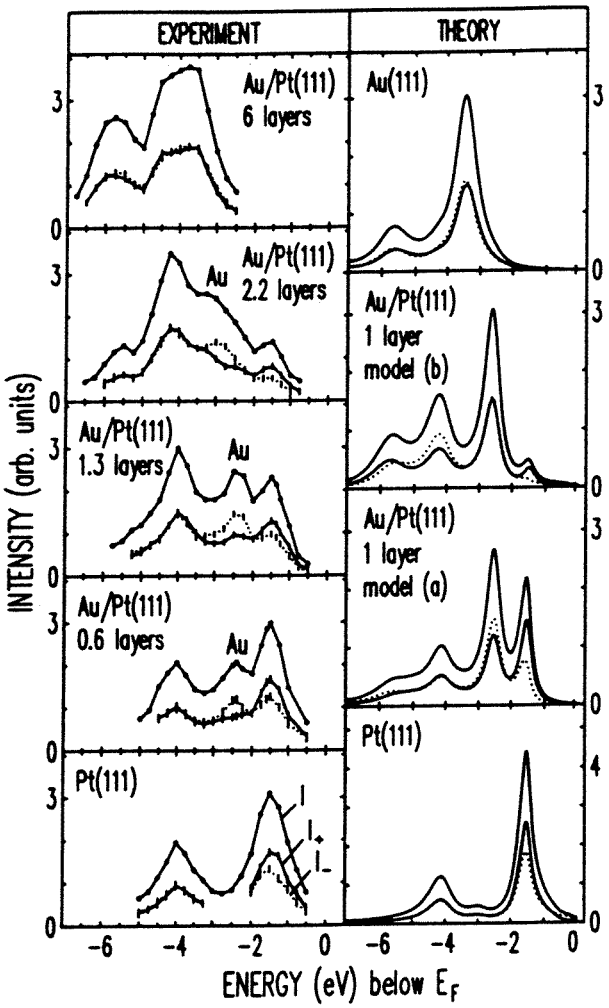


**Figure 42.** Spin-resolved photoemission spectra obtained for normal incidence of linearly polarized radiation (21.2 eV) and normal electron emission (left panel). Experimental spectra for Pt(111) and different Au coverages. The vertical dashes for $I+$ and $I-$ represent error bars including the uncertainty in the polarization of the incident light and the uncertainty in the detector asymmetry function (right panel). Calculated spectra for Pt(111) (bottom), Au(111) (top) and a monolayer Au adsorbate on Pt(111) for two different adsorption models: (a) in direct continuation of the Pt(111) lattice and (b) coinciding with the second Pt layer, i.e. opposite stacking sequence.

Stoppmanns *et al* (1991) used linearly polarized light to investigate the properties of an Au film deposited on the Pt(111) surface. Shown in figure 42, the authors identified in their photoemission spectra a spin-polarized Au derived feature at a binding energy of 2.5 eV for coverages in the vicinity of a monolayer. By comparing with calculations they were able to show that this state of $\Lambda_{45}$ double group symmetry had significant weight on both the gold layer and the surface Pt layer. Indeed, it might be more appropriate to describe it as an interface state. The authors were also able to show that the presence of this state was an indication that the gold atoms had occupied the site that would be available to the next Pt atom rather than modifying the sequence of stacking.

In a later study, circularly and linear polarized light were both used to investigate this system still further (Schmiedeskamp *et al* 1992). A second state at a binding energy of 5.7 eV below $E_F$ was identified in this study. The authors were able to show that the latter state was strongly localized in the Au layer. The observation of a strong spin polarization in the state for incident linearly polarized light was taken as evidence that either the initial state in the Au layer or the corresponding final state has strong threefold rotational symmetry.

Frentzen *et al* (1996) have recently reported a study of Au films deposited on Ag(111) using incident circularly polarized light. They reported the observation of 'confined' two(four) Au derived states for 1 ML (2 ML) thick films. However, on the basis of calculation it was concluded that intermixing of the Au and Ag was very likely. In the following section we will discuss the concept of confined states in more detail.

### *6.6. Quantum well states and magnetic multilayers*

Several magnetic multilayers consisting of ferromagnetic layers spaced by non-magnetic layers are known to exhibit an oscillatory exchange coupling between the adjacent ferromagnetic layers dependent on the thickness of the intervening spacer layer. The first observation of such exchange coupling was made in the Fe/Cr multilayer system (Grunberg *et al* 1986). Parkin *et al* (1990) later extended this observation with the demonstration that the antiferromagnetic coupling was, in fact, oscillatory, a behaviour that was identified and characterized in a number of other systems. Associated with the coupling, the multilayers have also been shown to exhibit a giant magnetoresistance (Baibich *et al* 1988). The potential technological applications of systems with these properties have spawned an enormous amount of research (Falicov 1992).

The early observations posed a dilemma however. Whilst the oscillations in the exchange coupling appeared 'RKKY-like', the period length was too long to be explained by such a theory. Indeed, within the RKKY framework, treating the non-magnetic layer as a free-electron gas resulted in a predicted period length of 1 atomic layer (AL), as opposed to the frequently observed 5–6 AL. A clearer picture emerged in a number of new theories which acknowledged the periodicity of the potential within the non-magnetic spacer (Bruno and Chappert 1991). These theories have shown that the observed period lengths are inversely related to spanning vectors characterizing the appropriate Fermi surface of the spacer layer. This is illustrated in figure 43 where the free-electron Fermi surface of a monovalent metal equivalent to copper is compared with the actual Fermi surface of copper. As will be discussed later the characteristic 'dog-bone' in the Fermi surface of figure 43(b) leads to two periods of oscillation.

An alternative approach to the problem recognizes that the multilayer is in fact composed of a series of thin films or quantum wells. In particular, the intervening non-magnetic layers are represented as quantum wells with electrons confined between the adjacent ferromagnetic layers (Edwards *et al* 1991). As in any one-dimensional quantum well, the binding energies of the confined electron states and the related coupling reflect the width of the well. Quantization effects have long been studied in semiconductor heterostructures (Weisbuch and Vinter 1991). They have also been extensively studied in thin metallic films (Miller *et al* 1988, Lindgren and Wallden 1988).

To examine the properties of these metallic thin films we first consider the film as a free electron gas trapped in the one-dimensional quantum well defined by the crystal potential of the substrate on one side and the vacuum barrier on the other. In the vicinity of the crystal barrier the wavefunction of the electron states in the well take the form

$$\Psi = \mathrm{e}^{-\mathrm{i}k\cdot z} + r_c\,\mathrm{e}^{\mathrm{i}\phi_c}\,\mathrm{e}^{\mathrm{i}k\cdot z} \tag{33}$$

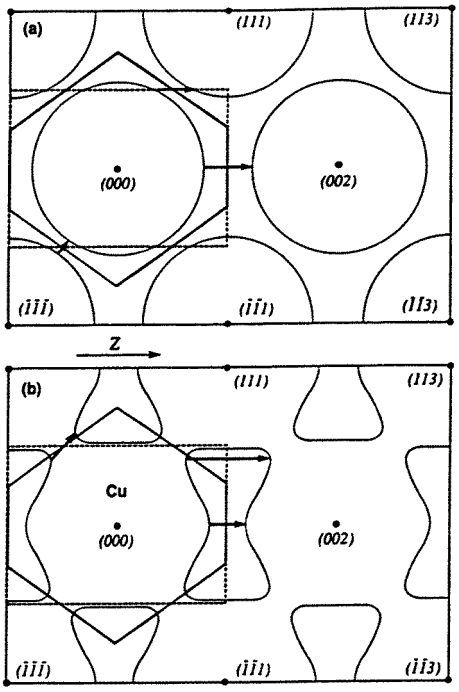


**Figure 43.** $(1\bar{1}0)$ cross section of the first Brillouin zone and of the Fermi surface (FS) for an fcc spacer. The upper part (a) shows the free-electron FS of a monovalent metal such as Cu and the lower part (b) shows the actual FS of Cu. For the [001] orientation there are two periods of oscillation as determined by the spanning vectors indicated with bold arrows.

where $r_c\,e^{i\phi_c}$ represents the complex reflectivity at the interface with the substrate. Matching to the logarithmic derivative of the crystal wavefunction, $L_C$, leads to the condition $\tan(\phi_c/2) = -(L_c/k)$. Moving to the other side of the well, matching logarithmic derivatives leads to a similar expression for the phase change $\phi_B$ at the vacuum or image barrier. Thus $\tan(\phi_B/2) = (L_B/k)$ with $L_B$ the logarithmic derivative of the wavefunction associated with the image barrier. A stationary or bound state exists whenever the total phase change within the well is given by

$$\phi_c + 2kma + \phi_b = 2\pi n. \tag{34}$$

Here $2kma$ represents the phase change accumulated on the round trip across a well consisting of $m$ atomic layers with interlayer spacing $a$.

This description has been applied in studies of noble metal films deposited on noble metal substrates where the potential well is defined by the bandstructure offset of the two metals involved. As an example, Miller and co-workers (1988) have studied the quantization of the Ag sp-band in Ag films deposited on a Au(111) substrate. Here the potential barrier was provided by an offset of 1 eV between the $L_4$ critical points for Au and Ag. Lindgren and Wallden (1987, 1988) have applied a similar model to the study of alkali metal films deposited on a Cu(111) substrate.

Quantum well states in a noble metal thin film deposited on a ferromagnetic substrate were first observed in silver films deposited on an Fe(001) substrate (Brookes *et al* 1991). In section 6.2, we discussed this system in connection with interfacial magnetism in the ultrathin regime. As the films become thicker than one monolayer, photoemission studies

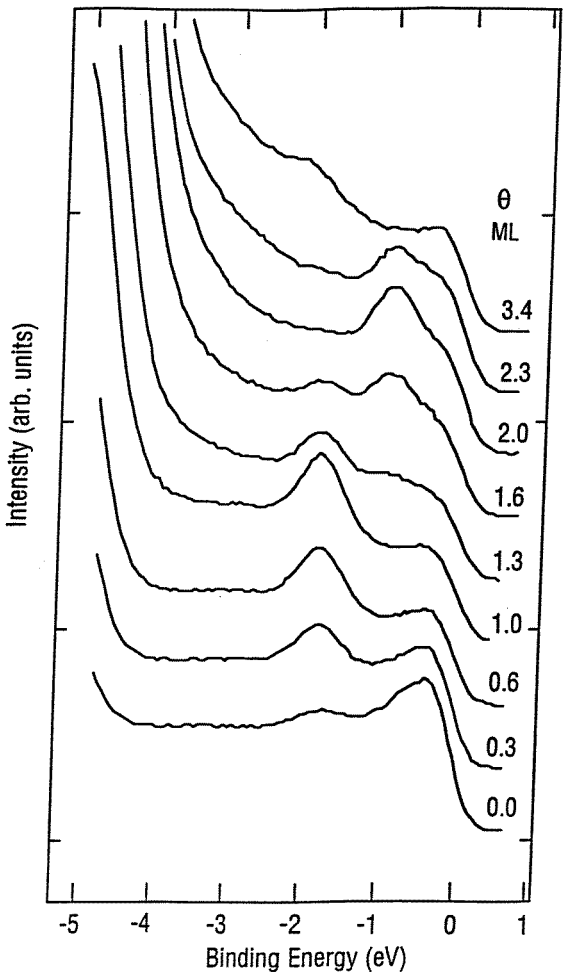


**Figure 44.** Spin-integrated photoemission spectra recorded along the surface normal from different thickness silver films deposited on an Fe(001) substrate as indicated. In the 3.4 ML thickness spectrum quantum well states corresponding to the 3 ML thickness and the 4 ML thickness can be seen at the Fermi level and a binding energy of 2.0 eV, respectively.

show that the interface state evolves into a series of states that move up to and through the Fermi level as shown in figure 44. The movement to lower binding energy simply reflects the fact that with each new layer the wavefunction describing the quantum well state has to gain an extra half-wavelength to accommodate the new atomic potential (Smith *et al* 1994). Thus the quantization condition of equation (34) becomes

$$\phi_c + 2(k + \Delta k)(m + 1)a + \phi_b = 2(n + 1)\pi. \tag{35}$$

The spin-polarized photoemission study of Brookes *et al* (1991) revealed that the Ag quantum well states are highly spin-polarized, preferentially with minority spin. This observation of a strong spin polarization can be explained in terms of the spin-dependent reflectivities at the interface with the ferromagnetic substrate. If one considers the spin-dependent bandstructure of iron in the ΓH direction, figure 45, one observes that in the

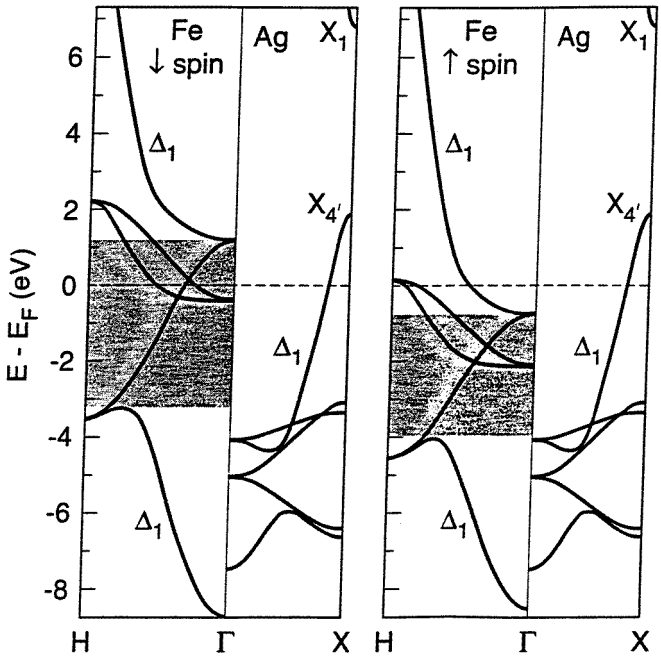


**Figure 45.** Energy bands of Fe and Ag along the Δ direction for both minority (↓) and majority (↑) spin electrons. The shaded areas indicate the range of the s–d hybridization gap in Fe for states of $\Delta_1$ symmetry.

minority spin band structure a $\Delta_1$ s–d hybridization gap exists in the vicinity of the Fermi level. At binding energies corresponding to this gap, propagating waves will be reflected back into the silver layer. Thus, it is this gap that defines the degree of confinement of the minority spin quantum well state. In the majority spin band structure, on the other hand, the hybridization gap is displaced to higher binding energies and the majority spin states in the silver layer in the vicinity of the Fermi level will be less strongly confined. The quantum well states that survive in the silver layer will, therefore, preferentially carry minority spin as observed experimentally.

Subsequent inverse photoemission studies have tracked the same states as they continue to evolve above the Fermi level eventually converging on the bulk $X_{4'}$ critical point (Ortega and Himpsel 1992, Ortega *et al* 1993). In the latter studies it was found in this and a number of other systems that the Fermi surface was sampled by the quantum well states with a frequency identical to that observed for the oscillatory exchange coupling in the associated multilayers. This is illustrated in figure 46 where the intensity observed at the Fermi level in inverse photoemission studies of copper films deposited on a Co(001) substrate is compared with the oscillatory coupling observed in the associated Cu/Co(001) multilayers.

It is relatively straightforward to show that the quantum well state sampling of the Fermi surface will be related to the period length of the oscillatory coupling and that this is not a coincidence. Consider the quantization condition of equation (34). The graphical solutions of this equation for the minority spin states in the Ag/Fe(001) system are reproduced in figure 47 (Smith *et al* 1994). Here curves of $2\pi n - \phi_c - \phi_b$ are compared with curves of $2kma$ where again $m$ represents the number of silver layers in the film. Following McRae

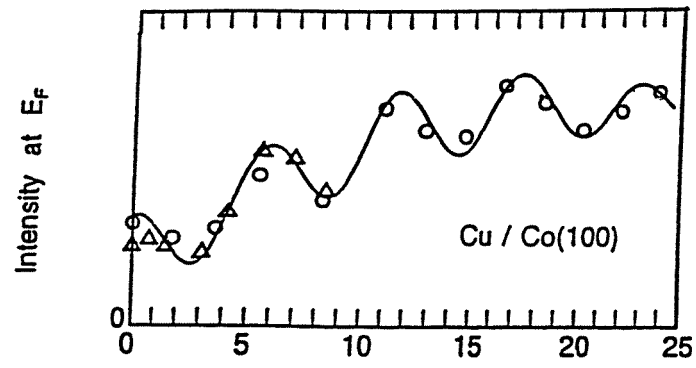


(a)

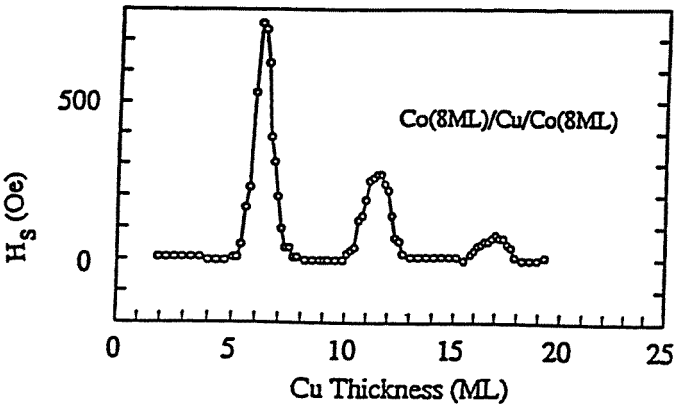


(b)

**Figure 46.** (a) Oscillations in the inverse photoemission intensity at $E_F$ for copper films deposited on a fcc Co(001) substrate from the study of Ortega *et al* (1993). (b) Results of a Kerr effect study showing the oscillatory antifferomagnetic coupling in Cu/Co(001) multilayers as a function of the copper thickness from the study of Qiu *et al* (1992).

(1979) the phase change from the image or vacuum barrier, $\phi_b$, has been generated within the WKB approximation such that

$$\phi_b/\pi = \left|\frac{3.4\ (\text{eV})}{E_V - E}\right|^{1/2} - 1. \tag{36}$$

Here the binding energy $E$ is referenced to $E_V$, the vacuum level.

The net phase change on reflection from the crystal $\phi_c$ must increase by $\pi$ on traversing the hybridization gap. Smith *et al* (1994) use the purely empirical formula

$$\phi_c = 2\arcsin[(E - E_L)/E_U - E_L)]^{1/2} - \pi \tag{37}$$

with $E_U$ and $E_L$ representing the energies of the upper and lower edges of the minority spin hybridization gap in Fe, respectively. Finally, moving away from the free electron model, the $2kma$ curves are generated from the standard two-band nearly-free electron expression for $k$, namely

$$k(E) = G^{1/2} - [(G + E) - (4GE + V_g^2)^{1/2}]^{1/2} \tag{38}$$

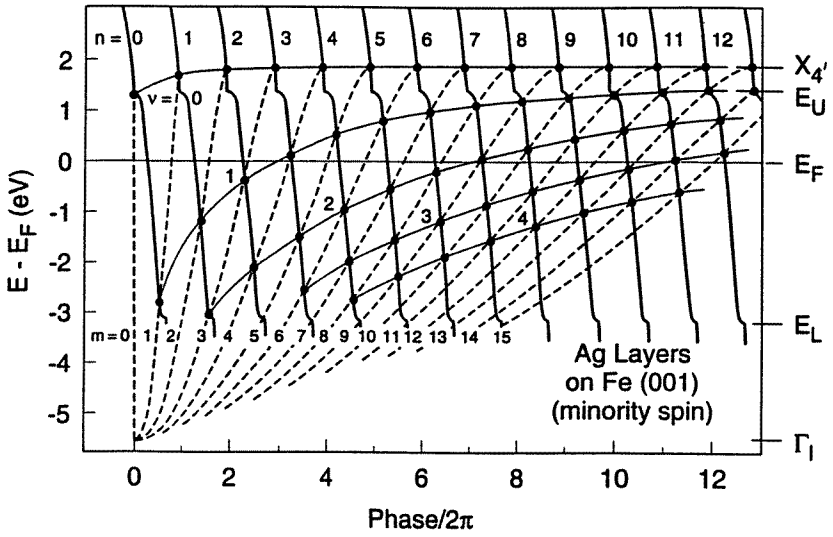


**Figure 47.** Graphical solutions (full circles) for the energies of quantum well states of Ag overlayers on Fe(001) using the phase accumulation model. Full bold waves represent the phase $2\pi n - \phi_C - \phi_B$ and dashed curves represent the quantum well phase accumulation $m2ka$. States characterized by the quantum number $v = (m - n)$ are connected by the full thin curves.

where the parameters $G = \hbar^2 k_{BZ}^2/2m$ and $V_g$ are chosen to reproduce the known band energies $\Gamma_1$, $X_1$ and $X_{4'}$ for Ag.

From the graphical solutions for the electron energies indicated in figure 47 Smith *et al* conclude that the appropriate quantum numbers for classifying the quantum well states are not $n$, the number of nodes, or $m$, the number of layers, but rather $v = m - n$. In this classification scheme the thickness against energy relationship may be written

$$\frac{D_v(E)}{a} = \frac{[\phi_c(E) + \phi_b(E)]/2\pi + v}{(1 - k(E)/k_{BZ})} \tag{39}$$

where $k_{BZ} = \pi/a$ represents the zone boundary wavevector. It is clear from equation (39) that the Fermi surface will be sampled every $\Delta m$ layers such that

$$\Delta m = (1 - k_F/k_{BZ})^{-1} \tag{40}$$

where $k_F$ represents the Fermi wavevector. Recognizing that $2(k_{BZ} - k_F)$ gives the associated bulk Fermi surface spanning vectors, $q$, one immediately retrieves from equation (40) a period length $\Delta ma$ given by $2\pi/q$, identical to that obtained by Bruno and Chappert (1991) in their analysis of the thickness dependence of the oscillatory exchange coupling in the related multilayers.

An interesting question arises as to whether or not majority spin quantum well states exist in the spin-polarized photoemission spectra recorded from the silver films deposited on the Fe(001) surfaces. Examination of figure 45 shows that in the Fe majority spin band structure the top of the s–d hybridization gap falls only 0.8 eV below the Fermi level and the top of the Ag d-bands falls 3.0 eV below. Thus one might anticipate seeing strong majority spin states in the region above the silver d-bands up to 0.8 eV below the Fermi level. In fact such states are predicted in calculations using both the phase model approach of equation (34) and the tight-binding method (Smith *et al* 1994) and *ab initio* calculations of the layered KKR type (Crampin *et al* 1996).

Experimental studies have, however, been less conclusive. Brookes *et al* (1994) examined the incident photon energy dependence of the spectra emitted from the Ag monolayer coverage. At a photon energy of 31 eV they found a majority spin peak in the spectra at a binding energy corresponding to that predicted for the majority spin quantum well state. They made the observation, however, that a bulk transition should also occur in the same vicinity. Vescovo *et al* (1995b) have also examined this system. At a silver coverage of one monolayer they identified the minority spin interface state at a binding energy of 1.8 eV but also concluded that any equivalent majority spin states were degenerate with bulk bands.

In a spin-polarized inverse photemission study of Ag on Fe(001), Crampin *et al* (1996) claim the observation of unoccupied majority spin quantum well resonances above the Fermi level for silver coverages up to four monolayers. Using lineshape fitting, they note that these resonances become sharper as they move away from the Fermi level and further into the energy range of the substrate continuum. They account for the resonance widths by extending the phase-accumulation model to complex energies identifying Im $\phi_c^*$ as the substrate parameter that governs the integrity of the quantum well levels. Here $\phi_c^*$ represents the phase change at the substrate interface associated with the reflection of a quantum well state described within the nearly-free electron framework. Above a thickness of approximately 4 ML, Crampin *et al* found that the width of a resonance scales inversely with the thickness of the film.

The spin-polarized photoemission study of Ag on Fe(001) (Brookes *et al* 1991) represented a study of the spin-polarization effects in very thin films. Indeed, at the monolayer limit it is probably more reasonable to describe the induced state as an interface state as we have discussed earlier in section 6.2. Two studies have examined the spin-polarization characteristics of quantum well states in thicker films. In both cases the studies were of copper films deposited on a fcc Co(001) substrate (Garrison *et al* 1993, Carbone *et al* 1993). As in the earlier Ag/Fe (001) study, the quantum well states shown in figure 48 were found to be highly spin polarized with minority spin. However, now the Cu films were grown to thicknesses of the order of six layers or more. In fact in a more recent study Carbone *et al* (1996) reported the observation of quantum well states in copper films of the order of 50 layers thick. At such thicknesses the escape depth of the photoelectrons ensures that the spin-polarization information in the spectrum clearly reflects emission from the Cu film itself rather than the cobalt substrate. In their study, Carbone *et al* also claimed the observation of majority spin quantum well states with considerably less intensity than the minority spin counterparts. They determined an exchange splitting of 0.15 eV between the two spin components.

A tight-binding simulation of the photoemission spectra observed in their study, led Garrison *et al* (1993) to the conclusion that the quantum well states have significant d as well as sp character. This interesting observation stems from the fact that, within the Cu film, as in bulk Cu, the s,p bands will hybridize with the d-bands of the same symmetry. This hybridization results in a small fraction of the d-electrons being carried up to and through the Fermi level and indeed in bulk Cu, approximately 3% of the d-electron manifold is unoccupied. A similar observation has also been made in a recent *ab initio* layered KKR calculation of copper films deposited on Co(001) (Van Gelderen *et al* 1996).

The observation that there is a small spin polarization in the Cu d-band, and further that this band crosses the Fermi level, is a clear indication that a small magnetic moment of d-character must exist on the Cu site, an observation that has been confirmed in a recent MCD study of Cu/Co multilayers (Samant *et al* 1994, Held *et al* 1996). Here the authors, exploiting the dipole selection rules, studied absorption at the Cu L-edge to obtain site and

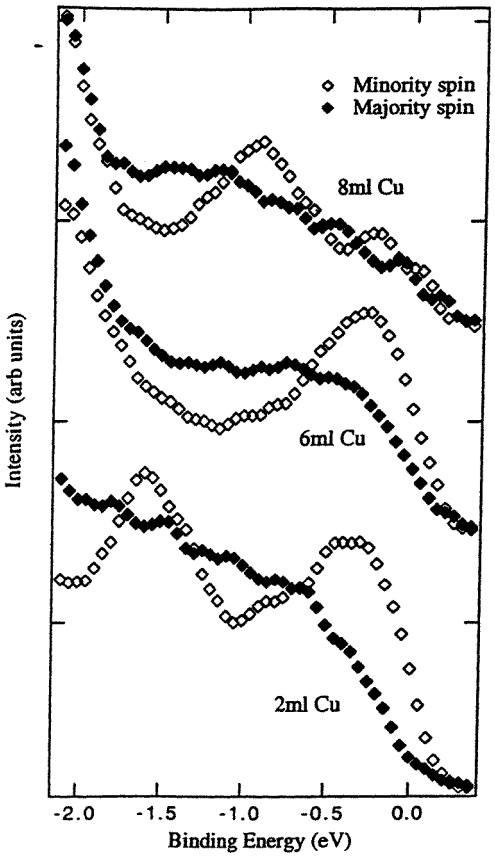


**Figure 48.** Spin-resolved photoemission spectra recorded from two, six and eight monolayer thick copper films deposited on a fcc Co(001) substrate. The minority and majority spin spectra are represented by the open and full diamonds, respectively. The spectra are recorded for photoelectrons emitted along the surface normal.

spin specific information on the unoccupied d-bands. The study found a small moment of d-character on the copper sites and further concluded that the largest moments exist in the interface where the hybridization with the neighbouring Co layers will be strongest.

As noted earlier, the strong minority spin polarization in the quantum well states is a direct consequence of the spin-dependent reflectivities in the vicinity of the hybridization gaps of the ferromagnetic substrate. Bruno (1995) has calculated these reflectivities specifically for the Cu/Co(001) system. His results are shown in figure 49. At energies corresponding to the gap the reflectivity $r^{\uparrow(\downarrow)}$ is equal to unity and the quantum well state will be completely confined. At energies outside of the gap, the reflectivity decreases and the states are no longer as strongly confined.

In fcc Co(001) the minority spin hybridization gap does not straddle the Fermi level, but is displaced to higher binding energies with the top falling 0.5 eV below the Fermi level. Strictly speaking, therefore, the electronic states that mediate the long period should be viewed as quantum well resonances rather than quantum well states. This has been clearly demonstrated in a recent theoretical study by Van Gelderen *et al* (1996). These authors found that as the quantum well state moved from the binding energy region corresponding to the

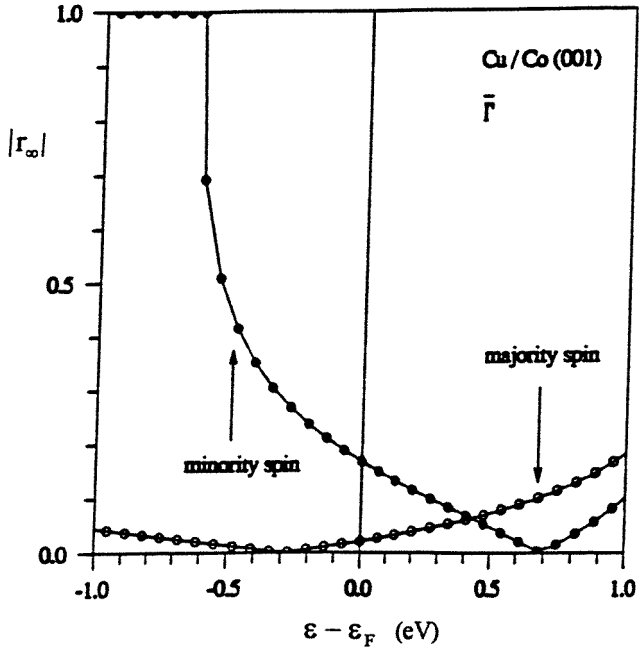


**Figure 49.** Calculated module of the spin-dependent reflection coefficient $|r_\infty|$ against energy for the Cu/Co(001) interface at the centre of the zone $\bar{\Gamma}$.

substrate bandgap into the continuum the energy width of the state broadened considerably. They also noted that with the addition of a second Co layer on the opposite side of the Cu film the width of the resonance increased even further.

As we noted earlier the Fermi surface of copper is characterized by a well defined 'dog-bone' shape. Bruno and Chappert (1991) in their analysis pointed out that the coupling in the Cu/Co multilayers should show two periods of oscillation; a long period, reflecting the spanning vector at the centre of the zone and a second shorter period reflecting a spanning vector farther out in the zone at the neck of the dog bone. These two spanning vectors are indicated earlier in figure 43. Experimentally the two periods of oscillation have been identified in Cu/Co(001) multilayers (Johnson M T *et al* 1992).

In the simplest approximation the exchange coupling in a thick well $J(t)$ is given by the difference between the sum of the energies for the spin-up and spin-down electrons in a ferromagnetically aligned sandwich and twice the energy for either spin in an antiferromagnetically aligned sandwich (Stiles 1993). Thus if $v_F$ and $k_F$ represent the Fermi velocity and Fermi wavevector, respectively,

$$J(t) = \frac{\hbar}{\pi}\frac{v_F}{2}[|R_\uparrow^\uparrow|^2 + |R_\downarrow^\uparrow|^2 - 2|R_\uparrow^\uparrow R_\downarrow^\uparrow|]\frac{1}{t}\sin(2k_F t + \phi_0) \tag{41}$$

where $R_\uparrow^\uparrow$ ($R_\downarrow^\uparrow$) is the reflection amplitude for a spin-up (-down) electron in the well reflecting from an up magnetization barrier, $R_\uparrow^\uparrow = R_\downarrow^\downarrow$ and $R_\downarrow^\uparrow = R_\uparrow^\downarrow$. It is clear from equation (41) that as the reflectivity and associated confinement increases the strength of the coupling increases. The important observation noted by several authors (Mathon *et al* 1995, Lang *et al* 1996) is that at the point in the Co substrate Brillouin zone corresponding to the neck

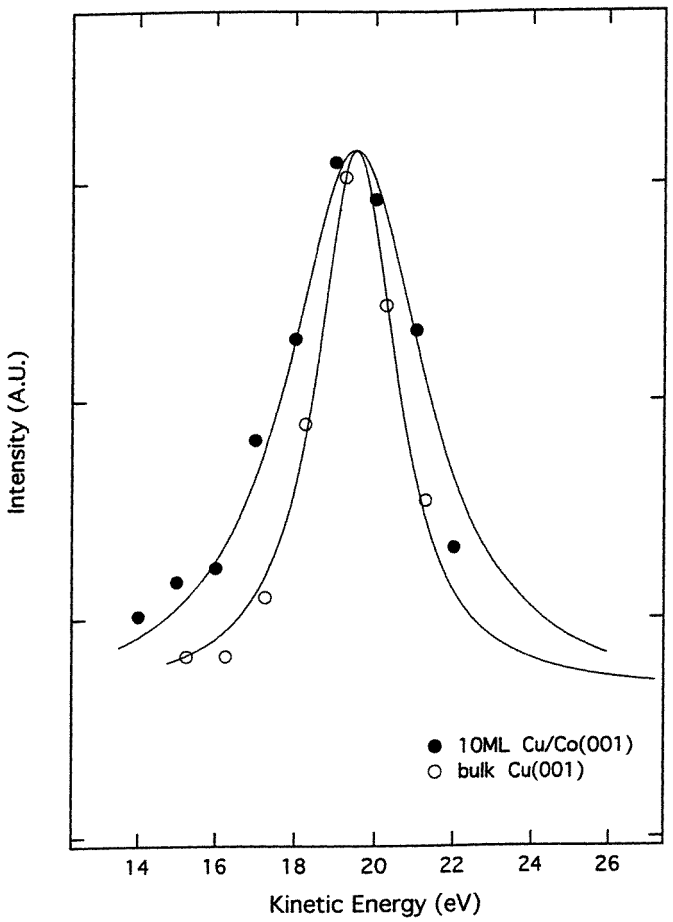


**Figure 50.** The intensities as a function of incident beam energy measured 0.6 eV above the Fermi level from bulk Cu(001) and from a quantum well state in a 10 ML Cu film deposited on fcc Co(001). The full curves represent Lorentzian fits to the experimental data.

of the Cu Fermi surface dog bone, a minority spin bandgap spans the Fermi surface. The resulting stronger confinement of the Cu quantum well states at this point should result in the short oscillation period dominating the coupling.

A recent experimental study has indeed shown that it is possible to grow samples in which the short period dominates (Weber *et al* 1995). However, in other films, the coupling showed both the long and short period of oscillation, an indication that the results can be strongly influenced by the quality of the sample, particularly the quality of the interfaces, a conclusion that has also been drawn and demonstrated in studies of the Fe/Cr multilayer system (Unguris *et al* 1991).

Two very recent studies have examined the possibility of quantum well states existing in the copper films at the appropriate point in the zone to mediate the short period of oscillation (Segovia *et al* 1996, Huang *et al* 1996). Segovia *et al* in a photoemission study of the occupied quantum well states report that the intensity at the Fermi level $E_F$ passes through a maximum with a periodicity of 14–19 ML. They suggest that this observation is consistent with the short period oscillation being sampled with a close but different

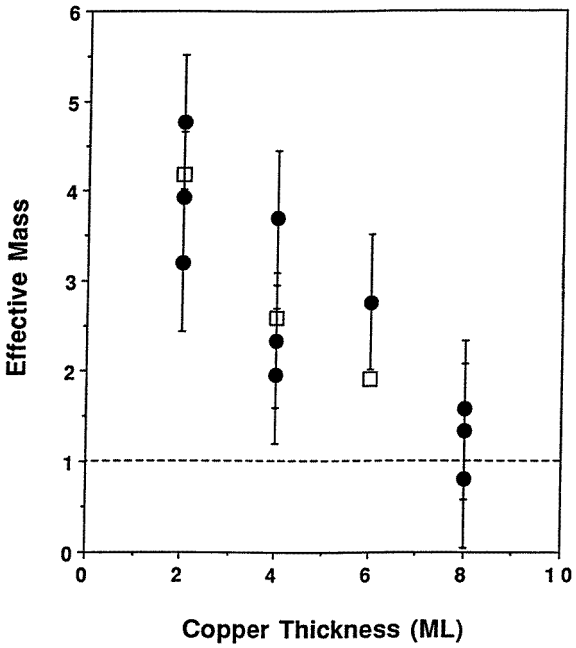


**Figure 51.** Plot of the effective masses of the quantum well states as a function of the copper film thickness in atomic layers. The full circles indicate the fits to the experimental data; the open circles indicate the results of tight-binding calculations of the effective masses. The dashed lines represents the free-electron mass.

periodicity. Whilst the idea of two close-lying frequencies producing a beating phenomena may be valid, the experimental observation is inconsistent with the model of Mathon *et al* (1995) who suggest that the photoemission intensity and the oscillatory exchange coupling are directly related to the same spectral density. Indeed this model appears to be verified at the centre of the zone as demonstrated earlier in figure 46.

In a second study Huang *et al* (1996) examined both the unoccupied states above the Fermi level with inverse photoemission and the occupied states below the Fermi level with photoemission. Their photoemission observation of states appearing close to the Fermi level for the thinner film coverages of six and nine monolayers are consistent with the observations in the higher energy resolution study of Segovia *et al* (1996). Huang *et al* suggested that the lack of a strong intensity in the states even though their binding energies coincided with a bandgap in the Co substrate probably reflected interfacial roughness.

In their inverse photoemission study Huang *et al* examined the intensity variation of a quantum well state immediately above the Fermi level as a function of the incident electron beam energy. Reproduced in figure 50 they were able to demonstrate that the cross section peaked at an energy corresponding to a direct transition for the associated bulk band and suggested that the intensity $I_0$ of the quantum well state reflected the thickness of the film $W$ according to the relationship

$$I_0 \propto \left| \frac{\sin(k - k')W/2}{(k - k')W/2} \right|^2 \tag{42}$$

where $k$ and $k'$ represent the wavevectors of the initial and final states, respectively. In the limit of an infinitely thick film equation (42) will collapse to a $\delta$-function corresponding to the direct transition characterizing the bulk.

In an earlier study, Johnson *et al* (1994) suggested that in a pre-asymptotic limit, the Fermi surface crossings of the quantum well states may be modified by strong hybridization with the substrate d-bands. In a study of copper films deposited on fcc Co(001) they found that the in-plane effective mass of the states showed a considerable enhancement in the ultrathin copper films. As the film becomes thicker the effective mass increases and as shown in figure 51 eventually approaches 1.0, characteristic of bulk Cu, for film thicknesses greater than five to six monolayers. Similar results were observed in a second study of the Cu/Co system (Carbone *et al* 1994). These observations have a simple explanation. In the thinnest films, the quantization condition of equation (34) is dominated by the interaction or phase changes at the interfaces. In the thicker films, on the other hand, the phase change within the film becomes more dominant and the film looks more like bulk Cu, as would be expected. Thicknesses at which the in-plane effective mass show a strong enhancement essentially define a pre-asymptotic regime where bulk Fermi surfaces of the type shown in figure 43 may not provide an appropriate description.

Similar enhancements of the effective masses have also been observed in two studies of quantum well states in silver films deposited on Fe(001) (Brookes *et al* 1994, Carbone *et al* 1994). Both studies reported a similar value for the effective mass of the quantum well state characterizing the monolayer coverage of silver, Brookes *et al* finding a value of $2.1m_e$ and Carbone *et al* a value of $2.0m_e$. For the two-monolayer coverage, Brookes *et al* reported that the effective mass for the quantum well state increased to $2.8m_e$. The authors suggested that the increase in the effective mass as the quantum well state moved to lower binding energies probably reflected the increased coupling to the substrate minority d-bands as the state moved into resonance. Interestingly the same observation has been made in a recent study of the quantum well states characterizing silver films deposited on a V(001) substrate (Valla *et al* 1996). In the latter study the authors reported that the effective mass increased from $2.2m_e$ to $3.1m_e$ on going from the one- to two-monolayer coverage. Examination of the hybridization bandgap in the vanadium substrate shows that at the centre of the zone it has a similar alignment with the Fermi level as the gap found within the Fe minority spin band structure.

Much of the above discussion has centred around the experimental and theoretical observations related to the oscillatory exchange coupling. There have also been some studies directed towards obtaining a better understanding of the magnetoresistive properties. However, before discussing this property we briefly examine the electronic structure of these systems when coupled in the antiferromagnetic phase.

An obvious question is what happens to the quantum well states when the system switches to antiferromagnetic alignment and how might these changes influence the observed magnetoresistance. Figure 52 shows a schematic of the spin-dependent quantum wells for the two different configurations, ferromagnetic and antiferromagnetic alignment of the two ferromagnetic layers. In the ferromagnetic configuration the two wells have a different depth producing a strong spin polarization in the quantum well states as observed in the experiment. However, in the antiferromagnetic configuration the two wells are identical but reversed. For a given spin the confinement on one side of the well is considerably reduced. The fact that the two potential wells are identical means that any separation in energy between the two states will be removed and there will no longer be a net spin polarization as a function of binding energy. However, there will be a level of spin localization in the quantum well in that one spin state will be favoured at one interface and the other spin state will be favoured at the other interface.

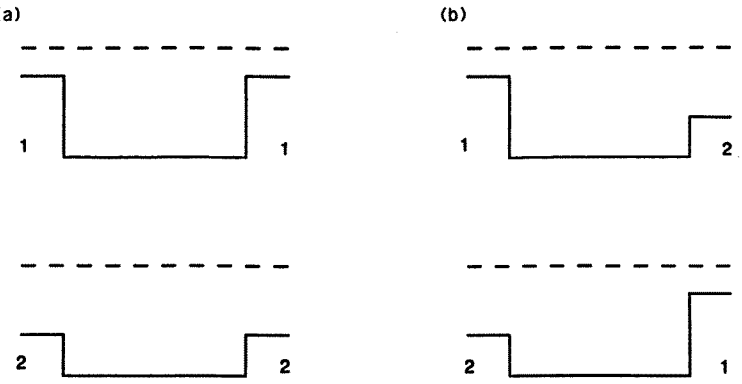


**Figure 52.** The potential wells appropriate to (a) ferromagnetic alignment of the Co layers and (b) antiferromagnetic alignment of the Co layers. In both cases the minority spin well is shown in the upper panel and the majority spin in the lower panel. The dashed lines indicate the position of the Fermi level and the numerals indicate the type of potential experienced by the different spins.

Using a tight-binding analysis, Johnson (1995b) has examined the quantum well states at the centre of the zone in a six-layer Cu slab sandwiched between two five-layer Co slabs. The calculation again produced a series of quantum well states for ferromagnetic alignment of the Co layers. As would be expected from the above discussion, the spin polarization in the quantum well states disappears in the antiferromagnetic case. However, more interestingly in the latter configuration a small gap appears at the Fermi level as the states are pushed to higher and lower binding energies. A similar observation has been made in a separate study reported by Lang (1995). Clearly examining the electronic structure at a single point in the zone does not represent the same level of sophistication as a total-energy calculation. However, the opening of the gap does provide a natural explanation for the switching between ferromagnetic and antiferromagnetic alignment as the reduction in the density of states at the Fermi level will lower the energy of the system. In fact we note that in the more recent tight-binding studies of the magnetic multilayers, Mathon *et al* (1995) have concentrated their total-energy calculations around key points representing calipers of the Cu Fermi surface.

Returning to the question of magnetoresistance we note that several studies have suggested that the interfaces play a crucial role. As an example, Parkin (1993) has examined the properties of the permalloy/copper multilayers with varying thicknesses of Co placed in the interface between the permalloy and copper. He found that as the thickness of the Co increased the magnetoresistance increased with a form given by $(1 + e^{x/\lambda})$ where the scaling parameter $\lambda$ takes the value 2.3 Å.

Possible insight into the properties determining the rate of increase of the magnetoresistance comes in two separate studies. Li *et al* (1995b) have studied the confinement of quantum well states by a ferromagnetic barrier of varying thickness. Here the authors measured the intensity of different quantum well states, a measure of the confinement, in a two-monolayer thick copper film deposited on a Co wedge. Two states representing the $sp_z$ derived state at a binding energy of 1.7 eV and a more tightly bound $d_{xz}$ quantum well state at higher binding energy were examined. The study found that as a function of Co thickness, the intensity of the more localized $d_{xz}$ state saturated more quickly than the $sp_z$ state, as shown in figure 53. Fitting the increase in intensity of the $sp_z$ quantum

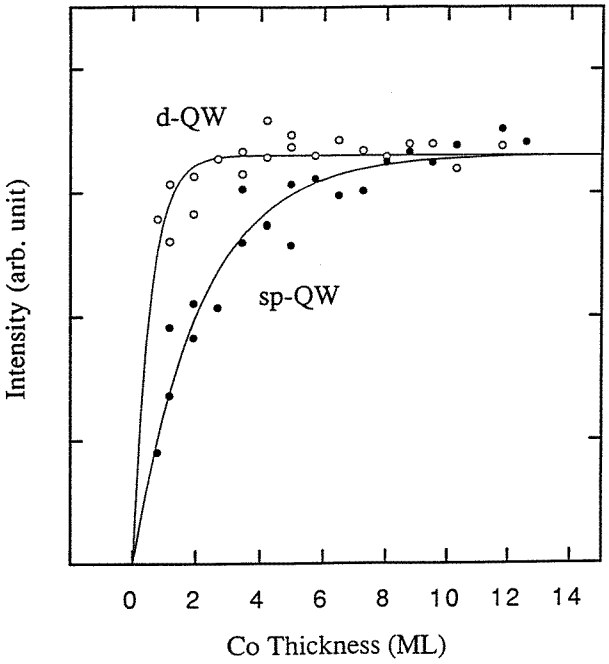


**Figure 53.** Peak intensities of the sp quantum well state at 1.6 eV (full circles) and d quantum well state at 2.4 eV (open circles; normalized to the same saturation intensity as the sp state) indicating a more pronounced quantum confinement by the Co barrier for the d quantum well state. Full and dashed curves represent the experimental fits described in the text, where $t_{Co}$ is the Co thickness.

well state with the functional form used by Parkin, the authors found a scaling parameter of 2.3 Å, identical with that found in the earlier magnetoresistance study. This supports the idea that the magnetoresistance property is essentially determined by interfacial effects with the thickness of the 'leaky' Co barrier determining the measured characteristics.

A note of caution might be added into the discussion at this point. A recent STM study of ion beam sputtered copper films grown on Co(001) and Co films grown on Cu(001) has shown that the degree of surface roughness tends to be higher in the latter (Minvielle *et al* 1996). However, as the authors note, in general the copper tends to act as a 'smoothing agent' when deposited on the pre-grown 'rough' Co films. Whilst such studies suggest that the observation of Li *et al* (1995b) could be influenced by the presence of Co islands it is clear that the presence of quantum well states down to the very thinnest Co layer is an indication that a barrier exists.

An alternative picture of the origin of the interfacial effect is given by Hwang and Himpsel (1995). In an inverse photoemission study of Co films deposited on a Ni(001) substrate they reported the observation of an interfacial state located 0.55 eV above the Fermi level. Monitoring the growth of this state as function of coverage they found a growth constant of 2.4 Å, i.e. close to that found for the enhancement of the GMR in the Cu/permalloy films with Co coated interfaces. Thus in this picture the interfacial effect in the GMR results from distinct changes in the electronic structure of the interface.

The quantization of the d-bands has also been observed in a number of thin films. The ability to resolve discrete quantum well states can depend on a number of different factors

including the experimental energy resolution. Another important factor reflects the lifetime of the photohole following excitation of the electron from the quantum well state. The width of a photoemission peak, $\Gamma$, may be related to both the lifetime of the photohole $\Gamma_h$ and the momentum broadening $\Gamma_e/|\delta E_e/\delta k|$ of the photoelectron in the final state (Knapp *et al* 1979, Chiang *et al* 1980). Thus

$$\Gamma = \frac{\Gamma_h + \Gamma_e((\delta E_h/\delta k)/(\delta E_e/\delta k))}{1 + ((\delta E_h/\delta k)/(\delta E_e/\delta k))}. \tag{43}$$

Because the quantum well state has no dispersion with $k_\perp$ equation (43) reduces to $\Gamma = \Gamma_h$ the inverse lifetime of the photohole. However, the latter may be strongly influenced by the quality of the film and of the interface.

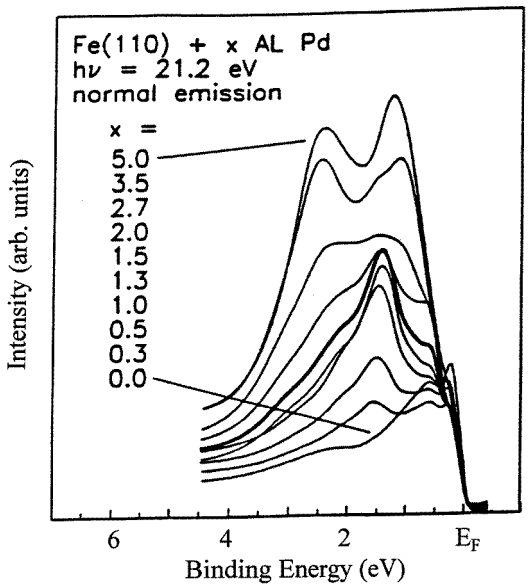


**Figure 54.** Spin-intgerated spectra recorded from Pd films deposited on an Fe(011) substrate. The different thicknesses of Pd are indicated.

The energy separation between consecutive quantum well states, $\Delta E$, is related to both the number of layers in the film, $N$, and the rate of dispersion of the bulk band from which the quantum well states are derived such that

$$\Delta E = \frac{2\pi}{Na}\frac{\delta E}{\delta k} \tag{44}$$

where $a$ is the separation between layers (Loly and Pendry 1983). One might anticipate, therefore, that quantization of the more localized d-bands will be seen more easily in thinner films. This is indeed the case.

Systems that have been studied include Cu, Au, Pd and Pt overlayers on Fe(110) and Co(0001) (Hartmann *et al* 1993, Wesner *et al* 1993). In general, all these systems show a similar behaviour. Two peaks appear in the coverage-dependent spectra which saturate in intensity at coverages of 1.5 AL and 2 AL, respectively. As an example we show in figure 54 the photoemission spectra obtained from Pd films deposited on an Fe(110) substrate. A peak at a binding energy of $-1.5$ eV appears in the 0.5 AL Pd coverage spectrum, saturates at 1.0 AL and then reduces in intensity. With further coverage a second peak appears at

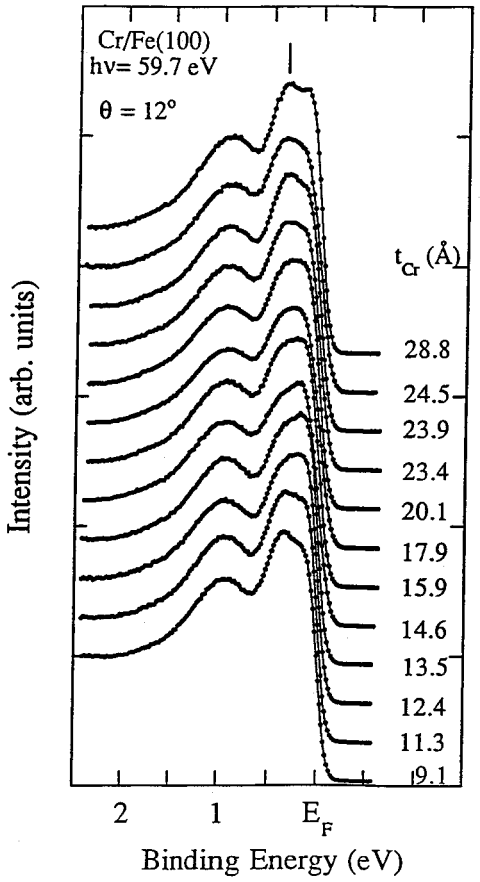


**Figure 55.** Photoemission spectra recorded from epitaxial Cr films deposited on an Fe(100) substrate. The incident photon energy is $h\nu = 59.7$ eV and the photoelectron emission angle away from the surface normal corresponds to $\theta = 12^{\circ}$.

−0.7 eV binding energy saturating at a coverage of 2 AL. By 4 AL the photoemission spectra resemble those characteristic of a Pd(111) surface. Similar quantization effects have also been observed in studies of the noble metals Cu and Ag deposited on Co(001) (Li *et al* 1995b, Mankey *et al* 1994) and Fe(001) (Brookes *et al* 1994), respectively.

Li *et al* (1997) have also reported the observation of quantization effects in the d-bands of Cr films deposited on an Fe(001) whisker. Looking out in the Brillouin zone the authors were able to show, as indicated in figure 55, that quantum well states were observable at one of the points proposed as the source for the long period oscillatory exchange coupling in the related Fe/Cr multilayers by Koelling (1994). Indeed the intensity of the quantized states oscillated with the same periodicity.

In a separate theoretical study of the spin-dependent reflectivities at the Cr/Fe(001) interface, Stiles (1996) also found that strong reflection did indeed exist at this point corresponding to a lens in the Fermi surface. However, he also indicated that the reflectivities were higher at the $N$-centred ellipsoids farther out in the zone. The importance of the type of studies carried out by Li *et al* (1997) is that they point to the potential utility of angle-resolved photoemission as a probe of the $k$-space origins of different oscillation periodicities in the interlayer magnetic coupling.

## 7. Summary and future outlook

We have seen that in the past 20 years the development and application of spin-polarized photoemission has been extensive. Because of its sensitivity to the surface region it has offered a number of new insights into the electronic structure of magnetic surfaces and thin films. However, we may anticipate still further developments in the future both in the area of spectroscopy and in the area of microscopy. Indeed, we have hardly touched on the latter area at all in the present review.

The development of more efficient spin polarimeters will allow experiments to be carried out with higher energy resolution than has been achieved to date. Amongst other things this will make accessible studies of the fine details associated with magnetic anisotropies in thin films. The greater part of this review has dealt with studies of ferromagnetic materials. This reflects the simple fact that in order to measure the spin polarization we have to define a quantization direction for the spin polarization. This is achieved in the ferromagnets when the domains are aligned in the remanent state. The use of incident circularly polarized light means that the quantization direction may be defined by the polarization axis or direction of propagation of the incident light. Thus we may anticipate seeing further developments in the combined use of circularly polarized incident light and spin-polarized detection of the photoemitted electrons. This opens up the possibility of spin-polarization effects in non-magnetic systems, some of which have already been demonstrated, and also antiferromagnetic materials, where the net long-range spin polarization is zero.

## Acknowledgments

The author is pleased to acknowledge many stimulating conversations with amongst others N Brookes, N V Smith, M Weinert, B Sinkovic, G Van der Laan, E Vescovo, S Blugel, D Li, S D Bader and D-J Huang. Work described in this review was partially supported by the Department of Energy under contract No DOE-AC02-76CH00016.

## References

Aebi P, Kreutz, T J, Osterwalder J, Fasel R, Schwaller P and Schlapbach L 1996 *Phys. Rev. Lett.* **76** 1150
Allenspach R, Taborelli M and Landolt M 1985 *Phys. Rev. Lett.* **55** 2599
Alvarado S F and Bagus P S 1978 *Phys. Lett.* **67A** 397
Arenholz E, Navasa E, Starke K, Baumgarten L and Kaindl G 1995 *Phys. Rev.* B **51** 8211
Bagus P S and Mallow J V 1994 *Chem. Phys. Lett.* **228** 695
Baibich M N, Broto J M, Fert A, Nguyen Van Dau F, Petroff F, Etienne P, Creuzet G, Fiedrich A and Chazelas J 1988 *Phys. Rev. Lett.* **61** 2472
Baumgarten L, Schneider C M, Petersen H, Schafers F and Kirschner J 1990 *Phys. Rev. Lett.* **65** 492
Bland J A C, Bateson R D, Riedi P C, Graham R G, Lauter H J, Penfold J and Shackleton C 1991 *J. Appl. Phys.* **69** 4989
Blugel S 1992 *Phys. Rev. Lett.* **68** 851
Blyholder G J 1964 *J. Chem. Phys.* **68** 2772
Brookes N B, Chang Y and Johnson P D 1991 *Phys. Rev. Lett.* **67** 354
——1994 *Phys. Rev.* B **50** 15 330
Brookes N B, Clarke A and Johnson P D 1989 *Phys. Rev. Lett.* **63** 2764
——1992 *Phys. Rev.* B **46** 237
Brookes N B, Clarke A, Johnson P D and Weinert M 1990 *Phys. Rev.* B **41** 2643
Brundle C R, Chuang T J and Wandelt K 1977 *Surf. Sci.* **68** 459
Bruno P 1995 *Phys. Rev.* B **52** 411
Bruno P and Chappert C 1991 *Phys. Rev. Lett.* **67** 1602
Burnett G C, Monroe T J and Dunning F B 1994 *Rev. Sci. Instrum.* **65** 1893

Bylander D M and Kleinman L 1994 *Phys. Rev.* B **50** 4996
Callaway J and Wang C S 1977 *Phys. Rev.* B **16** 2095
Carbone C and Kisker E 1987 *Phys. Rev.* B **36** 1280
——1988 *Solid State Commun.* **65** 1107
Carbone C, Kachel T, Rochow R and Gudat W 1991 *Solid State Commun.* **77** 619
Carbone C, Rochow R, Braicovich L, Jungblut R, Kachel T, Tillmann D and Kisker E 1990 *Phys. Rev.* B **41** 3866
Carbone C, Vescovo E, Klasges R, Eberhardt W, Rader O and Gudat W 1994 *J. Appl. Phys.* **76** 6966
Carbone C, Vescovo E, Klasges R, Sarma D D and Eberhardt W 1996 *J. Magn. Magn. Mater.* **156** 259
Carbone C,Vescovo E, Rader O, Gudat W and Eberhardt W 1993 *Phys. Rev. Lett.* **71** 2805
Carver J C, Schweitzer G K and Carlson T A 1972 *J. Chem. Phys.* **57** 973
Chen C T, Idzerda Y U, Lin H-J, Smith N V, Meigs G, Chaban E, Ho G H, Pellegrin E and Sette F 1995 *Phys. Rev. Lett.* **75** 152
Cherepkov N A 1983 *Adv. At. Mol. Phys.* **19** 395
——1994 *Phys. Rev.* B **50** 13 813
Chiang T C, Knapp J A, Aono M and Eastman D E 1980 *Phys. Rev.* B **21** 3513
Cho J-H and Kang M-H 1995 *Phys. Rev.* B **52** 13 805
Chubb S R and Pickett W E 1987 *Phys. Rev. Lett.* **58** 1248
——1988a *Phys. Rev.* B **38** 10 227
——1988b *Phys. Rev.* B **38** 12 700
Clarke A, Brookes N B, Johnson P D, Weinert M, Hulbert S L, Sinkovic B and Smith N V 1990 *Phys. Rev.* B **41** 9659
Clarke A, Jennings G, Willis R F, Rous P J and Pendry J B 1987 *Surf. Sci.* **187** 327
Clauberg R, Gudat W, Kisker E, Kuhlmann E and Rothberg G M 1981 *Phys. Rev. Lett.* **47** 1314
Clauberg R, Hopster H and Raue R 1984 *Phys. Rev.* B **29** 4395
Clemens W, Kachel T, Rader O, Vescovo E, Blugel S, Carbone C and Eberhardt W 1992a *Solid State Commun.* **81** 739
Clemens W, Vescovo E, Kachel T, Carbone C and Eberhardt W 1992b *Phys. Rev.* B **46** 4198
Crampin S, De Rossi S and Ciccaci F 1996 *Phys. Rev.* B **53** 13 817
Davis L C and Feldkamp L A 1979 *J. Appl. Phys.* **50** 1944
Donath M 1994 *Surf. Sci. Rep.* **20** 251
Donath M, Dose V, Ertl K and Kolac U 1990 *Phys. Rev.* B **41** 5509
Donath M, Passek F and Dose V 1993 *Phys. Rev. Lett.* **70** 2802
Dose V 1985 *Surf. Sci. Rep.* **5** 337
Durham P J, Staunton J and Gyorffy B L 1984 *J. Magn. Magn. Mater.* **45** 38
Eastman D E, Himpsel F J and Knapp J A 1980 *Phys. Rev. Lett.* **44** 95
Eberhardt W and Plummer E W 1980 *Phys. Rev.* B **21** 3245
Ebert H 1989 *J. Phys.: Condens. Matter* **1** 9111
Edwards D M, Mathou J, Muniz R B and Phan M S 1991 *Phys. Rev. Lett.* **67** 493
Egerton R F 1986 *Electron Energy Loss Spectroscopy in the Electron Microscope* (New York: Plenum)
Eib W and Alvarado S F 1976 *Phys. Rev. Lett.* **37** 444
Elliot G S, Smith K E and Kevan S D 1991 *Phys. Rev.* B **43** 3893
Erskine J L 1980 *Phys. Rev. Lett.* **45** 1446
Fadley C S, Shirley D A, Freeman A J, Bagus P S and Mallow J V 1969 *Phys. Rev. Lett.* **23** 1397
Falicov L M 1992 *Phys. Today* **45** 46
Falicov L M *et al* 1990 *J. Mater. Res.* **5** 1299
Feder R 1985 *Polarized Electrons in Surface Physics* ed R Feder (Singapore: World Scientific) p 125
Feder R, Gudat W, Kisker E, Rodriguez A and Schroder K 1983 *Solid State Commun.* **46** 619
Feder R, Rodriguez A, Baier U and Kisker E 1984 *Solid State Commun.* **52** 57
Federov A V, Starke K and Kaindl G 1994 *Phys. Rev.* B **50** 2739
Feldkamp L A and Davis L C 1979 *Phys. Rev. Lett.* **43** 151
Feuchtwang T E, Cutler P H and Nagy D 1978 *Surf. Sci.* **75** 490
Fink R L, Mulhollan G A, Andrews A B and Erskine J L 1992 *Phys. Rev.* B **45** 9824
Fink R L, Mulhollan G A, Andrews A B, Erskine J L and Walters G K 1991 *J. Appl. Phys.* **69** 4986
Freeman A J and Wu R 1991 *J. Magn. Magn. Mater.* **100** 497
Frentzen F, Henk J, Irmer N, David R, Schmiedeskamp B, Heinzmann U and Feder R 1996 *Z. Phys.* B **100** 575
Fu C l, Freeman A J and Oguchi T 1985 *Phys. Rev. Lett.* **54** 2700
Fuchs P, Petrov V N, Totland K and Landolt M 1996 *Phys. Rev.* B **54** 9304
Garrison K, Chang Y and Johnson P D 1993 *Phys. Rev. Lett.* **71** 2801

Getzlaff M, Bansmann J and Schonhense G 1993a *Solid State Commun.* **87** 467
——1993b *Phys. Lett.* **182A** 153
——1993c *Phys. Rev. Lett.* **71** 793
——1994 *J. Magn. Magn. Mater.* **131** 304
——1995 *Surf. Sci.* **323** 118
——1996 *J. Electron. Spectrosc. Relat. Phenon.* **77** 197
Getzlaff M, Bansmann J, Westphal C and Schonhense G 1992 *J. Magn. Magn. Mater.* **104–107** 1781
Gokhale M P and Mills D L 1991 *Phys. Rev. Lett.* **66** 2251
Gonzalez L, Miranda R, Salmeron M, Verges J A and Yndurain F 1981 *Phys. Rev.* B **24** 3245
Grunberg P, Schreiber R, Pang Y, Brodsky M B and Sowers H 1986 *Phys. Rev. Lett.* **57** 2442
Guillot C, Ballu Y, Paigne J, Lecante J, Jain R P, Thiry P, Pinchaux R, Petroff Y and Falicov L M 1982 *Phys. Rev. Lett.* **49** 72
Gunnarsson O 1976 *J. Phys. F: Met. Phys.* **6** 587
Haines E, Clauberg R and Feder R 1985a *Phys. Rev. Lett.* **54** 932
Haines E M, Heine V and Ziegler A 1985b *J. Phys. F: Met. Phys.* **15** 661
——1986 *J. Phys. F: Met. Phys.* **16** 1343
Harrison W A 1980 *Electronic Structure and the Properties of Solids* (San Francisco, CA: W H Freeman)
Hartmann D, Weber W, Rampe A, Popovic S and Guntherodt G 1993 *Phys. Rev.* B **48** 16 837
Hathaway K B, Jansen H J F and Freeman A J 1985 *Phys. Rev.* B **31** 7603
Heimann P, Himpsel F J and Eastman D E 1981 *Solid State Commun.* **39** 219
Heimann P and Neddermeyer N 1978 *Phys. Rev.* B **18** 3537
Heine V, Samson J H and Nex C M M 1981 *J. Phys. F: Met. Phys.* **11** 2645
Heinrich B, Arrott A S, Cochran J F, Liu C and Myrtle K 1986a *J. Vac. Sci. Technol.* A **4** 1376
Heinrich B, Arrott A S, Cochran J F, Purcell S T, Urquhart K B and Myrtle K 1987 *J. Crystal. Growth* **81** 562
Heinrich B, Purcell S T, Dutcher J R, Urquhart K B, Cochran J F and Arrott A S 1986b *Phys. Rev.* B **38** 12 879
Heinzmann U 1987 *Phys. Scr.* T **17** 77
Held G A, Samant M G, Stohr J, Parkin S S P, Hermsmeier B D, van Schilfgarde M and Nakajima R 1996 *Z. Phys.* B **100** 335
Hillebrecht F U, Jungblut R and Kisker E 1990 *Phys. Rev. Lett.* **65** 2450
Hillebrecht F U, Roth Ch, Jungblut R, Kisker E and Bringer A 1992 *Europhys. Lett.* **19** 711
Hillebrecht F U, Roth Ch, Rose H B, Finazzi M and Braicovich L 1995 *Phys. Rev.* B **51** 9333
Himpsel F J 1983 *Adv. Phys.* **32** 1
——1986 *Commun. Condens. Mater. Phys.* **12** 199
——1991 *Phys. Rev. Lett.* **67** 2363
Himpsel F J, Knapp J A and Eastman D E 1979 *Phys. Rev.* B **19** 2919
Hopster H, Raue R, Guntherodt G, Kisker E, Clauberg R and Campagna M 1983 *Phys. Rev. Lett.* **51** 829
Huang D-J, Johnson P D and Shi X 1996 *Phys. Rev.* B **54** 17 123
Huang D-J, Lee J-Y, Suen J-S, Mulhollan G A, Andrews A B and Erskine J L 1993 *Rev. Sci. Instrum.* **64** 3474
Huang D-J, Riffe D M and Erskine J L 1995 *Phys. Rev.* B **51** 15 170
Huang H and Hermanson J 1985 *Phys. Rev.* B **32** 6312
Huang H, Hermanson J, Gray J G, Richter R and Smith J R 1986 *Surf. Sci.* **172** 363
Hubinger F, Schusslerlangeheine C, Federov A V, Starke K, Weschke E, Hohr A, Vandre S and Kaindl G 1995 *J. Electron. Spect.* **76** 535
Hufner S and Wertheim G K 1975 *Phys. Lett.* **51A** 299
Hwang C and Himpsel F J 1995 *Phys. Rev.* B **52** 15 368
Idzerda Y U, Tjeng L H, Lin H-J, Gutierez C J, Meigs G and Chen C T 1993 *Surf. Sci.* **287/288** 741
Janak J F 1977 *Phys. Rev.* B **16** 255
Jansen H J F, Hathaway K B and Freeman A J 1984 *Phys. Rev.* B **30** 6177
Johnson M T, Purcell S T, Mcgee N W E, Coehoorn R ann de Stegge J and Hoving W 1992 *Phys. Rev. Lett.* **68** 2688
Johnson P D 1992 *Angle-Resolved Photoemission* ed S D Kevan (Amsterdam: Elsevier)
——1995a *Ann. Rev. Mater. Sci.* **25** 455
——1995b *Electronic Surface and Interface States on Metallic Systems* ed E Bertel and M Donath (Singapore: World Scientific) p 253
Johnson P D *et al* 1992 *Rev. Sci. Instrum.* **63** 1902
Johnson P D, Chang Y and Brookes N B 1993 *Proc. 10th VUV Conf. Vacuum Ultraviolet Radiation Physics* ed F J Wuilleumier, Y Petroff and I Nenner (Singapore: World Scientific) p 453
Johnson P D, Clarke A, Brookes N B, Hulbert S L, Sinkovic B and Smith N V 1988 *Phys. Rev. Lett.* **61** 2257

Johnson P D, Garrison K, Dong Q, Smith N V, Li D, Mattson J E, Pearson J and Bader S D 1994 *Phys. Rev.* B **50** 8954
Johnson P D, Liu Y, Xu Z and Huang D-J 1995 *J. Electron. Spectrosc.* **75** 245
Jonker B T, Walker K-H, Kisker E, Prinz G A and Carbone C 1986 *Phys. Rev. Lett.* **57** 142
Jungblut R, Roth Ch, Hillebrecht F U and Kisker E 1992 *Surf. Sci.* **269/270** 615
Kachel T, Carbone C and Gudat W 1993 *Phys. Rev.* B **47** 15 391
Kachel T, Gudat W, Carbone C, Vescovo E, Blugel S, Alkemper U and Eberhardt W 1992 *Phys. Rev.* B **46** 12 888
Kakehashi Y 1985 *Phys. Rev.* B **31** 7482
Kakizaki A, Fujii J, Shimada K, Kamata A, Ono K, Park K-H, Kinoshita T, Ishii T and Fukutani H 1994 *Phys. Rev. Lett.* **72** 2781
Kamper K-P, Schmitt W and Guntherodt G 1990 *Phys. Rev.* B **42** 10 696
Kamper K-P, Schmitt W, Wesner D A and Guntherodt G 1989 *Appl. Phys.* A **49** 573
Kessler K 1985 *Polarized Electrons* (Berlin: Springer)
Kevan S D 1992 *Angle-Resolved Photoemission* (Amsterdam: Elsevier)
Kim B, Andrews A B, Erskine J L, Kim K J and Harmon B N 1992 *Phys. Rev. Lett.* **68** 1931
Kirschner J and Feder R 1979 *Phys. Rev. Lett.* **42** 1008
Kirschner J, Globl M, Dose V and Scheidt H 1984 *Phys. Rev. Lett.* **53** 612
Kisker E 1987 *Metallic Magnetism* ed H Capellmann (Berlin: Springer) p 57
Kisker E, Clauberg R and Gudat W 1982 *Rev. Sci. Instrum.* **53** 50
Kisker E, Schroder K, Campagna M and Gudat W 1984 *Phys. Rev. Lett.* **52** 2285
Kisker E, Schroder K, Gudat W and Campagna M 1985 *Phys. Rev.* B **31** 329
Kisker E, Schroder K, Gudat W, Campagna M, Kuhlmann E, Hopster H and Moore I D 1979 *Phys. Rev. Lett.* **43** 966
Klebanoff L E, Van Campen D G and Pouliot R J 1994 *Phys. Rev.* B **49** 2047
Knapp J A, Himpsel F J and Eastman D E 1979 *Phys. Rev.* B **19** 4952
Koelling D D 1994 *Phys. Rev.* B **50** 273
Korenman V 1986 *Metallic Magnetism* ed H Capellmann (Berlin: Springer) p 109
Lang P 1995 Theory of the interlayer exchange coupling *PhD Thesis* Technical University of Aachen
Lang P, Nordstrom L, Wildberger K, Zeller R and Dederichs P H 1996 *Phys. Rev.* B **53** 9092
Lassailly Y, Drouhin H-J, van der Sluijs J, Lampel G and Marliere C 1994 *Phys. Rev.* B **50** 13 054
Lee J I, Hong S C, Freeman A J and Fu C L 1993 *Phys. Rev.* B **47** 810
Legg K O, Jona F, Jepsen D W and Marcus P M 1977a *Surf. Sci.* **66** 25
——1977b *Phys. Rev.* B **16** 5271
Li D, Hutchings W, Dowben P A, Hwang C, Wu R T, Onellion M, Andrews A B and Erskine J L 1991 *J. Magn. Magn. Mater.* **99** 85
Li D, Pearson J, Bader S D, McIlroy D N, Waldfried C and Dowben P A 1995a *Phys. Rev.* B **51** 13 895
Li D, Pearson J, Bader S D, Vescovo E, Huang D-J, Johnson P D and Heinrich B 1997 *Phys. Rev. Lett.* **78** 1154
Li D, Pearson J, Mattson J E, Bader S D and Johnson P D 1995b *Phys. Rev.* B **51** 7195
Li D *et al* 1993 *MRS Symp. Proc.* **313** 451
Li H, Quinn J, Li Y S, Tian D, Jona F and Marcus P M 1991 *Phys. Rev.* B **43** 7305
Liebsch A 1979 *Phys. Rev. Lett.* **43** 1431
——1981 *Phys. Rev.* B **23** 5203
Lindgren S A and Wallden L 1987 *Phys. Rev. Lett.* **59** 3003
——1988 *Phys. Rev. Lett.* **61** 2894
Liu C and Bader S D 1991 *J. Magn. Magn. Mater.* **93** 307
Liu Y, Xu Z, Johnson P D and van der Laan G 1995 *Phys. Rev.* B **52** R8593
Loly P D and Pendry J B 1983 *J. Phys. C: Solid State Phys.* **16** 423
Mankey G J, Willis R F, Orgega J E and Himpsel F J 1994 *J. Vac. Sci. Technol.* A **12** 2183
Marcus P M, Moruzzi V L, Wang Z Q, Li Y S and Jona F 1986 *Physical and Chemical Properties of Thin Metal Overlays and Alloy Surfaces (MRS Symp. Proc. 83)* ed D M Zehner and D W Goodman (Pittsburgh, PA: Materials Research Society) p 21
Mathon J, Villeret M, Muniz R B, d'Albuquerque e Castro J and Edwards D M 1995 *Phys. Rev. Lett.* **74** 3696
McRae E G 1979 *Rev. Mod. Phys.* **51** 541
Menchero J G 1996 *Phys. Rev. Lett.* **76** 3208
Miller T, Samsavar A, Franklin G E and Chiang T-C 1988 *Phys. Rev. Lett.* **61** 1404
Minvielle T J, White R L and Wilson R J 1996 *J. Appl. Phys.* **79** 5116
Miranda R, Chandesris D and Lecante J 1983 *Surf. Sci.* **130** 269
Moore I D and Pendry J B 1978 *J. Phys. C: Solid State Phys.* **11** 4615

Morrison I, Bylander D M and Kleinman L 1993 *Phys. Rev. Lett.* **71** 1083
Moruzzi V L 1986 *Phys. Rev. Lett.* **57** 2211
Moruzzi V L and Marcus P M 1988 *Phys. Rev.* B **38** 1613
Moruzzi V L, Marcus P M, Schwartz K and Mohn P 1986 *Phys. Rev.* B **34** 1784
Mott N F 1964 *Adv. Phys.* **13** 325
Mulhollan G A, Andrews B A and Erskine J L 1992a *Phys. Rev.* B **46** 11 212
Mulhollan G A, Fink R L, Erskine J L and Walters G K 1991 *Phys. Rev.* B **43** 13 645
Mulhollan G A, Garrison K and Erskine J L 1992b *Phys. Rev. Lett.* **69** 3240
Nolting W, Dambeck T and Borstel G 1994 *Z. Phys.* B **94** 409
Oed W, Dotsch B, Hammer L, Heinz K and Muller K 1988 *Surf. Sci.* **207** 55
Ohnishi S, Weinert M and Freeman A J 1984 *Phys. Rev.* B **30** 36
Ortega J E and Himpsel F J 1992 *Phys. Rev. Lett.* **69** 844
Ortega J E, Himpsel F J, Mankey G J and Willis R F 1993 *Phys. Rev.* B **47** 1540
Pappas D P, Kamper K-P, Miller B P, Hopster H, Fowler D E, Brundle C R, Luntz A C and Shen Z-X 1991 *Phys. Rev. Lett.* **66** 504
Parkin S S P 1991 *Phys. Rev. Lett.* **67** 3598
——1993 *Phys. Rev. Lett.* **71** 1641
Parkin S S P, More N and Roche K P 1990 *Phys. Rev. Lett.* **64** 2304
Penn D R 1979 *Phys. Rev. Lett.* **42** 921
Penn D R, Apell S P and Girvin S M 1985 *Phys. Rev. Lett.* **55** 518
Pierce D T, Celotta R J, Kelley M H and Unguris J 1988 *Nucl. Instrum. Methods* A **266** 550
Pierce D T, Stroscio J A, Unguris J and Celotta R J 1994 *Phys. Rev.* B **49** 14 564
Plummer E W and Eberhardt W 1979 *Phys. Rev.* B **20** 1449
Plummer E W and Eberhardt W 1982 *Adv. Chem. Phys.* vol 49, ed I Prigogine and S A Rice (New York: Wiley) p 533
Prinz, G A, Kisker E, Hathaway K B, Schroder K and Walker K-H 1985 *J. Appl. Phys.* **57** 3024
Purcell S T, Johnson M T, McGee N W E, Coehoorn R and Hoving W 1992 *Phys. Rev.* B **45** 13 064
Qiu Z Q, Pearson J and Bader S D 1992 *Phys. Rev.* B **46** 8659
——1993 *Phys. Rev. Lett.* **70** 1006
Rader O, Carbone C, Clemens W, Vescovo E, Blugel S, Eberhardt W and Gudat W 1992 *Phys. Rev.* B **45** 13 823
Rader O, Vescovo E, Redinger J, Blugel S, Carbone C, Eberhardt W and Gudat W 1994 *Phys. Rev. Lett.* **72** 2247
Rau C and Robert M 1987 *Phys. Rev. Lett.* **22** 2714
Raue R, Hopster H and Clauberg R 1983 *Phys. Rev. Lett.* **50** 1623
Rossi G, Sirotti F, Cherepkov N A, Farnoux R C and Panaccione G 1994 *Solid State Commun.* **90** 557
Roth Ch, Hillebrecht F U, Park W G, Rose H B and Kisker E 1994 *Phys. Rev. Lett.* **73** 1963
Roth Ch, Hillebrecht F U, Rose H B and Kisker E 1993a *Phys. Rev. Lett.* **70** 3479
Roth Ch, Kleeman Th, Hillebrecht F U and Kisker E 1995 *Phys. Rev.* B **52** R15691
Roth Ch, Rose H B, Hillebrecht F U and Kisker E 1993b *Solid State Commun.* **86** 647
Rothberg G M 1980 *J. Magn. Magn. Mater.* **15–18** 323
Roy D and Carette J D 1977 *Electron Spectroscopy for Surface Analysis* ed H Ibach (Berlin: Springer) p 13
Saitoh Y *et al* 1995 *Phys. Rev.* B **52** R11549
Sakisaka Y, Rhodin T and Mueller D 1985 *Solid State Commun.* **53** 793
Samant M G *et al* 1994 *Phys. Rev. Lett.* **72** 1112
Sandratskii L M and Kubler J 1993 *Europhys. Lett.* **23** 661
Scheinfein M R, Pierce D T, Unguris J, McClelland J J, Celotta R J and Kelley M H 1989 *Rev. Sci. Instrum.* **60** 1
Schmiedeskamp B, Irmer N, Stoppmanns P, Vogt B and Heinzmann U 1992 *Europhys. Lett.* **20** 657
Schmiedeskamp B, Vogt B and Heinzmann U 1988 *Phys. Rev. Lett.* **60** 651
Schmitt W, Hopster H and Guntherodt G 1985 *Phys. Rev.* B **31** 4035
Schmitt W, Kamper K-P and Guntherodt G 1987 *Phys. Rev.* B **36** 3763
Schneider C M, Hammond M S, Schuster P, Cebollada A, Miranda R and Kirschner J 1991a *Phys. Rev.* B **44** 12 066
Schneider C M, Miguel J J, Bressler P, Schuster P, Miranda R and Kirschner J 1990 *J. Electron. Spectrosc. Relat. Phenom.* **51** 263
Schneider C M, Schuster P, Hammond M, Ebert H, Noffke J and Kirschner J 1991b *J. Phys.: Condens. Matter* **3** 4349
Schneider C M, Schuster P, Hammond M S and Kirschner J 1991c *Europhys. Lett.* **16** 689
Schonhense G, Donath M, Kolac U and Dose V 1988a *Surf. Sci.* **206** L888
Schonhense G, Getzlaff, Westphal C, Heidemann B and Bansmann J 1988b *J. Physique Coll.* **8** C 1643

Schonhense G and Siegmann H C 1993 *Ann. Phys., Lpz.* **2** 465
Schröder K, Prinz G A, Walker K-H and Kisker E 1985 *J. Appl. Phys.* **57** 3669
Schultz A, Courths R, Schultz H and Hufner S 1979 *J. Phys. F: Met. Phys.* **9** L41
Seah M P and Dench W A 1979 *Surf. Interface Anal.* **1** 2
See A K and Klebanoff L E 1995a *Phys. Rev. Lett.* **74** 1454
——1995b *Phys. Rev.* B **51** 7901
——1995c *Phys. Rev.* B **51** 11 002
Segovia P, Michel E G and Ortega J E 1996 *Phys. Rev. Lett.* **77** 3455
Seiler A, Feigerle C S, Pena J l, Celotta R J and Pierce D T 1985 *Phys. Rev.* B **32** 7776
Shirley D A 1978 *Photoemission in Solids* vol 1, ed M Cardona and L Ley (Berlin: Springer) p 165
Sinkovic B, Friedman D J and Fadley C S 1991 *J. Magn. Magn. Mater.* **92** 301
Sinkovic B, Johnson P D, Brookes N B, Clarke A and Smith N V 1989 *Phys. Rev. Lett.* **62** 2740
——1990 *Phys. Rev. Lett.* **65** 1647
——1995a *Phys. Rev.* B **52** R6955
Sinkovic B and Shekel E 1994 *National Synchrotron Light Source (NSLS) Annual Report* ed E Z Rothman (Brookhaven National Laboratory, Upton, NY) p 49
Sinkovic B, Shekel E and Hulbert S L 1995b *Phys. Rev.* B **52** R8696
Sirotti F and Rossi G 1994 *Phys. Rev.* B **49** 15 682
Smith N V 1979 *Phys. Rev.* B **19** 5019
——1988 *Rep. Prog. Phys.* **51** 1227
Smith N V, Brookes N B, Chang Y and Johnson P D 1994 *Phys. Rev.* B **49** 332
Smith N V and Himpsel F J 1983 *Handbook on Synchrotron Radiation* ed E Koch (Amsterdam: North-Holland) p 905
Starke K, Erth K and Dose V 1992 *Phys. Rev.* B **45** 6154
Starke K, Kaduwela A P, Liu Y, Johnson P D, Van Hove M A, Fadley C S, Chakarian V, Chaban E E, Meigs G and Chen C T 1996 *Phys. Rev.* B **53** R10544
Stiles M D 1993 *Phys. Rev.* B **48** 7238
——1996 *Phys. Rev.* B **54** 14 679
Stoeffler D and Gautier F 1993 *J. Magn. Magn. Mater.* **121** 259
——1995 *J. Magn. Magn. Mater.* **147** 260
Stoppmanns P, Heidemann B, Irmer N, Muller N, Vogt B, Schmiedeskamp B, Heinzmann U, Tamura E and Feder R 1991 *Phys. Rev. Lett.* **66** 2645
Stroscio J A, Pierce D T, Davies A and Celotta R J 1995 *Phys. Rev. Lett.* **75** 2960
Taborelli M, Allenspach R, Boffa G and Landolt M 1986 *Phys. Rev. Lett.* **56** 2869
Tamura E, Piepke W and Feder R 1987 *Phys. Rev. Lett.* **59** 934
Tamura E, Waddill G D, Tobin J G and Sterne P A 1994 *Phys. Rev. Lett.* **73** 1533
Tang F C, Zhang X, Dunning F B and Walters G K 1988 *Rev. Sci. Instrum.* **59** 504
Tang H, Weller D, Walker T G, Scott J C, Chappert C, Hopster H, Pang A W, Dessau D S and Pappas D P 1993 *Phys. Rev. Lett.* **71** 444
Thole B T and van der Laan G 1991a *Phys. Rev. Lett.* **67** 3306
——1991b *Phys. Rev.* B **44** 12 424
——1994a *Phys. Rev.* B **49** 9613
——1994b *Phys. Rev.* B **50** 11 474
Tillman D, Thiel R and Kisker E 1989 *Z. Phys.* B **77** 1
Turner A M, Chang Y J and Erskine J L 1982 *Phys. Rev. Lett.* **48** 348
Turner A M, Donoho A W and Erskine J L 1984 *Phys. Rev.* B **29** 2986
Turner A M and Erskine J L 1983 *Phys. Rev.* B **28** 5628
——1984 *Phys. Rev.* B **30** 6675
Unguris J, Celotta R J and Pierce D T 1991 *Phys. Rev. Lett.* **67** 140
——1992 *Phys. Rev. Lett.* **69** 1125
Unguris J, Pierce D T and Celotta R J 1986 *Rev. Sci. Instrum.* **57** 1314
Valla T, Pervan P, Miles M, Hayden A B and Woodruff D P 1996 *Phys. Rev.* B **54** 11 786
Van Campen D G and Klebanoff L E 1994 *Phys. Rev.* B **49** 2040
Van Campen D G, Pouliot R J and Klebanoff L E 1993 *Phys. Rev.* B **48** 17 533
Van Gelderen P, Crampin S and Inglesfield J E 1996 *Phys. Rev.* B **53** 9115
Van der Laan G 1995 *Phys. Rev.* B **51** 240
Van der Laan G and Thole B T 1994 *Solid State Commun.* **92** 427
Van der Sluijs A, Drouhin H-J, Lampel G, Lassailly Y and Marliere C R 1994 *Acad. Sci., Paris* **319** Series II 753

Van Vleck J H 1934 *Phys. Rev.* **45** 405
Venus D 1993 *Phys. Rev.* B **48** 6144
——1994 *Phys. Rev.* B **49** 8821
Vescovo E, Carbone C, Alkemper U, Rader O, Kachel T, Gudat W and Eberhardt W 1995a *Phys. Rev.* B **52** 13 497
Vescovo E, Carbone C, Eberhardt W, Rader O, Kachel T and Gudat W 1993a *Phys. Rev.* B **48** 285
Vescovo E, Rader O and Carbone C 1993b *Phys. Rev.* B **47** 13 051
Vescovo E, Rader O, Redinger J, Blulgel S and Carbone C 1995b *Phys. Rev.* B **51** 12 418
Vescovo E, Rochow R, Kachel T and Carbone C 1992 *Phys. Rev.* B **46** 4788
Victora R H and Falicov L M 1985a *Phys. Rev. Lett.* **55** 1140
——1985b *Phys. Rev.* B **31** 7335
Walker T G and Hopster H 1993 *Phys. Rev.* B **48** 3563
Walker T G, Pang A W, Hopster H and Alvarado S F 1992 *Phys. Rev. Lett.* **69** 1121
Wang Z Q, Li Y S, Jona F and Marcus P M 1987 *Solid State Commun.* **61** 623
Watson R M 1959 *Solid-State and Molecular Theory Group, Technical Report* No 12 (Cambridge, MA: MIT Press)
Weber W, Allenspach R and Bischof A 1995 *Europhys. Lett.* **31** 491
Weber W, Wesner D A, Guntherodt G and Linke U 1991 *Phys. Rev. Lett.* **66** 942
Weinert M and Blugel S 1994 *Magnetic Multilayers* ed L H Bennett and R E Watson (Singapore: World Scientific) p 51
Weinert M, Blugel S and Johnson P D 1993 *Phys. Rev. Lett.* **71** 4097
Weisbuch C and Vinter B 1991 *Quantum Semiconductor Studies* (New York: Academic)
Weller D, Alvarado S F, Gudat W, Schroder K and Campagna M 1985 *Phys. Rev. Lett.* **54** 1555
Wesner D A, Weber W, Hartmann D, Guntherodt G and Effner U A 1993 *Phys. Rev.* B **48** 1806
Wohlfarth E P 1971 *Phys. Lett.* **36A** 131
——1977 *Phys. Rev. Lett.* **38** 524
Wu R and Freeman A J 1992 *Phys. Rev. Lett.* **69** 2867
——1995 *Phys. Rev.* B **51** 17 131
Wu R, Li C, Freeman A J and Fu C L 1991 *Phys. Rev.* B **44** 940
Wu S C, Garrison K, Begley A M, Jona F and Johnson P D 1994 *Phys. Rev.* B **49** 14 081
Xu Z, Liu Y, Johnson P D and Itchkawitz B S 1995a *Phys. Rev.* B **52** 15 393
Xu Z, Liu Y, Johnson P D, Itchkawitz B, Randall K, Feldhaus J and Bradshaw A 1995b *Phys. Rev.* B **51** 7912
Yeomans J M 1992 *Statistical Mechanics of Phase Transitions* (Oxford: Clarendon)
Ziman J M 1972 *Principles of the Theory of Solids* (Cambridge: Cambridge University Press)